Stability and Reliability Validation of Microgrid Systems

Song, Yubo

DOI (link to publication from Publisher):
10.54337/aau561825401

Publication date:
2023

Document Version
Publisher's PDF, also known as Version of record

STABILITY AND RELIABILITY VALIDATION OF MICROGRID SYSTEMS

BY
YUBO SONG

DISSERTATION SUBMITTED 2023

AALBORG UNIVERSITY
DENMARK

Stability and Reliability Validation of Microgrid Systems

Ph.D. Dissertation

Yubo Song

Dissertation submitted July 2023

Dissertation submitted: July 2023

PhD supervisor:: Prof. Frede Blaabjerg
Aalborg University, Denmark

PhD co-supervisors: Asst. Prof. Subham Swaroop Sahoo
Aalborg University, Denmark

Prof. Yongheng Yang
Zhejiang University, China

PhD committee: Associate Professor Sanjay K. Chaudhary (chair)
Aalborg University, Denmark

Professor Giovanni De Carne
Karlsruhe Institute of Technology, Germany

Professor Suryanarayana Doolla
Institute of Technology (IIT) Bombay, India

PhD Series: Faculty of Engineering and Science, Aalborg University

Department: AAU Energy

ISSN (online): 2446-1636
ISBN (online): 978-87-7573-670-6

Published by:
Aalborg University Press
Kroghstræde 3
DK – 9220 Aalborg Ø
Phone: +45 99407140
aauf@forlag.aau.dk
forlag.aau.dk

Printed in Denmark by Stibo Complete, 2023

Biography

Yubo Song

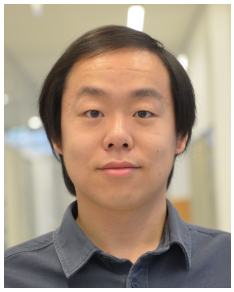

Yubo Song received the B.Sc. and M.Eng. degrees in Electrical Engineering with specializing in power electronics systems from Shanghai Jiao Tong University, Shanghai, China, in 2016 and 2019, respectively. Since 2020, he has been working toward Ph.D. degree in the Department of Energy (AAU Energy), Aalborg University, Aalborg, Denmark. From May to July 2022, he was a visiting Ph.D. researcher with the ELITE Grid Research Lab, in Department of Electrical and Computer Engineering, University of Alberta, Edmonton, AB, Canada.
His main research interests include the control, stability and reliability of power electronics systems.

Abstract

Power-electronics-based power systems (PEPS) are revolutionizing the utilization of renewable energy sources (RES) in modern society, playing a critical role in achieving the global net-zero carbon emission goal. As distributed power suppliers are becoming more prevalent, microgrids are formed, enhancing the functionality of PEPS. Meanwhile, the expanding applications of power electronics components in turn reduce the physical inertia in microgrid systems, thus inducing higher risk of failures. To address this issue, it is essential to develop methodologies that ensure safe and reliable operation of microgrids, specifically necessitating the study on stability and reliability of microgrids. By considering them in the design and operational planning of microgrids, the economic costs due to power outages or maintenances can be effectively reduced.

The stability and reliability of microgrids are conventionally examined separately due to their huge disparity in timescales and evaluation methodologies. Stability analysis encompasses system dynamics in shorter timescales (typically in a few milliseconds), while reliability evaluation pertains to long-term degradation of components in power electronics systems. However, the two performance indices literally interact with each other, unraveling unrecognized constraints or limitations on the operational planning. This Ph.D. project thereby aims to bridge the stability and reliability validation of microgrids and provide a comprehensive understanding of them at the system level.

This Ph.D. project begins with individual examinations on the stability and reliability of microgrids, primarily governed by their respective definitions. With a focus on dynamic stability, this project investigates various modeling methods and formulates quantitative metrics to facilitate an intuitive mapping of the methods. In terms of reliability, the physics-of-failure (PoF) based evaluation is emphasized, upon which a conditional reliability-oriented power sharing strategy for microgrids is formed, showing improved performances especially under fluctuated loading conditions. Moreover, the project presents methodologies for stability and reliability-oriented tests, including model-aggregated emulation of converters for stability validation and simplified real-time thermal evaluation for reliability validation.

Subsequently, this project explores the connections between stability and reliability of microgrids for the first time. The reliability-oriented control is further examined, revealing underlying stability constraints on reliability as practical interactions. To this end, solutions are demonstrated to tackle the stability concerns and achieve higher system reliability. From a theoretical standpoint, stability and reliability are linked through probabilistic analysis accounting for system uncertainties. The long-term reliability is decomposed into short-timescale frames, allowing for the evaluation of operational risk that incorporates both stability and reliability. Similarly, the conditional evaluation of their relationship is also implemented using the Bayesian inference methods.

In summary, the outcomes of this Ph.D. project offer new guidelines and frameworks for comprehensively considering stability and reliability in the operation of microgrids, so as to optimize the system costs. Acknowledging technical assumptions and limitations of this project, several research points have also been specified as potential future extensions.

Resumé

Effektelektronik-baserede elsystemer er betydningsfulde for en effektiv udnyttelse af den vedvarende energi og for dermed at opnå det CO_2-neutrale mål for verden. Med det stigende antal af distribuerede energileverandører bliver flere mikronet oprettet, som forbedrer elnettets funktionalitet, men imidlertid er der ulempen, at den traditionelle roterende inerti i elsystemer bliver reduceret, og det øger risikoen for operative fejl. Derfor er det vigtigt at udvikle nye metoder til at sikre stabilitet og høj pålidelighed af de fremtidige mikronet. Ved at tage hensyn til dem i designet og planlægningen af mikronet kan de økonomiske omkostninger reduceres som bl.a. opstår pga. strømsvigt eller vedligeholdelser i forbindelse med fejl.

Stabiliteten og pålideligheden af mikronet bliver normalt analyseret separat pga. deres forskelle i tidsskalaer og evalueringsmetoder. Stabiliteten handler om mikronettets dynamik på kortere tidsskalaer, mens pålideligheden vedrører analyser af svigt af de elektroniske dele på længere sigt. Dog påvirker de to faktorer faktisk hinanden, hvilket medfører nye begrænsninger i planlægningen af mikronet, som ikke tidligere er blevet undersøgt. Dette ph.d.-projekt når derfor som mål at kombinere stabilitet og pålidelighed af mikronet ved at udvikle en samlet forståelse af de to faktorer på systemniveau.

Projektet starter med individuelle undersøgelser af stabilitet og pålidelighed af mikronet, som er forankret i deres respektive definitioner. Med særlig fokus på den dynamiske stabilitet undersøger projektet forskellige evalueringsmetoder, og kvantitative metrikker bliver defineret for at muliggøre intuitive sammenligninger af metoderne. Mht. pålidelighed bliver de fysisk-baserede levetidsmodeller understreget for at derefter gennemføre en pålidelighed-orienteret kontrolstrategi, som i praksis er en betinget belastningsdeling imellem forskellige omformere i mikronet. Strategien udviser forbedret performance, især når belastningen ændrer sig over tid. Derudover præsenteres der metoder til at teste et mikronets stabilitet og pålidelighed, inkl. en samlet emulering af flere omformere med henblik på stabilitetsvalidering og en termisk evaluering af omformerne i realtid som karakteriserer pålideligheden.

Mht. forbindelserne imellem stabilitet og pålidelighed afsløres det desuden, at den pålidelighed-orienterede kontrol-strategi medfører underliggende grænser for pålideligheden i mikronet pga. stabiliteten, der kan betragtes som fysiske interaktioner. Således foreslås løsninger til grænserne for at opnå højere pålidelighed af mikronet. I et matematisk perspektiv er stabilitet og pålidelighed forbundet med en vis sandsynlighed, som handler om usikkerhederne der eksisterer i mikronet. Ved at opdele de langvarige pålidelighedsanalyser i kortere tidssegmenter kan en evaluering af den operative risiko foretages, som omfatter både stabilitet og pålidelighed. Ligeledes kan de betingede sandsynligheder beregnes ved brug af den Bayesianske inferens.

Dette ph.d.-projekt giver dermed nye retningslinjer og metoder til at kunne gennemføre en omfattende analyse af stabilitet og pålidelighed i mikronet. Projektet har dog tekniske antagelser, der betyder begrænsninger, hvorfor nye forskningsemner også bliver foreslået som potentielle fortsættelser af projektet i fremtiden.

Thesis Details

Thesis Title: Stability and Reliability Validation of Microgrid Systems
Ph.D. Student: Yubo Song
Supervisors: Prof. Frede Blaabjerg, Aalborg University, Denmark
Asst. Prof. Subham Swaroop Sahoo, Aalborg University, Denmark
Prof. Yongheng Yang, Zhejiang University, China

This thesis serves as a summary based on the following papers, highlighting the outcome of the Ph.D. project:

Publications in journals:

[J1] **Y. Song**, S. Sahoo, Y. Yang, and F. Blaabjerg, "Quantitative Mapping of Modeling Methods for Stability Validation in Microgrids," *IEEE Open J. Power Electron.*, vol. 3, pp. 679-688, Oct. 2022.
doi: 10.1109/OJPEL.2022.3214200.

[J2] **Y. Song**, S. Sahoo, Y. Yang, and F. Blaabjerg, "Conditional Droop Adjustment for Reliability-Oriented Power Sharing in Microgrid Systems," *IEEE Trans. Circuits Syst. II Express Briefs*, vol. 70, no. 7, pp. 2465-2469, Jul. 2023.
doi: 10.1109/TCSII.2023.3242139.

[J3] **Y. Song**, S. Sahoo, Y. Yang, and F. Blaabjerg, "Stability Constraints on Reliability-Oriented Control of AC Microgrids – Theoretical Margin and Solutions," *IEEE Trans. Power Electron.*, vol. 38, no. 8, pp. 9459-9468, Aug. 2023.
doi: 10.1109/TPEL.2023.3270640.

[J4] **Y. Song**, S. Sahoo, Y. Yang, and F. Blaabjerg, "Probabilistic Risk Evaluation of Microgrids Considering Stability and Reliability," *IEEE Trans. Power Electron.*, vol. 38, no. 8, pp. 10302-10312, Aug. 2023.
doi: 10.1109/TPEL.2023.3278037.

Publications in conference proceedings:

[C1] **Y. Song**, S. Sahoo, Y. Yang, and F. Blaabjerg, "System-Level Mapping of Modeling Methods for Stability Characterization in Microgrids," in *Proc. 2021 IEEE ECCE*, Vancouver, BC, Canada, Oct. 2021, pp. 2943-2949.

doi: 10.1109/ECCE47101.2021.9594979.

[C2] **Y. Song**, S. Sahoo, Y. Yang, and F. Blaabjerg, "System-Level Stability of the CIGRE Low Voltage Benchmark System: Definitions and Extrapolations," in *Proc. 2021 IEEE COMPEL*, Cartagena, Colombia, Nov. 2021, pp. 1-6.

doi: 10.1109/COMPEL52922.2021.9645971.

[C3] **Y. Song**, S. Sahoo, Y. Yang, F. Blaabjerg, and Y. W. Li, "Aggregated Emulation of Multiple Converters with Heterogeneous Dynamics in Low-Voltage Microgrids – A Clustering Approach," in *Proc. 2022 IEEE ECCE*, Detroit, MI, USA, Oct. 2022, pp. 1-5.

doi: 10.1109/ECCE50734.2022.9948214.

[C4] **Y. Song**, S. Sahoo, Y. Yang, F. Blaabjerg, and Y. W. Li, "Real-Time Thermal Evaluation of Power Converters in Microgrids by Device Current Reconstruction," accepted by *IEEE CPE-POWERENG 2023*, Tallinn, Estonia, Jun. 2023.

[C5] **Y. Song**, S. Sahoo, Y. Yang, and F. Blaabjerg, "Probabilistic Mapping of Stability and Reliability in Microgrids – A Bayesian Interpretation," accepted by *EPE'23 ECCE Europe*, Aalborg, Denmark, Sept. 2023.

This thesis has been submitted for assessment in partial fulfillment of the PhD degree. Parts of the papers above are used directly or indirectly in the extended summary of the thesis. The co-author statements have been made available to the assessment committee and are also available at the Faculty of Engineering and Science, Aalborg University.

Preface

This thesis serves as a summary of the main outcomes of the Ph.D. project entitled "*Stability and Reliability Validation of Microgrid Systems*", which was performed at the Department of Energy (AAU Energy), Aalborg University, Denmark. This Ph.D. project was supported by the REliable Power Electronic-Based Power System (REPEPS) project at Department of Energy, Aalborg University, as a part of the Villum Investigator Program funded by the Villum Foundation, Denmark, to whom I would like to deliver my deep acknowledgement.

I would like to express my sincere gratitude to my supervisor, Prof. Frede Blaabjerg, for his invaluable mentorship, support and encouragement throughout my Ph.D. study. His profound knowledge and diligent attitude to work and research have impressed and influenced me a lot. I would also like to thank my co-supervisors, Asst. Prof. Subham Sahoo and Prof. Yongheng Yang. They have provided me with fantastic inspirations and earnest assistance in my research and my life in Aalborg.

I would like to thank Prof. Yun Wei (Ryan) Li, for providing me with the opportunity to visit University of Alberta in Canada as well as the collaborations. I am also grateful for the help from the Postdocs and the PhDs in Ryan's lab during my stay in U of A.

I would also like to thank all my friends, my colleagues, and the secretaries and technicians in our department, especially Prof. Francesco Iannuzzo and Prof. Huai Wang for the discussions and collaborations, Mads Lund for the technical assistance, and Tianbao Gu, Zongzhe Xuan, Jiahui Wu, Kaichen Zhang, Monika Sandelić, Liang Huang, Jing Yuan, Meng Chen, and Zhongting Tang for all the support and help during these three years. Wish them all the best in the future.

Last but not least, I would like to express the sincerest gratitude to my family who are back in China – my parents and my grandparents. This work would never be possible without their love and support.

Yubo Song
1st July, 2023, in Aalborg

Table of Contents

Part I

Report

Chapter 1

Introduction

1.1. Background

Electricity is one of the most essential types of energy in the nature. In modern society, electrical energy is functioning everywhere, including automated manufacturing, modern transportation and information technology, etc. With the convenience of being transmitted in electric power systems, electrical energy has been acting as an interface of many other types of energy to be efficiently utilized.

There is an enormous global consumption of electricity nowadays, and electricity can be generated in many ways, e.g., fossil fuels, hydropower, solar panels, wind turbines, and nuclear power plants, etc., wherein Renewable Energy Sources (RES) are appealing for the sake of sustainable development of the planet. People have been seeking for the possibilities to reduce the CO_2 emission, and a net-zero goal of emission by 2050 has been set in many countries all over the world [1]-[3]. According to the Renewables 2022 Global Status Report by the Renewable Energy Policy Network for the 21st Century (REN21) [1], there is currently an amount of 3146 GW of renewable power capacity installed globally, where the newly installed capacity in 2021 was 314.5 GW (statistics of 2022 are not yet available). As depicted in Fig. 1.1, the share of renewable electricity has increased to 28.3% in 2021, and a significant increase lies in solar and wind power, thanks to the development of power electronics as their interfaces to the power grids. In Fig. 1.2, it is again shown that photovoltaic (PV) and wind power generation with much potential are supposed to contribute the major parts to meet the net-zero goal by 2050, and technically, this goal is in turn promoting the penetration of power electronics converters in modern power systems.

Subsequently, more power systems are becoming power-electronics-based power systems (PEPS). Not only has the flexibility of power conversion been remarkably elevated, but also can the RES be utilized via more extensively distributed energy suppliers, which is generally known as Distributed Energy Resources (DERs). To strive for such advantages, a power system can be thereby decomposed into smaller subdivisions that can operate either autonomously or cooperatively, while the entire system is governed hierarchically. Under this scenario, the concept of microgrids is formed as the local power systems

considering smaller scale of suppliers and users [4]. A typical example of a microgrid is shown in Fig. 1.3, which is the CIGRE Low-Voltage (LV) benchmark system [5]. Compared with conventional power systems like the standard systems in [6], microgrids can involve conventional microturbines, various DERs (e.g., wind turbines, PV panels and fuel cells) and energy storage facilities (e.g., flywheels or batteries) with changeable energy flow directions or heterogeneous dynamics, and should be able to operate in either islanded or grid-connected mode. The functionability of power systems is enhanced, whereas new challenges arise accordingly. The higher penetration of power electronics converters in microgrids has notably decreased the physical inertia, which used to be primarily provided by synchronous generators [7]. Also, the lower capacity of power electronics has limited the ride-through performances with higher short-circuit current during fault conditions [8]. Hence, methodologies should be developed and improved to accommodate the new scenarios and to ensure safe and reliable operation of microgrids, which is the basic motivation of this Ph.D. project.

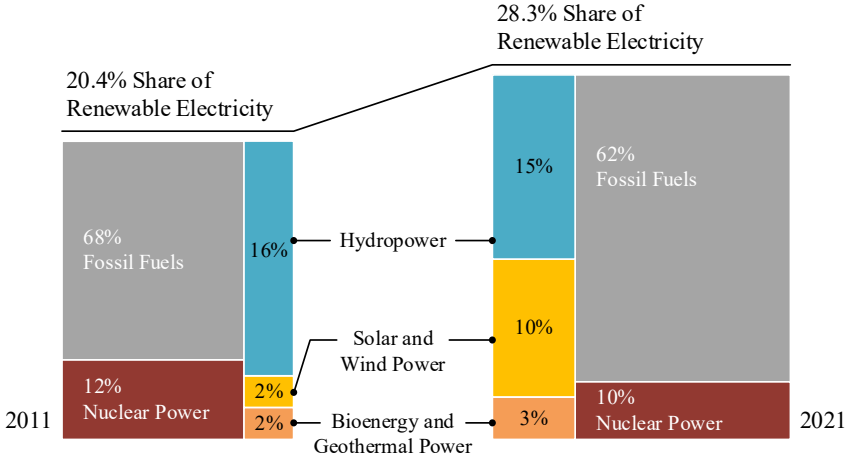

Fig. 1.1: Comparison in the shares of power generation categories in 2011 and 2021 worldwide. Source: [1].

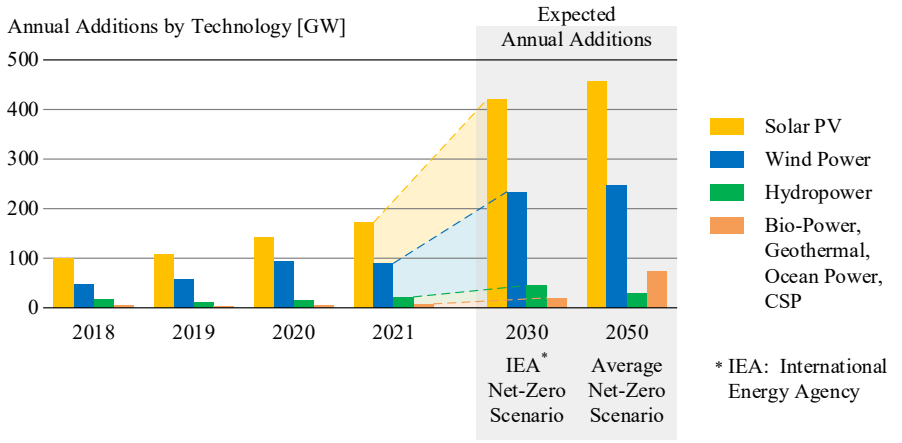

Fig. 1.2: Annual additions of renewable power capacity in the previous years and the expectation of annual additions to achieve the net-zero scenarios. Source: [1].

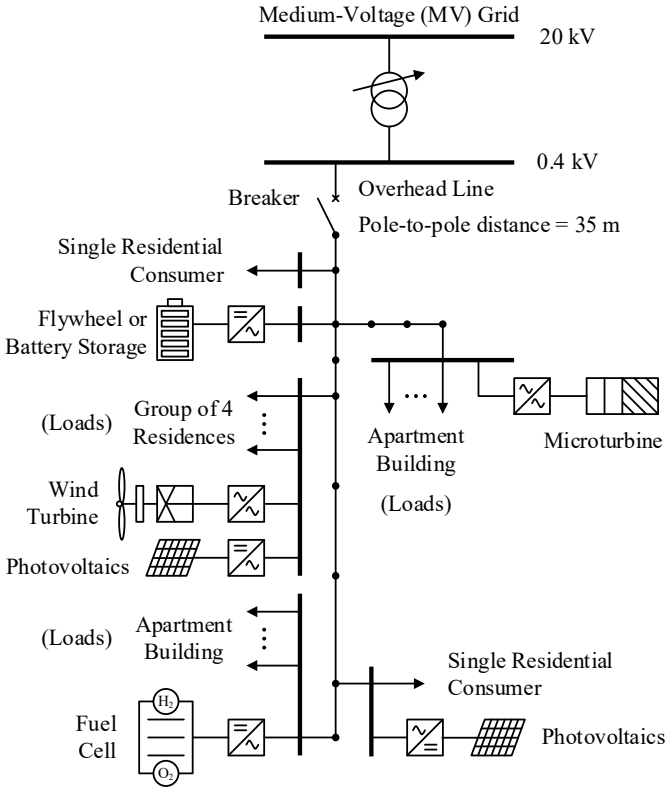

Fig. 1.3: The CIGRE Low-Voltage (LV) benchmark system, which is a typical example of local distributive microgrids. Source: [5].

1.1.1. Challenges in Modern Microgrids: Failures and Uncertainties

The safe and reliable operation of power systems is an ever-focused point, where faults and failures may lead to dangers and economic losses both for utilities and consumers. According to [9], the most severe historical power outages can last from hours up to several days and affect more than hundreds of millions of people, and even in the 2010s, there are still more than 20 severe outages that have taken place worldwide [10]. Earlier in 2003, a blackout occurred in eight states in the U.S. and the province of Ontario in Canada, known as the most serious one in the North American history [11]-[13]. It was originally caused in Ohio by reactive power deficiencies [11], ending up with over 6 billion dollars cost and over 50 million people being influenced [12], [13]. People are relying more on electrified automation and electronic information technologies nowadays, and the security and reliability of electrical power systems should consequently be emphasized more to avoid harsher aftermaths, yielding design and operation guidelines like [14] and [15].

Also, for microgrids, more variety of distributed generations and loads have increased the risk of failures, and more uncertainties appear inside. The uncertainties in microgrids basically include the uncertainties of internal system parameters and external working conditions, where the latter can be classified into *operational variables* (system quantities, like wind and solar power) and *disturbance variables* (events, like faults and load contingencies) [16]. The uncertainties can be time-variant variables and affect the secure and reliable operation state of microgrids via system architectures, configurations or mission profiles. Hence, in order to better design and operate such systems, the stability and reliability evaluations are introduced to formalize methodologies and characterize the role of the uncertainties.

Those variables can also be mathematically modelled into probability distributions, e.g., normal distribution (Gaussian distribution) for ordinary loads and component parameters, Weibull distribution for wind speed [17], and Poisson distribution for fault incidents [18], etc. To this end, a combination of deterministic and probabilistic approaches can simplify both stability and reliability analysis on microgrids in such cases.

1.1.2. Stability of Microgrids and Its Evaluation

The concept of stability stems from control theory. Systems are designed for certain objectives, yet disturbances naturally exist in practice, which influence the outputs of the systems. The time-domain responses of a system under disturbances basically include steady-state and transient responses, wherein the

most important dynamic behavior of the system is absolute stability. In control theory, *a linear time-invariant* (*LTI*) *system is said to be stable if it can eventually achieve an equilibrium state after being subject to a disturbance* [19]. The dynamics of both the plants and the controllers are involved, and system modeling is thereby a must.

Electric power systems are typical systems with mathematical models based on Kirchhoff's current and voltage laws (KCL and KVL). Being responsible for energy conversion and transmission, it is always desired that power systems should operate safely and stably, whereby the stability is defined. Based on the definition in control theory, power system stability is defined in [20]-[22] as: *the ability that a power system can operate steadily under normal conditions and regain an acceptable state of equilibrium after a disturbance*. In addition to the requirement on dynamic performance, the system variables are also supposed to be bounded within a desired region, which ensures the quality of electric energy service during normal operation.

With respect to microgrids, the stability also involves both the steady-state and the dynamic performances, yet it is redefined to exclude involuntary load shedding due to the relatively smaller number of users and lower capacity [23]. Intentional tripping of loads can be considered as instability even if the remaining parts of the system are able to continue operating. Meanwhile, in conventional power systems, stability analysis is basically classified into rotor angle stability, frequency stability and voltage stability corresponding to the resulting modes [21], [22]. In contrast, more diverse controllers and source dynamics in microgrids or PEPS have prompted additional stability concerns other than the synchronization of generators. The classification of stability in microgrids or PEPS is thereby modified into control system stability and power supply and balance stability in [23], [24], as illustrated in Fig. 1.4. In practice, instability in microgrids or PEPS could occur in different modes [25], and more than one could occur all at once due to the heterogeneous dynamics of the RES and the converters. Among them, dynamic stability of converters is a frequently discussed topic in microgrids due to the wide use of power electronics converters and the variety of controllers [26], and it is selected as a major consideration in this project in terms of microgrid stability, as highlighted in red in Fig. 1.4.

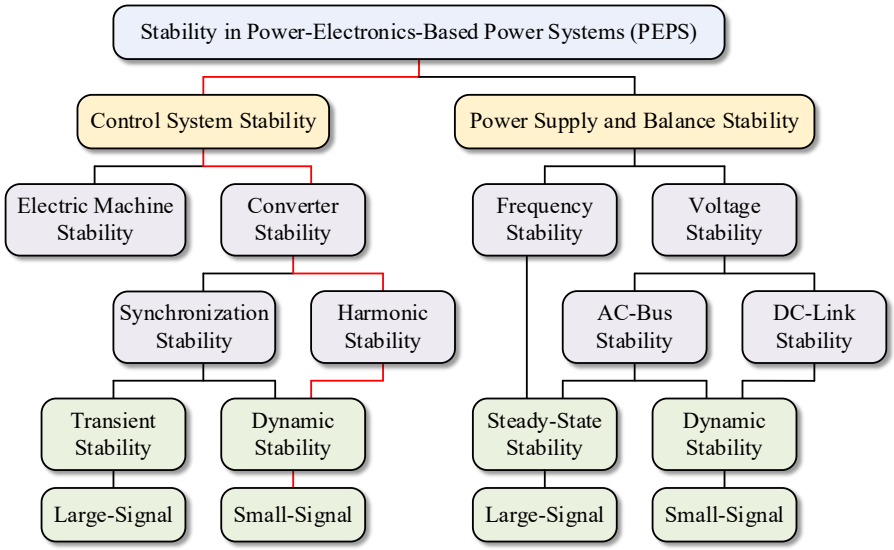

Fig. 1.4: Classification of stability in power-electronics-based power systems (PEPS) or microgrids [23].

With the above classification, stability in microgrids can be modeled by many approaches. In existing literature, the state-space-based modeling (e.g., [27]-[29]) and impedance-based modeling (e.g., [30]-[37]) originated from control theory are two major approaches for small-signal stability, while phasor portraits (e.g., [38]-[40]) are introduced for angular transient stability and power flow analysis for steady-state stability. Stability criteria could accordingly be formulated based on the employed tools in control theory, like the eigenvalue loci/root loci [27]-[29] and the Nyquist diagrams [30], [33]-[35] in the frequency domain, and the Lyapunov criteria in the time domain [41], [42]. On top of this, advanced methodologies have also been specified for particular instability modes or applications, e.g., using complex transfer functions to simplify the multiple-in-multiple-out (MIMO) system models or deal with unbalanced cases [31], [35]-[37].

The state-space-based modeling and impedance-based modeling have been compared in [43]-[45], and their respective pros and cons have been discussed under different scenarios like the scalability when the scale of microgrids expands. However, these comparisons have not defined a clear borderline between the modeling methods, and the validation can be ambiguous and challenging in multi-converter systems. It is consequently profitable to have an intuitive mapping of the modeling methods, namely the following research gap:

Research Gap 1 (Investigation on the stability of microgrids and comparison of the modeling methods)
The heterogeneous dynamics in microgrids may give rise to various types of instability, depending on the controllers, sources and loads. To clearly define the scope of the project, it is critical to explore the instability modes and intuitively compare the modeling methods, which lays a base for stability and reliability validation of microgrids.

Moreover, to deal with the system uncertainties mentioned in Section 1.1.1, the concept of probabilistic stability has also been introduced [16], where the stability of power systems is measured by probability instead of deterministic binary values. The uncertainties can be integrated into stability analysis, e.g., by Monte-Carlo methods, mathematical regression or artificial intelligence modeling [46]. In existing literature, such approaches have provided possibilities to quantify the influences of, e.g., power generation uncertainties [47]-[49]. As a new perspective of microgrid stability, the probabilistic approaches can be inspiring for exploring the connection between stability and reliability, the latter of which is essentially a probabilistic index of microgrid performance.

1.1.3. Reliability of Microgrids and Its Evaluation

Reliability engineering has been established on top of system engineering aimed at preventing unexpected failures and ensuring the operation quality of systems. It is expected that the systems should not only operate in a failure-free state, but also keep functioning as desired for a sufficient period of time. To measure how the expectations are met, the concept of *reliability* has been thereby proposed as a representative for the four aspects *reliability*, *availability*, *maintainability* and *safety* (RAMS) [50], and metrics have been formulated to quantify these performances.

Systems behave naturally in a stochastic way. The reliability of a system is thereby defined as *the probability that it performs its required functions under given conditions for a specified time interval* [50], and the mean-time-to-failure/restoration (MTTF/MTTR) are employed to reflect the time dimension in terms of system operation. Generally, the failure of systems follows the "*Bathtub Curve*" [50], as shown in Fig. 1.5. The failure rate λ, which indicates the occurrence of failures per unit time period, changes by three phases throughout the lifetime of the item or system: the early failure related to "infant mortality" after manufacturing/realization of the system, the constant failure during useful lifetime, and the increasing failure when approaching the end-of-life (EOL). This curve has been instructing the design of systems as well as the scheduling of maintenance before the systems are completely worn out.

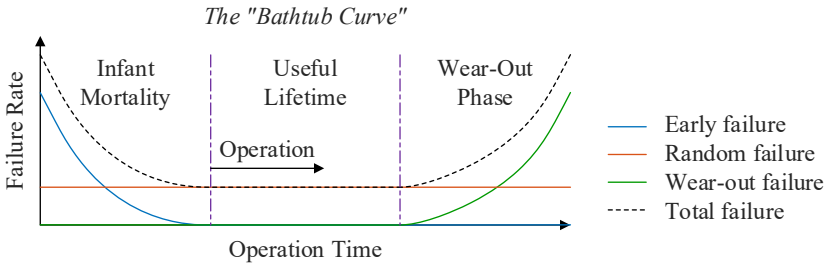

Fig. 1.5: The "*Bathtub Curve*" in reliability engineering [50].

In electrical engineering, reliability analysis has been widely performed on power systems and power components, where different methodologies have been formalized based on the definition of reliability.

Power systems supply electrical power to a number of users, and unexpected load shedding should be avoided [23], [51], [52]. In conventional power systems, there is a relatively low variety of facilities, e.g., synchronous generators, transmission lines and transformers, and interactions between the supplier and the user are rarely seen. Thus, MTTF, MTTR and failure rate could be easily modeled to characterize the time-domain influence of failures, and Markov techniques can be applied to represent the state transformation [51]. Meanwhile, as electrical energy cannot be efficiently stored in a large amount, the economic aspect is also an important concern in power system planning, where the power flow is designed to minimize the economic cost. To this end, the reliability can be interpreted as a measurement of source adequacy and load capability of the power systems (e.g., loss-of-load-expectation (LOLE) or expected-energy-not-supplied (EENS)), or the economic loss due to the failures (e.g., expected customer interruption cost (ECOST)) [51]. Besides, the "*N*–1 contingency" or "*N*–*a* contingency" has been proposed as deterministic adequacy criteria [53] herein.

On the other hand, with respect to power electronics components, reliability is discussed more in individual performance than systematic planning, as there is less proportion of adequacy in power electronics converters compared to power systems. This requires satisfactory lifetime before the EOL. Apart from statistics and empirical failure-rate models (e.g., the MIL-HDBK-217 [54]), the physics-of-failure (PoF) based analysis has been developed in recent years to better accommodate power electronics applications involving multiple components and miscellaneous mission profiles (operation conditions) [55], [56]. In existing literature, many methodologies have been proposed for the testing or condition monitoring of power semiconductors [57]-[61] and capacitors [62], [63], etc., which are among the most fragile components (Fig. 1.6 [64]). It has been concluded that both electrical (e.g., loading) and non-electrical (e.g., ambient temperature or

humidity) factors are contributing to the degradation of power electronics components [65]. Based on this, mathematical models can be derived by combining physical and regressive approaches for both internal (the damage models for power semiconductors [66]-[68] or capacitors [69]-[71]) and external (thermal networks [72]-[77]) characteristics. These models have provided more flexible prediction of the reliability and lifetime of the components under different conditions.

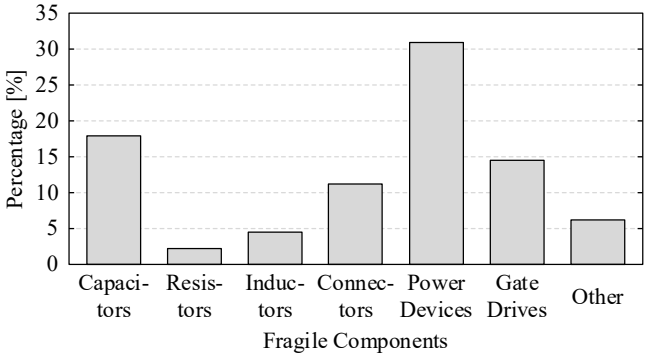

Fig. 1.6: An industrial-based study [64] conducted in 2008 on the most fragile components in power electronics applications, where 56 effective responses have been received.

Grounded by the above, the reliability of power converters [78], [79] and modern microgrids/PEPS [80]-[82] is accordingly formed, which is generally perceived as the combination of component-level and system-level reliability [83]. The reliability evaluation on power electronics systems principally follows the framework of reliability engineering, which is formulated according to the logical relationship of components in reliability block diagrams [50], [78], [83], whereas the reliability of components is additionally obtained by the PoF-based models and mission profiles. It is aimed to utilize the data of component-level tests and be well adaptive to both the numerous component types and varying mission profiles.

Subsequently, reliability-oriented control is formed owing to the reliability models, intended for achieving the desired lifetime or scheduling preventive maintenance to reduce the overall cost of power electronics systems. It is developed into several sub-topics, including power routing within power converters [84]-[87], operation point scheduling of RES-interfacing converters [88], [89] and power sharing among converters in microgrids or other PEPS [90]-[93]. The basic idea stems from the *Barrel Effect* [84], [86], [90]-[92]: the components or converters with lower reliability or higher cost, should share as less loading as

possible. In microgrids, the power sharing can be implemented by modifying the controllers of power converters, e.g., the droop controllers [90]-[93].

Nevertheless, the guidelines for achieving more reliable microgrids are sometimes ambiguous. For example, in existing literature, the pros and cons of the reliability-oriented power sharing in AC microgrids are not fully addressed, among which the variation of loads may lead to a contradiction from higher reliability in [93]. The control strategies could be accordingly improved. Thus, the following research gap has been identified:

> **Research Gap 2 (General guidelines for achieving more reliable microgrids)** The guidelines for achieving more reliable microgrids should be speculated. For example, the pros and cons of reliability-oriented power sharing for multi-converter AC microgrids are not fully addressed, and issues may arise when the power ratings change over time. There should be more encyclopedic guidelines on design or control strategies formed to accommodate the mission profiles.

1.1.4. Relationship between Stability and Reliability of Microgrids

In power system analysis, the adequacy for planning and the security for normal operation are two major concerns, which respectively correspond to reliability and stability [94]. In conventional power systems, the stability was passively assured by synchronous generators and slow dynamics [95], and the reliability was considered by adding as much redundancy as needed. Hence, there was not much critical connection between power system stability and reliability.

In modern microgrids, as mentioned above, power electronics converters and controllers are involved, whilst the stability and reliability evaluations are normally discussed in different timescales. As shown in Fig. 1.7, the degradation of components is an accumulation of stresses, which can last for up to several years, while the stability analysis is performed within the timescale of seconds (dynamic stability) or minutes to hours (steady-state stability). As a result, it is often assumed that the system is reliable when conducting stability analysis, and is stable for reliability analysis. Also due to the disparity in stability and reliability evaluation methodologies, the two indices are barely considered simultaneously. Though stability and reliability analysis are both performed in researches like [91], the purpose is simply to validate the design of parameters for reliability-oriented control, and little emphasis has been laid on the underlying relationships between the two indices.

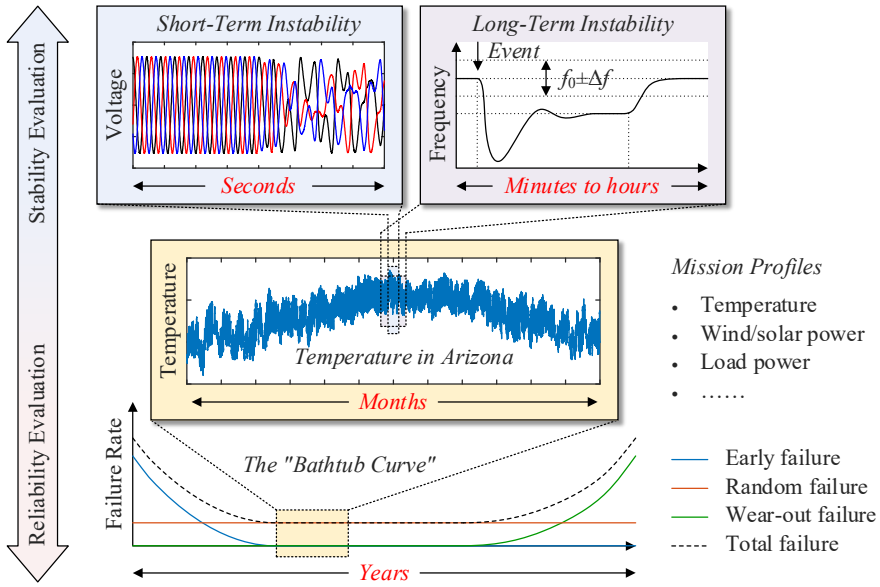

Fig. 1.7: Relationship on timescales of microgrid stability and reliability. Source: [J4].

However, the interactions between the two indices are not always negligible. Component failures may physically lead to large-signal instability events, and challenges emerge when additional methodologies are applied such that the two indices have time-domain coupling via one or more variables. For instance, the reliability-oriented power sharing in [92], [93] modifies the control parameters, which may change the dynamic performance of the system and have an impact on system stability. Such application-based scenario could yield a basic understanding of the relationship between stability and reliability, inspiring the subsequent research points of this project:

> **Research Gap 3 (Understanding of the relationship between stability and reliability of microgrids)**
> Due to the mismatch in timescales, the relationships between stability and reliability have not been well addressed. This limits the practicability of applied control or optimization strategies. To this end, mutual influences of the two indices should be identified. As a basic example, the reliability-oriented power sharing could be inspected by performing stability analysis, and potential issues could be revealed accordingly.

On the other hand, the collective impacts of the two indices also remain unclarified in existing literature, which corresponds to the operational risk of

microgrids. Risk is originally specified as the probabilistic consequence of unstable events [96], or how likely the system will fail due to unforeseen contingencies [97], [98]. However, microgrids are principally supposed to operate both stably and reliably, whereas the two indices do not always guarantee each other. To this end, the risk of microgrid operation should be re-evaluated more comprehensively by considering both two indices, and a combined index should be formed to reflect the performance of microgrids more genuinely. This project is also expected to fill in the following gap:

> **Research Gap 4 (Unified performance evaluation of microgrids considering both stability and reliability)**
> The stability and reliability of microgrids are normally analyzed separately, which leads to an ignorance of their collective impacts on the system performance. Both indices should be considered simultaneously to establish a comprehensive insight into this aspect, and the combined index should be interpreted for microgrid applications.

1.2. Project Motivations

As mentioned in the previous section, several research gaps have been identified with respect to microgrid stability and reliability, as well as their connections. The challenges may be attributed to the difference in the evaluation approaches and the mismatch in the timescales.

Firstly, there is much difference in the modeling and evaluation methodologies of stability and reliability, which separates the two topics, yet their connections should be enlightened out of the common aspects of methodologies. To this end, the modeling and evaluation of stability and reliability in microgrids should be investigated.

Secondly, the reliability-oriented power sharing could be an inspiring case to study as it involves both control parameters and reliability metrics. Stability analysis can be performed on it, and conclusions are to be drawn and explained based on the security of microgrids.

Thirdly, the combination of stability and reliability of microgrids should be considered to fill the research gap, which could be either under specific scenarios or using techniques that are in common for them. The combined index should be able to reflect both the stability and reliability performance, while its interpretation is desired.

In summary, the major motivation of this Ph.D. project is basically to explore the unseen connections between stability and reliability analysis of microgrids,

and have a comprehensive understanding of the two performance indices that can be also generalized up to large power system analysis.

1.3. Project Objectives and Limitations

1.3.1. Project Objectives

Motivated by the aforementioned research challenges, this Ph.D. project can be summarized into a major research question as following:

> "*How can we bridge stability and reliability analysis in microgrids to comprehensively validate the performances at system level?*"

To answer this question, the stability and reliability of microgrids should first be modeled. The connection between the two performance indices is the major focus in this project, and the possibility to combine the two performances is supposed to be explored. To this end, how to link the different timescales of the two indices is a necessity. Besides, when the two indices are unified, the combination should be interpreted in contrast with them.

Based on the research gaps and the major question, multiple sub-questions to proceed this project can be formed as following:

Q1. What are the definitions of stability and reliability in microgrids, how to evaluate the stability and reliability in microgrids, and in what cases will a microgrid become unstable or unreliable?

Q2. What are the connections between the two performances, and how are the two performances influencing each other?

Q3. How to unify stability and reliability together considering the timescales, and how to interpret the combined index in microgrid applications?

Q4. What methodologies can be employed to perform the validation of stability and reliability, and how to further improve the validation methods by advanced approaches?

Based on those sub-questions, the Ph.D. project can be subsequently decomposed into several objectives as following:

O1. To investigate the modeling and evaluation of microgrid stability:

This project is mainly aimed at studying the relationship between stability and reliability, and the modeling and evaluation of the two performances should be one of the bases. To address this objective, the stability modeling approaches should be classified and compared in terms of heterogeneous

dynamics and instability modes of microgrids. The modeling methods should be accordingly selected for the exemplary study cases in this project.

O2. To investigate microgrid reliability and the reliability-oriented control in microgrids

The modeling and evaluation of reliability is also an underlying part in this project. System-level reliability of the study cases will be modeled. To eventually connect microgrid stability and reliability together, the reliability-oriented control could be inspiring as it essentially covers both long-term degradation of power converters and short-term system dynamics. More general guidelines will be formed throughout the detailed analysis on reliability-oriented control, and its pros and cons will be discussed.

O3. To explore the mutual influence of microgrid stability and reliability:

In existing researches, it is mostly assumed that a microgrid is reliable in stability analysis, and vice versa. Their connections are usually neglected. To this end, one of the major objectives of this project is to explore their mutual influences. As the two indices have much difference in timescales, the reliability-oriented control could be a possible intermediary between them. The approaches for previous objectives will be employed to reveal the potential issues, and to form the framework addressing the issues in practice.

O4. To combine stability and reliability analysis and identify the interpretation behind the combination:

Based on the conclusions on their relationship, it could be theoretically possible to combine stability and reliability analysis. It is expected in this objective that their combination could reflect the collective impacts on system performance, and probabilistic assumptions and techniques could be required herein. The interpretation of the combined index could be practical, which should be demonstrated by case studies.

O5. To develop methodologies for stability and reliability validation of microgrids:

To validate the stability and reliability in microgrids, certain techniques could be required for experimental or simulation tests. This objective is a supplement of the previous objectives. Several methodologies that could simplify the tests or adapt certain scenarios should be developed, which could serve as useful tools for more general tests.

An overview of the aforementioned objectives can be summarized in Fig. 1.8.

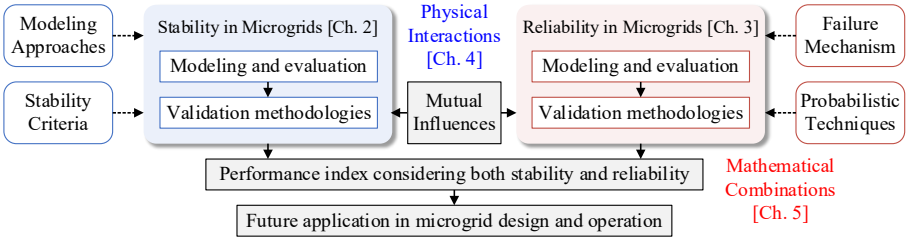

Fig. 1.8: An overview of the research objectives of the Ph.D. thesis.

1.3.2. Project Limitations

This Ph.D. project focuses on the relationships between stability and reliability analysis in microgrids, as well as a framework to bridge stability and reliability. With the general research topics, there are some assumptions that need to be taken in this project, which are associated with technical limitations.

In this thesis, only AC microgrids operating in islanded mode are studied. The studied microgrids are all distribution networks with no loops formed in terms of topology, and the studied microgrids are three-phase ones and balanced without faults.

In this thesis, the CIGRE LV benchmark is first studied, but to simplify the experimental validation, typical study cases are employed consisting of parallel DC-AC converters, and the power rating is decreased in certain situations. In terms of the study cases, assumptions and limitations are as following:

- It is assumed that the power lines are inductive with low parasitic resistance. Accordingly, inductors are used as the lines in the experiments.
- All the converters are controlled by *P*-*f* and *Q*-*V* droop controllers [99], where the frequency and voltage are adjusted for active and reactive power control, respectively:

$$\begin{aligned} f &= f_0 - m_p \left(P - P_0 \right) \\ V &= V_0 - n_q \left(Q - Q_0 \right) \end{aligned} \tag{1.1}$$

  The dynamics of primary voltage control loops (e.g., the cascaded voltage loops of grid-forming voltage source inverters in [99]) are neglected unless specified.
- The DC links of the DC-AC converters are assumed to be ideally steady unless specified. In other words, the DC-link dynamics are not considered.
- All the loads are assumed to be resistive. Other *ZIP* loads (*Z* for constant-impedance loads, *I* for constant-current loads, and *P* for constant-power loads) and non-linear loads are not considered in this project unless specified.

In the reliability analysis, there are further assumptions and limitations:

- All the power semiconductors are assumed to be silicon IGBTs or diodes. Other types of power semiconductors are not studied. All power semiconductors are assumed to follow the power cycling curves in [100].
- As the DC links are assumed to be ideal, the DC-link capacitors are not considered in the reliability analysis.
- The filters, lines and loads are assumed to be sufficiently reliable unless specified.

Therefore, though this project is conducted by keeping as much generality as possible, some of the conclusions may still not apply to exceptional cases. But the basic ideas could be an inspiration for further discussions and research work.

1.4. Thesis Outline

The outcomes of this Ph.D. project are summarized in this thesis as a collection of publications. The thesis consists of two major parts, the *Report* and the *Selected Publications*, and the structure of this thesis is elaborated in Fig. 1.9.

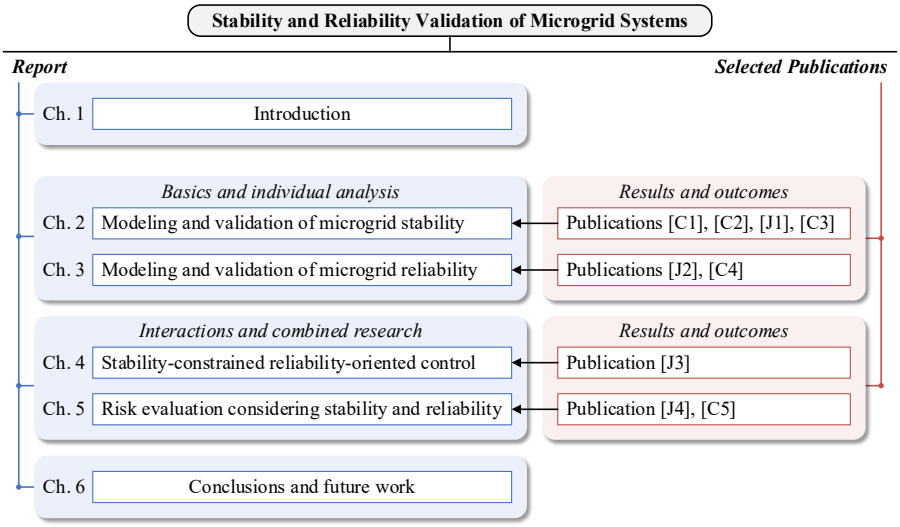

Fig. 1.9: Outline of this thesis, including the framework of the report part and the adherence of selected publications to the chapters in the report.

Navigated by the objectives, the *Report* includes six chapters, which are briefly introduced as following:

Chapter 1: Introduction

This chapter, *Chapter 1*, is aimed at depicting the background and motivation of this Ph.D. project. The objectives are established based on the research challenges, followed by assumptions and limitations in this project. In this chapter, the structure of this thesis is also presented, as well as the publications supporting this thesis.

Chapter 2: Microgrid Stability: System-Level Modeling and Its Validation

In *Chapter 2*, the definition of microgrid stability is first explored in a typical study case, i.e., the CIGRE LV benchmark system. In terms of different instability modes, the modeling and evaluation approaches of microgrid stability are investigated and compared, and the approaches are assessed by quantitative metrics. Meanwhile, to simplify the validation of multi-converter buses, a model-aggregated approach is proposed by emulating the multiple converter dynamics in clusters, which is demonstrated by real-time simulations.

Chapter 3: Microgrid Reliability and Reliability-Oriented Power Sharing

In *Chapter 3*, the modeling and evaluation of system-level reliability of microgrids is investigated, and the reliability-oriented power sharing is studied in details. A conditional power sharing strategy is proposed to improve the overall lifetime of microgrids in more general cases, where its pros and cons are also explained. Moreover, an approach demonstrating thermal performances of power semiconductors is presented based on device current reconstruction to validate reliability performance in real-time tests, showing advantages in reducing the computational burden in validation.

Chapter 4: Stability Constraints on the Reliability-Oriented Control

Chapter 4 is aimed at revealing the interactions between microgrid stability and reliability. The aforementioned reliability-oriented power sharing is effective to extend the overall lifetime of microgrids, yet it could lead to stability issues. It is elaborated in *Chapter 4* how the stability criteria should be considered in microgrid reliability, and a framework of stability-constrained reliability-oriented control is proposed. Alternative solutions to this issue are introduced, and the approaches are validated by simulation and experimental tests.

Chapter 5: Performance Evaluation Considering Both Stability and Reliability

In *Chapter 5*, the evaluation of stability and reliability is combined. The probability of microgrid stability considering system uncertainties is investigated by Monte-Carlo methods, which contributes to the probabilistic combination of the two indices. A more comprehensive concept, the *operational risk* of microgrids, is thereby introduced including both stability and reliability, and the concept of *lifetime* is generalized to match the new scenario. A trade-off between stability and reliability could lie in the design of microgrids, and the system-level performance could be comprehensively optimized accordingly.

Chapter 6: Conclusions and Future Work

Chapter 6 summarizes the outcomes and contributions of this project according to the research questions. Future research perspectives will also be discussed, which could be focused to address the limitations of this project or inspire possibilities in this field.

1.5. List of Publications

The research outcomes of the Ph.D. project have been disseminated in the form of a collection of publications in journals and conference proceedings, which are encompassed in this Ph.D. thesis. The list of the publications is as following:

Publications in journals:

[J1] **Y. Song**, S. Sahoo, Y. Yang, and F. Blaabjerg, "Quantitative Mapping of Modeling Methods for Stability Validation in Microgrids," *IEEE Open J. Power Electron.*, vol. 3, pp. 679-688, Oct. 2022. doi: 10.1109/OJPEL.2022.3214200.

[J2] **Y. Song**, S. Sahoo, Y. Yang, and F. Blaabjerg, "Conditional Droop Adjustment for Reliability-Oriented Power Sharing in Microgrid Systems," *IEEE Trans. Circuits Syst. II Express Briefs*, vol. 70, no. 7, pp. 2465-2469, Jul. 2023. doi: 10.1109/TCSII.2023.3242139.

[J3] **Y. Song**, S. Sahoo, Y. Yang, and F. Blaabjerg, "Stability Constraints on Reliability-Oriented Control of AC Microgrids – Theoretical Margin and Solutions," *IEEE Trans. Power Electron.*, vol. 38, no. 8, pp. 9459-9468, Aug. 2023. doi: 10.1109/TPEL.2023.3270640.

[J4] **Y. Song**, S. Sahoo, Y. Yang, and F. Blaabjerg, "Probabilistic Risk Evaluation of Microgrids Considering Stability and Reliability," *IEEE Trans. Power Electron.*, vol. 38, no. 8, pp. 10302-10312, Aug. 2023. doi: 10.1109/TPEL.2023.3278037.

Publications in conference proceedings:

[C1] **Y. Song**, S. Sahoo, Y. Yang, and F. Blaabjerg, "System-Level Mapping of Modeling Methods for Stability Characterization in Microgrids," in *Proc. 2021 IEEE ECCE*, Vancouver, BC, Canada, Oct. 2021, pp. 2943-2949. doi: 10.1109/ECCE47101.2021.9594979.

[C2] **Y. Song**, S. Sahoo, Y. Yang, and F. Blaabjerg, "System-Level Stability of the CIGRE Low Voltage Benchmark System: Definitions and Extrapolations," in *Proc. 2021 IEEE COMPEL*, Cartagena, Colombia, Nov. 2021, pp. 1-6. doi: 10.1109/COMPEL52922.2021.9645971.

[C3] **Y. Song**, S. Sahoo, Y. Yang, F. Blaabjerg, and Y. W. Li, "Aggregated Emulation of Multiple Converters with Heterogeneous Dynamics in Low-Voltage Microgrids – A Clustering Approach," in *Proc. 2022 IEEE ECCE*, Detroit, MI, USA, Oct. 2022, pp. 1-5. doi: 10.1109/ECCE50734.2022.9948214.

[C4] **Y. Song**, S. Sahoo, Y. Yang, F. Blaabjerg, and Y. W. Li, "Real-Time Thermal Evaluation of Power Converters in Microgrids by Device Current Reconstruction," accepted by *IEEE CPE-POWERENG 2023*, Tallinn, Estonia, Jun. 2023.

[C5] **Y. Song**, S. Sahoo, Y. Yang, and F. Blaabjerg, "Probabilistic Mapping of Stability and Reliability in Microgrids – A Bayesian Interpretation," accepted by *EPE'23 ECCE Europe*, Aalborg, Denmark, Sept. 2023.

1.6. Experimental Platform Used in the Ph.D. Project

The experimental results for this Ph.D. thesis are obtained with the setup shown in Fig. 1.10 unless otherwise specified.

An exemplary configuration is an islanded AC microgrid consisting of two converters connected in parallel through *LC* filters and lines at a Point of Common Coupling (PCC). The common DC-link is created by passively rectifying from an AC voltage source. Inductors are used as line impedances, and a resistor as the load.

In particular, the Imperix© converter racks are employed, where in each rack two Silicon Carbide (SiC) converters (PEB8024) are installed together with a B-Box RCP 3.0 digital controller and sensors with high capability of control bandwidth. A Spitzenberger© power amplifier is adopted as the AC source.

The hardware specifications of the experimental platform are listed in Table 1.1, while the exemplary configuration of the system under test is presented in Table 1.2. Configurations for exceptional cases will be specified additionally in corresponding chapters of the thesis.

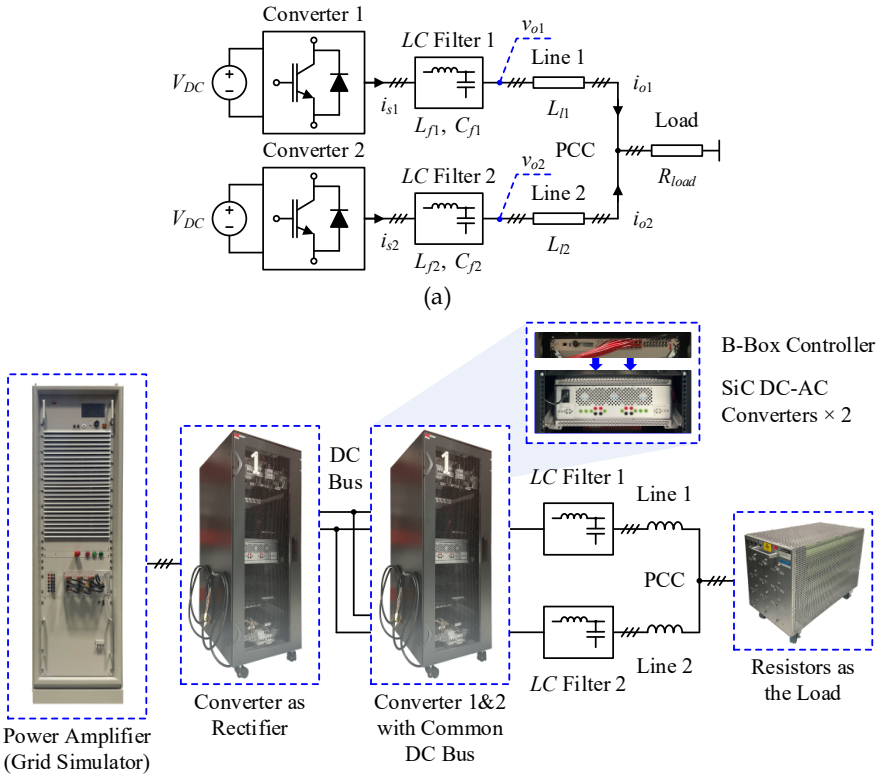

Fig. 1.10: Experimental platform used in the Ph.D. project: (a) an exemplary topology, and (b) the setup configured based on the topology shown in (a).

TABLE 1.1: HARDWARE SPECIFICATIONS OF THE EXPERIMENTAL PLATFORM

Facility	Description	Value
Imperix© Converters	Nominal DC-link voltage	800 V
	Power rating of the converters	1200 V/60 A
	Maximum switching frequency	70 kHz
Spitzenberger© Power Amplifiers	Power rating of the amplifiers	15 kW×3 ph
	Maximum signal bandwidth	30 kHz

TABLE 1.2: DEFAULT CONFIGURATIONS OF THE SYSTEM UNDER TEST

Description	Symbol	Default Value
DC-link voltage	V_{DC}	400 V
Nominal phase voltage	V_n	110 V_{RMS}
Fundamental frequency	f_n	50 Hz
Switching frequency	f_{sw}	10 kHz
Sampling frequency	f_s	10 kHz
LC filter inductance	L_{f1}, L_{f2}	2.0 mH
LC filter capacitance	C_{f1}, C_{f2}	10 µF
Line inductance	L_{l1}, L_{l2}	0.5 mH
Load resistance	R_{load}	57.5 Ω or 28.75 Ω (Specified by case)

Specially, the real-time simulations in Sections 2.4 and 3.4 are conducted based on an FPGA-based OPAL-RT platform (OP5700), as part of the work during the collaborative stay in University of Alberta, Edmonton, AB, Canada.

Chapter 2

Microgrid Stability: System-Level Modeling and Its Validation

2.1. Background

This Ph.D. project is aimed at bridging stability and reliability analysis in microgrids at system level, wherein the system stability should be firstly modeled. It has been mentioned in Section 1.1.2 that stability in a PEPS or a microgrid is defined as its ability to attain an acceptable equilibrium of state variables [20]-[22], which is contingent on both the plants and the controllers. In practice, the heterogeneous dynamics of the RES and the controllers can lead to multiple types of instability, which is classified in Fig. 1.4. To form an explicit and systematic view of the stability issues in microgrids, the instability in microgrids is firstly identified in this chapter based on the CIGRE LV benchmark system, and an explanatory inspection is provided accordingly [C2].

Secondly, to mathematically characterize the system behaviors, modeling methods have been proposed for specific scenarios, like the Nyquist-based stability criteria normally used for grid-connected inverters [30], and the state-space-based approach [27] or component connection method (CCM) [33] for multi-converter systems. The modeling methods can exhibit distinct accuracy or complexity for various scenarios in microgrids, which has been preliminarily discussed in [43]-[45]. Nonetheless, the existing comparisons have not yet provided a transparent mapping of the modeling methods for general microgrid systems and not fully addressed the borderline between the methods. The second focus of this chapter is thereby devoted to a further exploration into this point by formalizing quantitative metrics for benchmarking the modeling methods [C1], [J1], of which the efficacy is demonstrated by case studies.

Besides, the validation methodologies are also discussed from the perspective of real-time tests. The grids are normally regarded as a voltage source with an inductive impedance in series, whereas in microgrids, distributive generations are inducing heterogeneous dynamics. Hence, it can be challenging to test the performance of microgrid systems with multiple converters. Inspired by [101], a

model-aggregated emulation of multiple converters is proposed for time-domain stability validation [C3].

2.2. Microgrid Stability and Exemplary Instability in a Microgrid

As mentioned in Fig. 1.4, microgrid stability can be basically classified into control system stability, and power supply and balance stability [23]. Power supply and balance stability is concerned with maintaining safe operation points, while the control system stability is focused on ensuring system robustness against disturbances. Navigated by the classification, several cases have been carried out based on the CIGRE LV benchmark shown in Fig. 1.3, illustrating how the DERs and loads affect microgrid stability.

For better clarification, the converters, sources and loads are labeled in Fig. 2.1 (a), and the study cases are organized as shown in Fig. 2.1 (b). Simulations are performed on part of the benchmark system in each case, involving specified converters and loads connected to the same bus. The instability issues are accordingly demonstrated in [C2] as following.

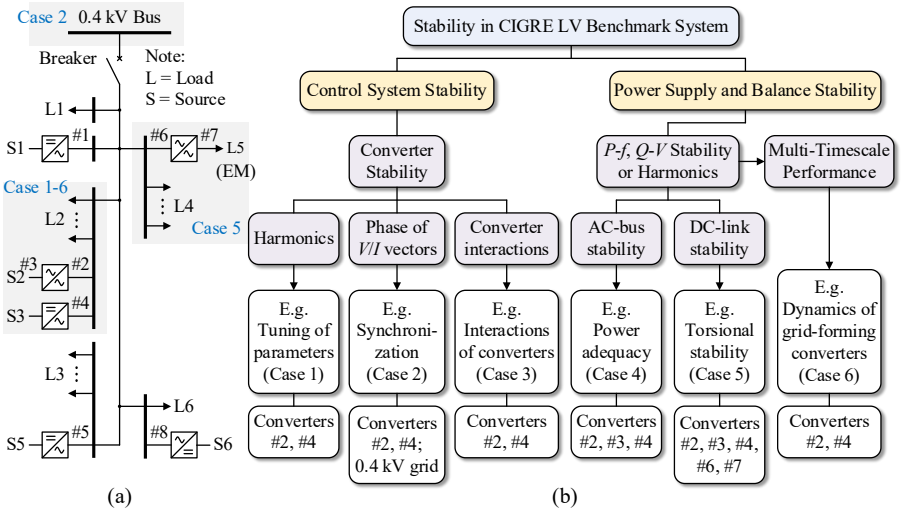

Fig. 2.1: Overview of the study cases in this section on the exemplary CIGRE LV benchmark system. (a) Illustration for the indices of converters, sources and loads. (b) Stability concerns and corresponding study cases in the exemplary system. Source: [C2].

Remark 2.2.1:
The electric machine stability in Fig. 1.4 concerns the oscillations of synchronous generators. In this section, the electric machine (EM) L5 is assumed to be a Permanent Magnet Synchronous Machine (PMSM) and is treated as a rotational load driven by back-to-back converters. Thus, the torsional stability (Case 5) is categorized as DC-link stability.

A. Instability from Mismatched Control System

The control system stability necessitates the adequacy of control schemes, and corresponding issues may arise due to the mismatch between controllers and plants [23]. In microgrids, the synchronization of electric machines and the tuning of controllers for converters are typically considered, while the latter is more common with the advanced control strategies.

In power electronics converters, the Pulse-Width Modulation (PWM) is known as a major harmonic source, and the mismatched controllers may magnify the harmonics at certain resonance frequency and lead to system failure. Supposing that the grid-interfacing converters are controlled typically as Fig. 2.2 [27], the control system stability is considered from the following aspects:

(1) The tuning of the control parameters,
(2) The frequency and phase generated locally, which pertains to synchronization,
(3) The current feedforward gain F, which ranges between 0 and 1 and indicates the interaction among converters.

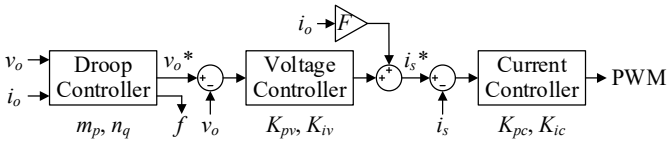

Fig. 2.2: A typical droop-based control scheme for a grid-forming converter with an interfacing filter, where i_s, i_o and v_o stand for the converter-side current and grid-side current and voltage, respectively.

Case 1: Tuning of Control Parameters

Poor tuning of controllers, like the voltage controller, may lead to an oscillation around the equilibrium operation point, which is known as the harmonic stability [25], [33]. Such oscillations are not necessarily diverging, while the resonance frequency can range from around the fundamental frequency (f_1) up to several kHz according to the control scheme [25]. One of the most typical scenarios is presented in Fig. 2.3, when the gain of voltage controllers K_{pv} is decreased.

Harmonics spring up around hundreds of Hertz, which can deteriorate the power quality and also increase the thermal stresses on power electronics components.

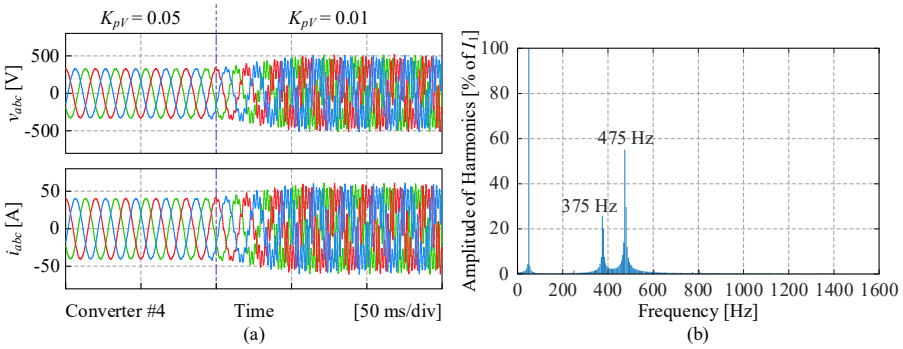

Fig. 2.3: Simulation results of instability Case 1 – Tuning of parameters. Resonance occurs along with a reduction of the voltage control gain K_{pv}, (a) voltage and current waveforms of Converter #4, and (b) harmonic spectrum of i_{abc} with respect to the fundamental component I_1. Source: [C2].

Case 2: Synchronization of Converters

The synchronization of converters is critical when controllers are implemented in the rotational control frame. Unlike synchronous generators where the synchronism can be adaptively built by the rotors, more stiffness exists in power electronics converters due to less inertia. A case is presented in Fig. 2.4 where the local microgrid is connected to an external strong grid with large Short-Circuit Ratio (SCR). The asynchronization at PCC will cause a loss of control and eventually a system failure. Here, grid-following strategies with synchronization techniques or decoupling of frequencies (e.g., via a DC link) could be considered as possible solutions.

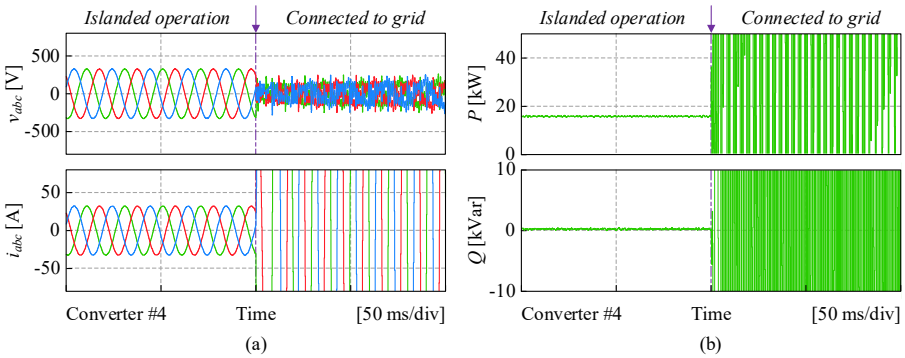

Fig. 2.4: Simulation results of instability Case 2 – Synchronization of Converters. Instability caused by poor synchronization, (a) voltage and current waveforms, and (b) active and reactive power of Converter #4. Source: [C2].

Case 3: Interactions of Converters

From a system-level perspective, converters in a microgrid are physically coupled with each other and the interactions are also leading to instability. In light of this, the feedforward gain F in Fig. 2.2 can be exemplified, which normally serves for decoupling the disturbances from grid-side current. In Fig. 2.5, when F is decreased, an oscillatory behavior appears between converters, driving the system away from the equilibrium point. Nevertheless, the divergence in this case may proceed gradually compared to the immediate loss of synchronization in Fig. 2.4.

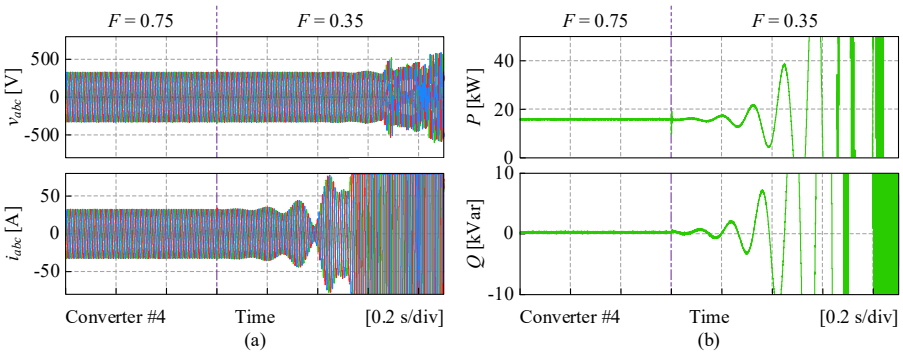

Fig. 2.5: Simulation results of instability Case 3 – Interactions of converters. Instability along with a reduction of the feedforward gain F, (a) voltage and current waveforms, and (b) active and reactive power of Converter #4. Source: [C2].

B. Instability from Insufficient Power Supply

The power supply stability concerns the demand-supply balance and the effectiveness of power sharing among DERs [23], which may be disrupted by, e.g., loss of generation, violation of DER power limits, improper power sharing among DERs, or involuntary load tripping, etc. In this part, the power capacity of Converter #4 is limited, which facilitates the following study cases with respect to power supply inadequacies.

Case 4: Power Inadequacy

Constrained by the mission profiles, the power generated by DERs cannot always be adjusted as needed. Hence, power adequacy should be an underlying concern for a microgrid operating in islanded mode. Fig. 2.6 exemplifies a scenario where the source S2 is considered to be a Permanent Magnet Synchronous Generator (PMSG)-based wind turbine, and the power capacity of Converter #4 is limited. Since wind power cannot be altered abruptly, and an increase in load L2 may result in system malfunctions due to the power supply limitation.

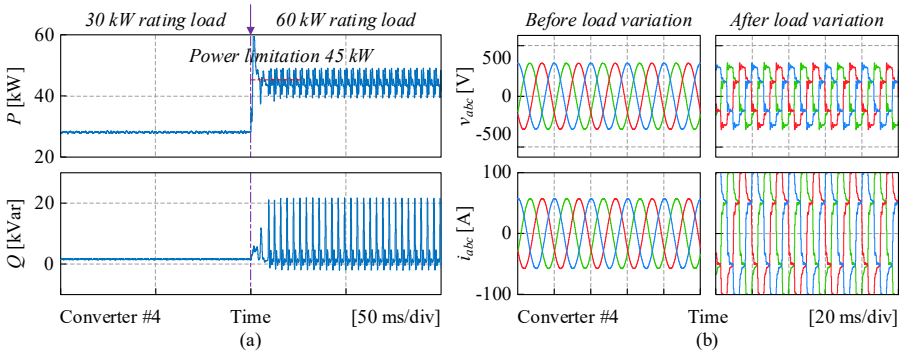

Fig. 2.6: Simulation results of instability Case 4 – Power inadequacy. Instability when the load L2 increases beyond the available power supply, (a) active and reactive power, and (b) voltage and current waveforms. The maximum power of source S3 is set as 45 kW of Converter #4. Source: [C2].

Case 5: Torsional and DC-Link Instability

Likewise, Fig. 2.7 depicts another unstable scenario in microgrids that also stems from power inadequacy, specifically torsional and DC-link instability. Different from Case 4, the following conclusions are drawn:

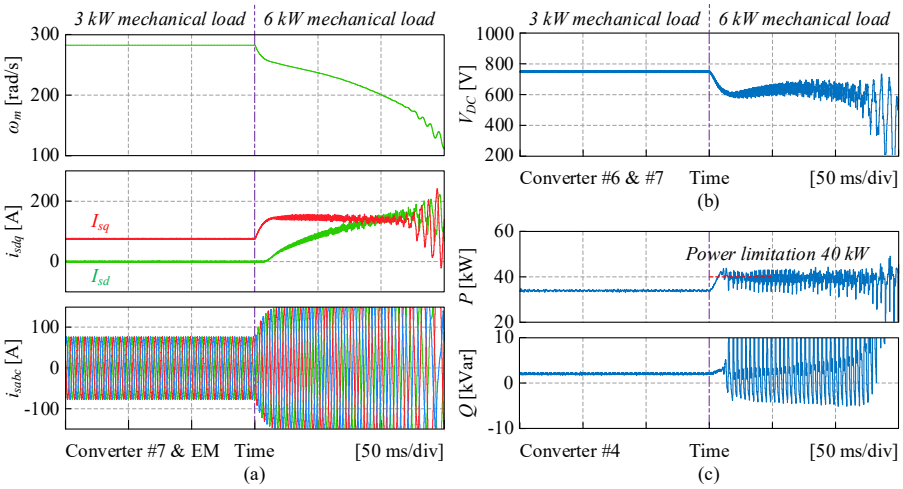

Fig. 2.7: Simulation results of instability Case 5 – Torsional and DC-link instability. Instability when the mechanical load of L5 increases beyond the available power supply, (a) rotational speed and stator current of the electric machine, (b) DC-link voltage of Converters #6 and #7, and (c) active and reactive power of Converter #4. The maximum power of source S3 is set as 40 kW. Source: [C2].

(1) In back-to-back converters, the DC-link voltage may drop when the power supply is insufficient, where the DC-link dynamics will lead to system instability.
(2) Overloading of electric machines can cause a loss of speed control, which will affect the electric system performance through rotational magnetic flux.

C. Instability from Multiple Time Constants

In microgrids, the RES normally have different dynamics. For instance, fuel cells have slower dynamics than PVs and batteries, and the difference in dynamics may lead to large-signal oscillations when subject to a load change. Similarly, the disability of RES to track load changes will possibly induce transient power inadequacy and also impair the system instability.

Case 6: Multi-Dynamics Instability

Fig. 2.8 thereby highlights the impacts of difference in source dynamics by exemplifying two grid-forming converters #3 and #4. The achieved steady state can be delicate in this scenario, as a large-signal disturbance can trigger system divergence in the form of low-frequency oscillations. This should be considered by system designers, ensuring that at least one grid-forming converter is equipped with sources that have sufficient dynamics and power capacity.

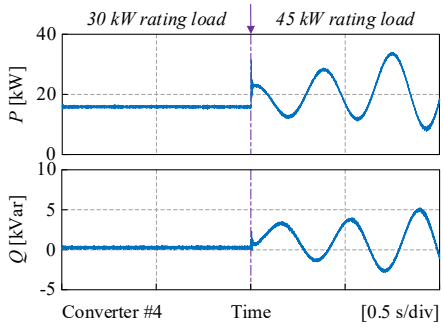

Fig. 2.8: Simulation results of instability Case 6 – Dynamics of grid-forming inverters. Instability in active and reactive power of Converter #4 caused by the difference in source dynamics. The load is increased from 30 kW to 45 kW, and the additional delays of Converters #3 and #4 are 3% and 0.3% of the fundamental frequency, respectively. Source: [C2].

2.3. Quantitative Mapping of Stability Modeling in Microgrids

In order to address the instability issues discussed in Section 2.2, numerous modeling methods have been proposed in existing literature for grid-connected converters and microgrid systems, given that the systems are linearized [C1]. In terms of small-signal dynamic stability, these modeling methods can be classified based on the underlying mechanisms of the models, with impedance- and state-space-based modeling being two primary types [43]-[45].

Impedance-based modeling is derived from the physical architecture of systems. Converters with interfacing filters are represented by Thevenin- or Norton- equivalent sources, and their interconnections are mapped into an admittance matrix. Controllers can also be incorporated into the impedances, as demonstrated in [35], [36]. Specifically, two common approaches for impedance-based modeling are: (1) developing input-to-output transfer functions and characterizing system dynamics by Bode plots or zero-pole plots, and (2) partitioning the system into source and load parts and applying the Nyquist criteria.

On the other hand, state-space-based modeling is an approach more inspired by mathematics, in that the Lyapunov definition of system stability aligns with the small-signal stability defined by equilibriums. By defining state variables and constructing a state matrix, the performances of multiple-in-multiple-out (MIMO) systems can be described mathematically, e.g., stability by eigenvalues, controllability and observability by the rank of the state matrix, etc. Alternatively, Lyapunov functions can be a more capable candidate approach even for nonlinear or large-signal scenarios.

Hence, the selection of appropriate modeling methods is crucial for effectively studying the performances of microgrid systems, concerning the features of the studied system and the type of instability under focus. These two types of stability modeling have been compared in [43]-[45], and their respective pros and cons are further summarized in Table 2.1 [J1]. There is usually a tradeoff considering the complexity, accuracy and intuitiveness of the modeling methods.

Furthermore, it has been recognized in [C1] that modeling complexity can be tailored as a quantitative criterion among the different modeling methods. By delving into this aspect, a more explicit guideline for stability validation has been concluded in [J1], which will be expanded in the remaining part of this section.

TABLE 2.1: COMPARISON OF STATE-SPACE- AND IMPEDANCE-BASED METHOD

	State-Space-Based Method	Impedance-Based Method
Size of matrix	Dependent on state variables	Dependent on impedance nodes
Order of elements in the matrix	Low	High
Domain of modeling	Time domain	Mostly frequency domain
Applicable frequency range	Wide	From around f_1 to control bandwidth
For large-scale systems	Easy for dimensional expansion	Moderate
For high-order systems	More state variables. Lyapunov functions are not influenced	Higher order of transfer functions. Bode plots are not influenced
For black-box systems	Difficult	Frequency scanning can be used for modeling
Possible source of inaccuracy	Linearization and approximations for numerical purpose	Linearization and ignoring coupling / asymmetry in dq / $a\beta$ components

Note: f_1 is the fundamental frequency (normally 50 or 60 Hz).
Source: [J1].

2.3.1. Quantification of Complexity of Modeling Methods

In terms of the complexity of system modeling, it is often necessary to evaluate the computational burden, particularly the differentials and integrals inside the system model that defines the *order* of the system. While non-elementary matrix operations (e.g., inversions) and eigenvalue calculations can also be time-consuming, the large number of differentials and integrals can primarily exacerbate the complexity to a greater extent.

Microgrids are composed of DERs and loads that are interfaced by converters and filters, and the behaviors of converters are usually modeled by averaging over the switching period. By linearizing the units in a microgrid and deriving their transfer functions, the contributions can be summarized as shown in Table 2.2, with a specific focus on two-level DC-AC converters. The *order* in Table 2.2 represents the maximum order of the numerator and denominator when the model is written in polynomial forms, corresponding to the highest order of inputs and outputs in the differential equations.

TABLE 2.2: ORDER CONTRIBUTION OF TYPICAL UNITS IN A MICROGRID

Units	Contribution to System Order
Proportional (P) controller	0
Integral (I) controller	1
Control delays in *Padé* approximation [102], [103]	Dependent on the order of the approximation employed
Simple resistor	0
An inductor or capacitor in filters	1
Synchronous-reference-frame phase-locked loop (SRF-PLL) [104]	2
P-f / *Q-V* droop controllers	0
First-order low-pass filters (LPF) for power in droop controllers	1 for active power 1 for reactive power
Integration of ω in *P-f* droop	1
Loads or lines in resistor-inductor (*RL*) equivalence	1
Transmission lines in π model	3

Source: [J1].

The metrics for quantifying the modeling complexity are formulated by analyzing the state-space- and impedance-based modeling as following. Assuming that there are m converters (nodes) in the studied microgrid system, then the state space can be constructed as (2.1), and the impedance-based model is (2.2) and (2.3):

$$\begin{aligned} \dot{\boldsymbol{x}}_{\mathrm{MG}}(t) &= \boldsymbol{A}_{\mathrm{MG}}\boldsymbol{x}_{\mathrm{MG}}(t) + \boldsymbol{B}_{\mathrm{MG}}\boldsymbol{u}_{\mathrm{MG}}(t) \\ \boldsymbol{y}_{\mathrm{MG}}(t) &= \boldsymbol{C}_{\mathrm{MG}}\boldsymbol{x}_{\mathrm{MG}}(t) + \boldsymbol{D}_{\mathrm{MG}}\boldsymbol{u}_{\mathrm{MG}}(t) \end{aligned} \tag{2.1}$$

where, $\boldsymbol{x}_{MG}$, $\boldsymbol{u}_{MG}$ and $\boldsymbol{y}_{MG}$ are the state vector, the input vector (e.g., the references, initial states and disturbances) and the output vector (the performances), respectively, and $\boldsymbol{A}_{MG}$, $\boldsymbol{B}_{MG}$, $\boldsymbol{C}_{MG}$, $\boldsymbol{D}_{MG}$ are the state matrices. If a number of λ state variables are defined, then the dimension of $\boldsymbol{x}_{MG}$ should be $\lambda \times 1$.

$$\begin{bmatrix} I_{\mathrm{conv,I}} \\ I_{\mathrm{conv,II}} \end{bmatrix}_{\mu\times 1} = \left[\boldsymbol{Y}_{\mathrm{MG}}\right]_{\mu\times\mu} \begin{bmatrix} V_{\mathrm{conv,I}} \\ V_{\mathrm{conv,II}} \end{bmatrix}_{\mu\times 1} \tag{2.2}$$

$$\begin{cases} V_{\mathrm{conv,I}} = G_{1,\mathrm{I}} V_{\mathrm{conv,I}}^{\ *} + G_{2,\mathrm{I}} I_{\mathrm{conv,I}} \\ I_{\mathrm{conv,II}} = G_{1,\mathrm{II}} I_{\mathrm{conv,II}}^{\ *} + G_{2,\mathrm{II}} V_{\mathrm{conv,II}} \end{cases} \tag{2.3}$$

where, V_{conv} and I_{conv} are respectively the node voltage and current, and G_1 and G_2 are the transfer functions from the references or disturbances. The subscripts I and II indicate the types of converters: Type I for voltage-source converters and Type II for current-source converters. $\boldsymbol{Y}_{MG}$ is the admittance matrix, and μ is the dimension of the admittance matrix, which can be an integer multiple of m dependent on the applied reference frame.

Based on this, the vector that contains the variables under observation is named as *state vector* (like $\boldsymbol{x}_{MG}$ or $[V_{conv,\mathrm{I}}, I_{conv,\mathrm{II}}]^{\mathrm{T}}$), and the matrix that describes the system architecture (like $\boldsymbol{A}_{MG}$ and $\boldsymbol{Y}_{MG}$) is named as *representative matrix*. Subsequently, two metrics *Maximum-Order Complexity* (MOC) and *Apparent-Order Complexity* (AOC) are defined as following to represent the complexity of a modeling method [J1].

Definition 2.3.1: Maximum-Order Complexity (MOC)
The MOC is defined as the sum of the following two parts:
a) Vector Part (VP): the total order of calculations directly applied to the state vector;
b) Matrix Part (MP): the sum of the maximum orders in each row in the representative matrix

Definition 2.3.2: Apparent-Order Complexity (AOC)
The AOC is defined as the sum of the following two parts:
a) Vector Part (VP): the total order of calculations directly applied to the state vector;
b) Matrix Part (MP): the sum of the orders of all elements in the representative matrix.

The MOC and AOC of state-space- and impedance-based modeling can be calculated as given in Table 2.3 [J1]. Generally, the MOC can provide a description on an order-defined size of the system, where both the number of nodes and the complexity inside each node are engaged. On the other hand, in AOC, the coupling among states is also fully considered, indicating the overall computational complexity. Hence, the MOC can be seen as the lower bound of AOC, namely AOC ≥ MOC.

An AC microgrid is thereby exemplified in Fig. 2.9 to illustrate the proposed metrics, supposing m droop-based converters connected in parallel with RL lines and loads. For a single converter modeled in dq frame, its order can be obtained as:

TABLE 2.3: CALCULATIONS OF MAXIMUM-ORDER COMPLEXITY AND APPARENT-ORDER COMPLEXITY

		State-Space-Based Modeling	Impedance-Based Modeling
Maximum-Order Complexity (MOC)	Vector Part (VP)	$VP_{\text{SS, MOC}} = \sum_{x_i \in \boldsymbol{x}} Ord\left\{\frac{\mathrm{d}}{\mathrm{d}t} x_i\right\} = \lambda$	$VP_{\text{Imp, MOC}} = Ord\left\{\begin{bmatrix} \frac{V_{conv,\text{I}}}{V_{conv,\text{I}}^{*}}(s) \\ \frac{I_{conv,\text{II}}}{I_{conv,\text{II}}^{*}}(s) \end{bmatrix}\right\} = \sum_{i=1}^{\mu} Ord\left\{g_{1,ii}\right\}$
	Matrix Part (MP)	$MP_{\text{SS, MOC}} = \sum_{i=1}^{\lambda} MaxOrd\left\{\left[\boldsymbol{A}_{\text{MG}}\right]_i\right\} = \sum_{i=1}^{\lambda} Ord\left\{a_{\text{MG},ii}\right\} = 0$	$MP_{\text{Imp, MOC}} = \sum_{i=1}^{\mu} MaxOrd\left\{\left[\boldsymbol{Y}_{\text{MG}}\right]_i\right\} = \sum_{i=1}^{\mu} Ord\left\{y_{\text{MG},ii}\right\}$
Apparent-Order Complexity (AOC)	Vector Part (VP)	$VP_{\text{SS, AOC}} = \sum_{x_i \in \boldsymbol{x}} Ord\left\{\frac{\mathrm{d}}{\mathrm{d}t} x_i\right\} = \lambda$	$VP_{\text{Imp, AOC}} = Ord\left\{\begin{bmatrix} \frac{V_{\text{conv, I}}}{V_{\text{conv, I}}^{*}}(s) \\ \frac{I_{\text{conv, II}}}{I_{\text{conv, II}}^{*}}(s) \end{bmatrix}\right\} = \sum_{i=1}^{\mu} Ord\left\{g_{1,ii}\right\}$
	Matrix Part (MP)	$MP_{\text{SS,AOC}} = \sum Ord\left\{\boldsymbol{A}_{\text{MG}}\right\} = \sum_{i=1}^{\lambda}\sum_{j=1}^{\lambda} Ord\left\{a_{\text{MG},ij}\right\} = 0$	$MP_{\text{Imp, AOC}} = \sum Ord\left\{\boldsymbol{Y}_{\text{MG}}\right\} = \sum_{i=1}^{\mu}\sum_{j=1}^{\mu} Ord\left\{y_{\text{MG},ij}\right\}$

Note: $Ord\{\cdot\}$ denotes the order of a certain element, and $MaxOrd\{\cdot\}$ indicates the maximum order in a group of elements (or elements of a matrix).
Source: [J1].

$$Ord\{\text{Conv}\} = \underbrace{(1\times 2+1)}_{\substack{\text{LPF and } \int \omega dt \text{ in} \\ \text{droop controllers}}} + \underbrace{(1+1)\times 2}_{\substack{\text{Voltage and current} \\ \text{PI controllers } (dq)}} + \underbrace{(1+1)\times 2}_{LC \text{ filter } (dq)} = 11 \tag{2.4}$$

Or if the model is reduced into a single-output (SO) model by considering only one of the symmetric phases in the impedance-based modeling (denoted as *single-axis* or *single* in subscripts):

$$Ord\{\text{Conv}_{\text{single}}\} = \underbrace{(1\times 2+1)}_{\substack{\text{LPF and } \int \omega dt \text{ in} \\ \text{droop controllers}}} + \underbrace{(1+1)\times 1}_{\substack{\text{Voltage and current} \\ \text{PI controllers}}} + \underbrace{(1+1)\times 1}_{LC \text{ filter}} = 7 \tag{2.5}$$

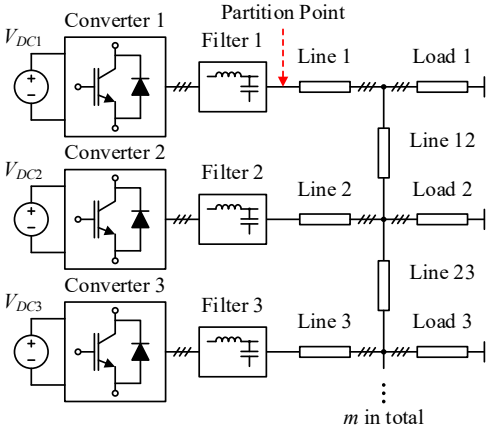

Fig. 2.9: An exemplified islanded microgrid with m converters in parallel and controlled by the droop-based scheme in Fig. 2.2. The power transmission lines and loads are all RL series, and the partition point for impedance-based modeling is labeled. Source: [J1].

The calculation of the MOC and AOC in terms of the two aforementioned types of modeling methods are accordingly presented in Table 2.4. In this case, the MOC is linearly related to the size of the system (number of nodes), while the AOC increases faster for large-scale systems by considering the interactions among the converters. The AOC is a more accurate reflection of the computational burden of a modeling method, and the MOC can serve as a benchmark for optimizing the modeling methods with sparse representative matrices.

TABLE 2.4: MAXIMUM-ORDER COMPLEXITY AND APPARENT-ORDER COMPLEXITY IN TERMS OF THE NUMBER OF CONVERTERS

	State-Space-Based Modeling	**Impedance-Based Modeling**
Maximum-Order Complexity (MOC)	$MOC_{\text{SS}} = \underbrace{1\cdot(17m-2)}_{\text{VP: state variables}} + \underbrace{0\cdot(17m-2)}_{\text{MP: state matrix}} = 17m-2$	$MOC_{\text{Imp}} = \underbrace{11\cdot m}_{\text{VP: } m \text{ Converters}} + \underbrace{1\cdot 2m}_{\text{MP: } 2m\times 2m\ \boldsymbol{Y}_{\text{MG}} \text{ Network of lines and loads}} = 13m$ $MOC_{Imp,\,\text{single}} = 8m$
Apparent-Order Complexity (AOC)	$AOC_{\text{SS}} = \underbrace{1\cdot(17m-2)}_{\text{VP: state variables}} + \underbrace{0\cdot(17m-2)^2}_{\text{MP: state matrix}} = 17m-2$	$AOC_{\text{Imp}} = \underbrace{11\cdot m}_{\text{VP: } m \text{ Converters}} + \underbrace{1\cdot(2m)^2}_{\text{MP: } 2m\times 2m\ \boldsymbol{Y}_{\text{MG}} \text{ Network of lines and loads}} = 4m^2+11m$ $AOC_{\text{Imp, single}} = m^2+7m$

Note: m denotes the number of converters in the system.
Source: [J1].

2.3.2. Comparison and Mapping of Stability Modeling in Microgrids

The AOCs of different modeling methods are plotted in Fig. 2.10 (a). In addition to the approaches shown in Table 2.4, the method proposed in [30] is also included, in which the microgrid system is partitioned into a source part (voltage source with impedance Z_g in series) and a load part (current source with impedance Z_0 in parallel), and the Nyquist criteria is applied to Z_g/Z_0. It is carried out under the *single-axis* condition.

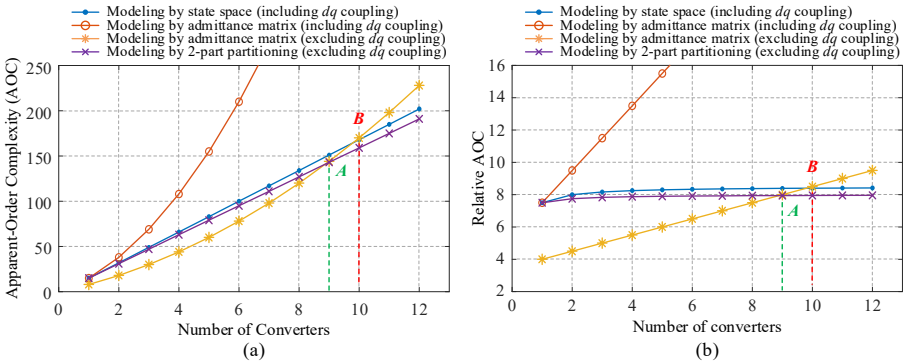

Fig. 2.10: Comparison of (a) Apparent-Order Complexity (AOC) and (b) relative AOC with respect to the number of converters. The base value for relative AOC is $2m$. Source: [J1].

As the number of converters (nodes) increase, the difference among the modeling methods can be observed intuitively, and the recommended application regions of the modeling methods can be specified by the intersection points of the curves, in terms of complexity. From the comparison, state-space-based methods are essentially more suitable for larger-scale systems, but techniques like zero-pole cancellation or model-order reduction in [105] and [106] may in turn help to reduce the complexity of the modeling methods.

The AOC can be normalized into *relative* AOC as Fig. 2.10 (b). The base value of AOC can be defined as the number of independent state variables, or the *freedom* of the state variables. In the exemplary case, the base value is $2m$ given that all converter voltages and currents are observed. In comparison with the AOC, the relative AOC provides a clearer delineation of the boundaries between modeling methods, and more notably, its increasing rate can quantitatively reflect the scalability of the modeling methods.

Furthermore, the modeling methods can also be mapped by applications with varied accuracy, and an example is depicted in Fig. 2.11 [C1], [J1]. The frequencies of interest can be another dimension independent from the size of systems. The

mapping relationship is not unique in general cases, but it could offer practical options for optimizing the selection of modeling methods at system level.

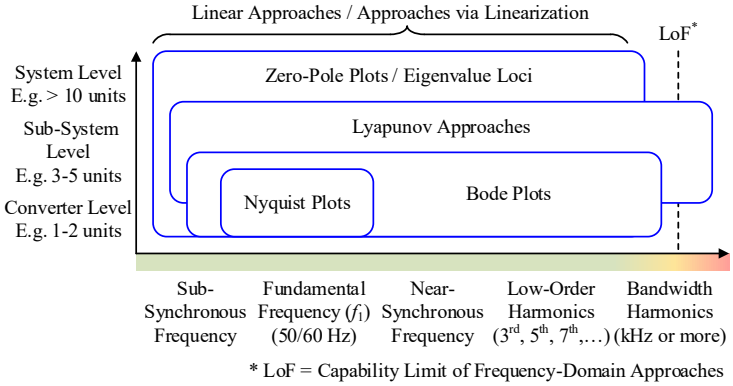

Fig. 2.11: Mapping of stability modeling for microgrids by applications. Source: [J1].

2.3.3. Case Study on the Validation of Microgrid Stability

A study case is presented in [J1] to demonstrate the stability validation. The case is designed based on the platform introduced in Section 1.6, which is shown in Fig. 2.12, and the *dq* decoupling used in the current controller of Fig. 2.2 is analyzed to identify the modeling methods. Several parameters are specified differently from Table 1.2, including: $L_{f1} = L_{f2} = L_{l2} = 1.5$ mH and $R_{load} = 57.5$ Ω, and the load is considered as locally connected to Converter 1 by neglecting Line 1.

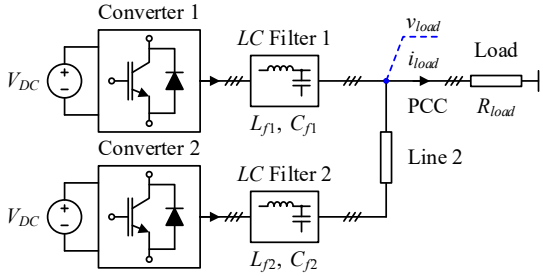

Fig. 2.12: Architecture of the study case for stability validation. Source: [J1].

Based on Sections 2.3.1 and 2.3.2, the complexity is evaluated as $AOC_{SS} = 26$ and $AOC_{Imp} = 38$. Since the eigenvalue loci are capable of characterizing harmonic stability, the state-space-based modeling in *dq* frame is accordingly adopted, and the system can be modeled into the state space equations as following [27]:

$$\frac{\mathrm{d}}{\mathrm{d}t}\begin{bmatrix}\Delta\boldsymbol{x}_{\mathrm{conv}}\\ \Delta\boldsymbol{i}_{\mathrm{line}}\\ \Delta\boldsymbol{i}_{\mathrm{load}}\end{bmatrix} = \boldsymbol{A}_{\mathrm{MG}}\begin{bmatrix}\Delta\boldsymbol{x}_{\mathrm{conv}}\\ \Delta\boldsymbol{i}_{\mathrm{line}}\\ \Delta\boldsymbol{i}_{\mathrm{load}}\end{bmatrix} \tag{2.5}$$

where the state vector is:

$$\Delta \boldsymbol{x}_{\text{conv}} = \begin{bmatrix} \Delta \boldsymbol{x}_{\text{conv, 1}} \\ \Delta \boldsymbol{x}_{\text{conv, 2}} \end{bmatrix} \tag{2.6}$$

$$\Delta \boldsymbol{x}_{\text{conv},k,dq} = \Delta \begin{bmatrix} \delta_k & P_k & Q_k & E_{v,k,dq} & E_{i,k,dq} & i_{s,k,dq} & v_{o,k,dq} & i_{o,k,dq} \end{bmatrix}^T \tag{2.7}$$

where, δ is the phase angle with regard to the rotational dq frame, and E_v, E_i are the time-domain integrals of the control errors of v_o and i_s, respectively.

The modeling and test results are compared in Fig. 2.13. The eigenvalue loci in Fig. 2.13 (a) theoretically indicate that the coupling between the dq components affects the system stability, resulting in a resonance frequency around 3512 rad/s in the unstable case. It is confirmed by the experimental waveforms in Fig. 2.13 (b) and (c), where the system becomes unstable when the dq decoupling is disabled, with the presence of harmonics at around 550 Hz (11 cycles per fundamental period).

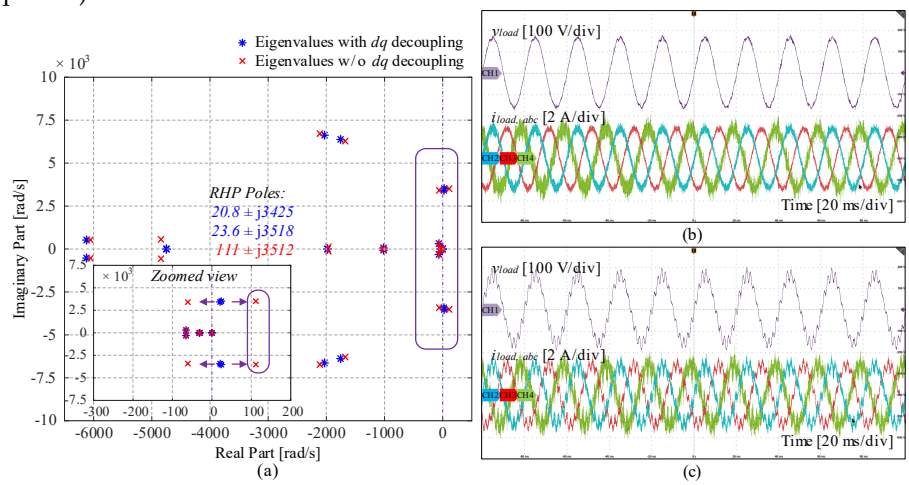

Fig. 2.13: Modeling and experimental results of the case study in Fig. 2.12, including: (a) the eigenvalue loci of the system in terms of the dq decoupling in the current loop, (b) voltage and current waveforms with dq decoupling, and (c) voltage and current waveforms without dq decoupling. Control parameters: $K_{pv} = 0.04$, $K_{iv} = 168$, $K_{pc} = 10.5$, $K_{ic} = 16000$. Source: [J1].

Through this case, the proposed metrics on the modeling complexity have been verified, and the mapping of stability modeling turns out to be feasible. Similar procedures can be applied for microgrids with larger size or higher penetration of RES, where more significant differences can be concluded among the discussed modeling methods.

Besides, this section has also laid a theoretical basis for using the state-space-based modeling to characterize the system-level stability of multi-converter microgrids, which is generally employed in the remaining parts of this thesis.

2.4. Model-Aggregated Emulation of Converters for Stability Validation

To facilitate the stability validation, real-time tests are generally essential. As power-electronics-based emulation is widely used to mimic the behaviors of loads and grids [101], it has provided the possibility of reducing the complexity of the system under test by aggregating multiple converters into clusters. For microgrid systems, it is also appealing to include the heterogeneous dynamics of DERs that also contribute to system stability.

The basic idea is illustrated in Fig. 2.14. The renewable generations (RGs) are considered as source with dynamics and impedances, and the emulation rule is accordingly formed as control references. If the variables are defined as labeled, then the following relationships hold:

$$\begin{cases} v_1 - v_{\text{bus}} = i_1 Z_{\text{line1}} \\ v_2 - v_{\text{bus}} = i_2 Z_{\text{line2}} \end{cases} \tag{2.8}$$

$$i_{\text{bus}} = i_1 + i_2 = \left(\frac{v_1}{Z_{\text{line1}}} + \frac{v_2}{Z_{\text{line2}}} \right) - v_{\text{bus}} \left(\frac{1}{Z_{\text{line1}}} + \frac{1}{Z_{\text{line2}}} \right) \tag{2.9}$$

The bus is thereby equivalent to a cluster with the impedance $Z_{bus} = v_{bus} / i_{bus}$.

With this, the behavior of the entire bus can be emulated without much loss of fidelity, by plotting the *V*-*I* relationships in *X*-*Y* planes, constructing small-signal state spaces or equivalent transfer functions. Concerning the control references of the converters that are determined by the dynamics of the RGs, three cases are exemplified to demonstrate this scheme:

(1) Buses only consisting of grid-forming converters (voltage as variable under control, or voltage-source converters), where:

$$v_j = V_j^* G_j(s), \ j = 1, \ 2 \tag{2.10}$$

(2) Buses only consisting of grid-following converters (current as variable under control, or current-source converters), where:

$$i_j = I_j^* G_j(s), \ j = 1, \ 2 \tag{2.11}$$

(3) Buses consisting of both grid-forming and grid-following converters.

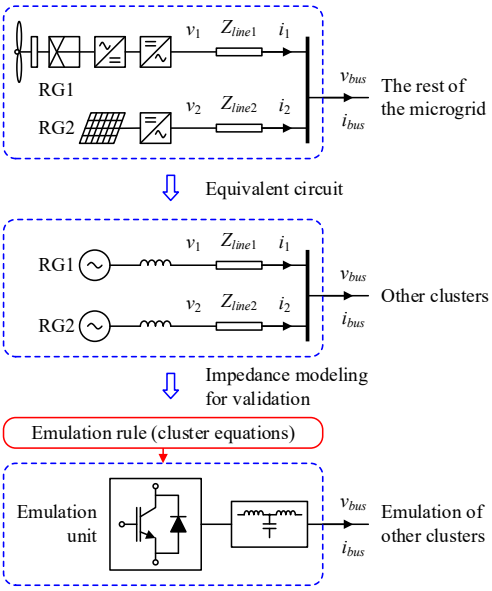

Fig. 2.14: Aggregated modeling and emulation of a multi-converter bus with renewable generations (RGs). Source: [C3].

The cases are validated by real-time simulations on an OPAL-RT platform as mentioned in Section 1.6, where the dynamics G_j are modeled as first-order delays with cut-off frequencies f_{c1} = 5 Hz and f_{c2} = 2 Hz. The step size of real-time simulation is 10 μs with switching-frequency averaging.

A. Emulation of Grid-Forming Buses

For grid-forming converters, the voltage at PCC is controlled, implying that the converters function as voltage sources. The architecture of the example is specified in Fig. 2.15 (a), where the references V_1* and V_2* are intentionally set equal to prevent synchronization instability. The emulation unit should operate in the same mode, adhering to the following *V-I* relationship that designates the voltage reference:

$$v_{\text{bus}} = \frac{V_1^* G_1 Z_{\text{line2}} + V_2^* G_2 Z_{\text{line1}}}{Z_{\text{line1}} + Z_{\text{line2}}} - i_{\text{bus}} \frac{Z_{\text{line1}} Z_{\text{line2}}}{Z_{\text{line1}} + Z_{\text{line2}}} \tag{2.11}$$

With this, the emulation unit is controlled as Fig. 2.15 (b), and the corresponding performances are presented in Fig. 2.16. The dynamics of the two converters in Fig. 2.15 (a) are merged while an appropriate level of accuracy is maintained in the overall behaviors. However, it should be noted that inaccuracies can be introduced by the impedance $Z_{line1}Z_{line2}/Z$, which essentially involves a

differential calculation and is sensitive to noise. To mitigate this issue, anti-noise filters can be employed together with discretization in a relatively lower bandwidth, which is a tradeoff between system robustness and the emulation fidelity during transients.

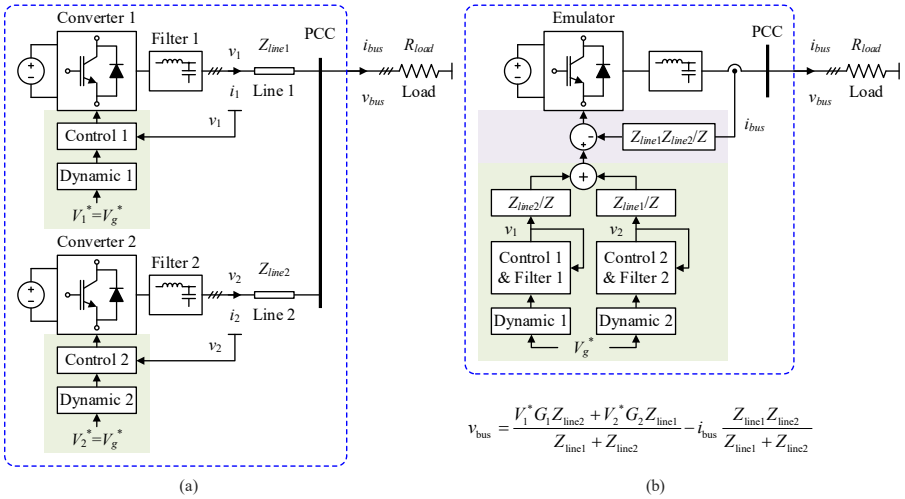

$$v_{bus} = \frac{V_1^* G_1 Z_{line2} + V_2^* G_2 Z_{line1}}{Z_{line1} + Z_{line2}} - i_{bus} \frac{Z_{line1} Z_{line2}}{Z_{line1} + Z_{line2}}$$

Fig. 2.15: A solution for emulating a grid-forming bus, including: (a) architecture of the example, and (b) proposed emulation scheme. Source: [C3].

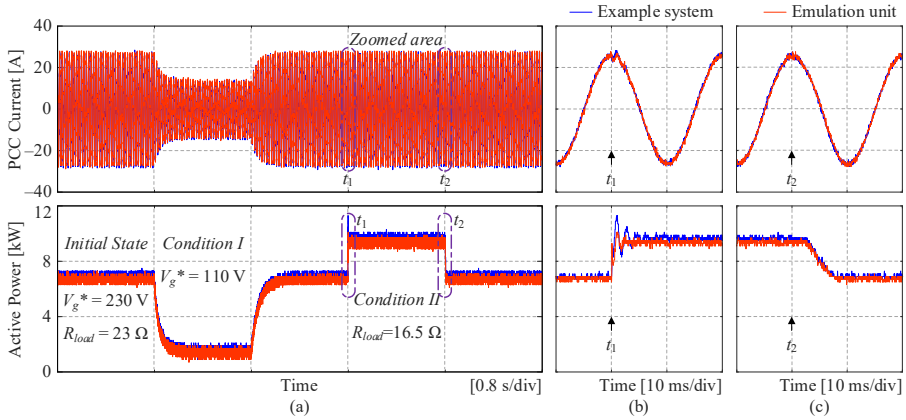

Fig. 2.16: The performance of the aggregation scheme in Fig. 2.15 by real-time simulations, including: (a) the current at PCC, (b) zoomed view around time t_1, and (c) zoomed view around time t_2. Source: [C3].

B. Emulation of Grid-Following Buses

On the other hand, grid-following converters operate as current sources or loads. Considering the grid-following bus in Fig. 2.17 (a), the currents of Converters 1 and 2 both flow into the PCC. If the currents in capacitor branches

of the *LCL* Filters 1 and 2 are neglected, then the following current reference can be obtained as governed by the Kirchhoff's current law:

$$i_{\text{bus}} = i_1 + i_2 = I_1^* G_1 + I_2^* G_2 \tag{2.12}$$

Therefore, the solution can be formed as shown in Fig. 2.17 (b), with the total current being the control reference. Its performance is demonstrated in Fig. 2.18.

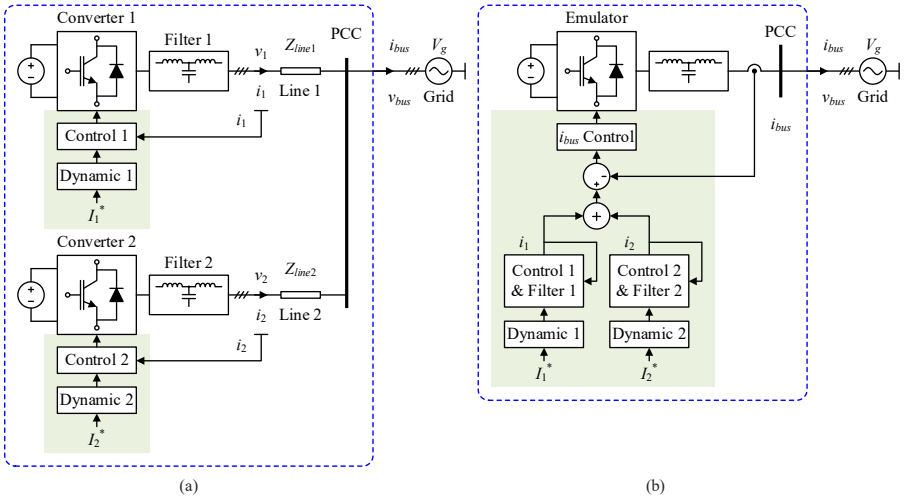

Fig. 2.17: A solution for emulating a grid-following bus, including: (a) architecture of the example, and (b) proposed emulation scheme. Source: [C3].

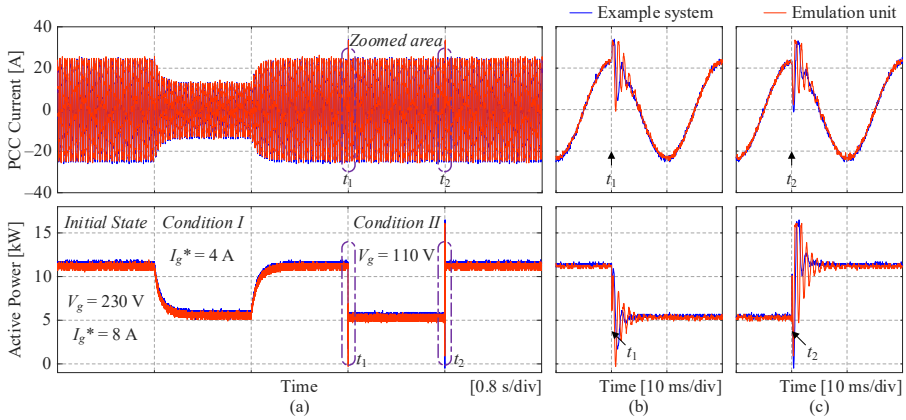

Fig. 2.18: The performance of the aggregation scheme in Fig. 2.17 by real-time simulations, including: (a) the current at PCC, (b) zoomed view around time t_1, and (c) zoomed view around time t_2. Source: [C3].

In this case, the accuracy may be affected by the current control loop of i_{bus}, which resembles the philosophy presented in [107]. To address such inconsistency in dynamics, a first-order proportional-differential (PD) regulator can be utilized for compensation. Moreover, it is also necessary to examine the damping of the filter in the emulation unit for stability validation to avoid unexpected unstable modes.

C. Emulation of Hybrid Buses

When both grid-forming and grid-following converters are involved, the bus behaves similarly to a grid-forming bus that shapes the voltage at PCC. To attain the voltage reference, (2.9) is formed into:

$$v_{\text{bus}} = v_1 - (i_{\text{bus}} - i_2) Z_{\text{line1}} = V_1^* G_1 - (i_{\text{bus}} - I_2^* G_2) Z_{\text{line1}} \tag{2.13}$$

which is expanded into the control scheme in Fig. 2.19.

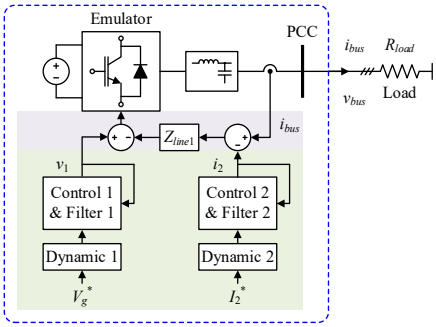

Fig. 2.19: A solution for emulating a hybrid bus involving both grid-forming and grid-following converters. Source: [C3].

2.5. Summary

In this chapter, the stability of microgrids has been extensively investigated with the focus on its definition, modeling and validation methodologies. The inherent features of microgrids give rise to miscellaneous unstable modes, which have been manifested in the CIGRE LV benchmark system. By narrowing the scope of this project down to small-signal dynamic stability, different modeling methods are intuitively compared using quantitative metrics. Accordingly, a case study is performed to illustrate the stability validation of a microgrid system. The selected state-space-based modeling sets the stage for the methodologies to be employed in subsequent sections. In terms of real-time tests, the emulation of multi-converter buses has been tested, thus offering more possibilities for stability validation methodologies in general microgrid systems.

Related Publications:

- **Section 2.2:**

[C2] **Y. Song**, S. Sahoo, Y. Yang, and F. Blaabjerg, "System-Level Stability of the CIGRE Low Voltage Benchmark System: Definitions and Extrapolations," in *Proc. 2021 IEEE COMPEL*, Cartagena, Colombia, Nov. 2021, pp. 1-6. doi: 10.1109/COMPEL52922.2021.9645971.

- **Section 2.3:**

[C1] **Y. Song**, S. Sahoo, Y. Yang, and F. Blaabjerg, "System-Level Mapping of Modeling Methods for Stability Characterization in Microgrids," in *Proc. 2021 IEEE ECCE*, Vancouver, BC, Canada, Oct. 2021, pp. 2943-2949. doi: 10.1109/ECCE47101.2021.9594979.

[J1] **Y. Song**, S. Sahoo, Y. Yang, and F. Blaabjerg, "Quantitative Mapping of Modeling Methods for Stability Validation in Microgrids," *IEEE Open J. Power Electron.*, vol. 3, pp. 679-688, Oct. 2022. doi: 10.1109/OJPEL.2022.3214200.

- **Section 2.4:**

[C3] **Y. Song**, S. Sahoo, Y. Yang, F. Blaabjerg, and Y. W. Li, "Aggregated Emulation of Multiple Converters with Heterogeneous Dynamics in Low-Voltage Microgrids – A Clustering Approach," in *Proc. 2022 IEEE ECCE*, Detroit, MI, USA, Oct. 2022, pp. 1-5. doi: 10.1109/ECCE50734.2022.9948214.

Chapter 3

Microgrid Reliability: System-Level Enhancement and Validation

3.1. Background

In addition to stability discussed in *Chapter 2*, the reliability of microgrid systems serves as the second basis of this Ph.D. project. In contrast to stability, microgrid reliability is defined upon system functionability over a certain period of time [51]-[53], as mentioned in Section 1.1.3. As such, the evaluation on system reliability is normally performed in longer timescales. The reliability of a PEPS or microgrid can be measured either by cost-related (such as LOLE and EENS) or PoF-based metrics (such as the probability of reliability and lifetime), and the latter is applied in this thesis. In this chapter, reliability modeling in microgrids will firstly be elaborated from component level to system level [79]-[83], establishing a theoretical foundation for the reliability analysis in this thesis.

With the reliability models, methodologies have been developed for enhancing the reliability of power electronics systems, among which the tailoring of controllers turns out favorable at converter and system level, namely the reliability-oriented control. In a microgrid system, it may be implemented via primary controllers, single-node operation points, or coordination among multiple nodes. However, to ensure a better compliance with more general scenarios, specific guidelines are still desirable. As a typical example, the reliability-oriented power sharing [93], [94] is studied in this Ph.D. project. The underlying principle is to balance the lifetime among converters, yet existing methods like [94] may prompt an exception under load fluctuations. To this end, the pros and cons of reliability-oriented power sharing are manifested in this chapter. A conditional droop adjustment strategy is proposed to form an improved power sharing framework [J2], implying more practical solutions for achieving higher reliability in microgrids.

Another focus of this chapter is to explore the validation of microgrid reliability from the perspective of real-time tests. Considering the power semiconductors emphasized in Section 1.1.3, the junction temperature plays a vital role in the degradation and thereby system reliability. However, thermal

measurement normally involves advanced and costly facilities in practice, showing much inconvenience to be accommodated to miscellaneous applications. Concerning the real-time testing platforms like OPAL-RT and dSPACE, the simulation of switching transients is still a must in the literature [108]-[110], requiring considerably high sampling rate. Hence, inspired by [108]-[112], a simplified approach is introduced in this chapter for real-time thermal evaluation of power converters using fundamental-frequency AC currents [C4]. The demand for a high sampling rate is alleviated, and real-time thermal evaluation is thereby enabled for more testing scenarios.

3.2. Lifetime and Reliability Modeling of Microgrid Systems

High system-level reliability necessitates the proper functioning of a certain number of components in the system for desired timespan. In PoF-based reliability analysis, systems are first decomposed into individual components to better understand their failure mechanisms. It has been underlined in Section 1.1.3 that power semiconductors and capacitors are among the most fragile components in power electronics systems. Hence, this section is aimed at elucidating the reliability modeling of microgrid systems based on the lifetime models of power semiconductors and capacitors, which are further adopted in [J2], [J3] and [J4].

One of the most frequently-used lifetime models for power semiconductors is described in [113]. The lifetime of power semiconductors is measured by the number of thermal cycles that they can withstand before a failure occurs. It is determined by the average junction temperature (T_{jm}) and the junction temperature swing (ΔT_j) in each thermal cycle:

$$N_{\mathrm{f}} = A \cdot \Delta T_{\mathrm{j}}^{\alpha} \cdot \exp\left(\frac{\beta_1}{T_{\mathrm{jm}}}\right) \cdot {t_{\mathrm{on}}}^{\gamma} \tag{3.1}$$

where, A, a, β_1 and γ are the coefficients that are dependent on the type of converters, which can be acquired through power-cycling tests like [100].

> **Remark 3.2.1:**
> It is noted in [114] that the accuracy of this model is limited when ΔT_j is small, whereas this will not undermine the validity of using this model in this thesis.

The damage of power devices accumulates over time as described by the Miner's rule [115], which is the sum of normalized consumed lifetime from the initial state:

$$D_{\mathrm{sw}} = \sum_{i} \frac{n^{(i)}}{N_{\mathrm{f}}{}^{(i)}} \tag{3.2}$$

where, in terms of the i-th time interval, $n^{(i)}$ and $N_f{}^{(i)}$ are the number of counted power cycles and corresponding rated cycles-to-failure, respectively. If multiple thermal cycle patterns are involved, $n^{(i)}$ is obtained by rainflow counting. The accumulated damage should be 1 when a device is expected to reach its end-of-life (EOL).

The lifetime of capacitors is defined based on the rated voltage and temperature operating condition (V_0, T_0) and the corresponding lifetime L_0, while actual operating condition (V, T) will influence the lifetime L as following [69]:

$$L = L_0 \cdot 2^{\frac{T_0 - T}{n_1}} \cdot \left(\frac{V}{V_0} \right)^{-n_2} \tag{3.3}$$

where, n_1 and n_2 are constant coefficients subject to the type of capacitors.

Likewise, the damage accumulation of capacitors also follows the Miner's rule:

$$D_{\mathrm{cap}} = \sum_{i} \frac{\Delta t^{(i)}}{L^{(i)}} \tag{3.4}$$

where the duration of the i-th time interval $\Delta t^{(i)}$ is normalized by the corresponding lifetime $L^{(i)}$.

For power semiconductors and capacitors, the obtained time-to-failure data both follow Weibull distribution in terms of time. Consequently, the probability of reliability can be formulated as the Cumulative Density Function (CDF) of Weibull distribution, given as:

$$R(t) = \exp\left[-\left(\frac{t}{\eta} \right)^{\beta} \right] \tag{3.5}$$

where, β is the shaping parameter, and η denotes the characteristic lifetime of the component. The lifetime estimated by (3.2) and (3.4) principally stands for the B_{10} lifetime, which implies that 10% of the device population is expected to fail, corresponding to the time t when $R(t)$ in (3.5) equals 90%.

The reliability block diagram can be plotted as a visual representation of the functional relationship among components [78]. For a power electronics converter, assuming that there are no parallel paths in its reliability block diagram, i.e., it is designed with no redundancy, then its reliability R_{conv} is the product of the reliability of all components within it:

$$R_{\text{conv}} = \prod_{j} R_{\text{sw or cap}}^{(j)} \tag{3.6}$$

And the accumulated damage of a converter can be taken as the averaged damage of the considered M components in the converter [92]:

$$D_{\text{conv}} = \frac{1}{M}\sum_{j=1}^{M} D_{\text{sw or cap}}^{(j)} \tag{3.7}$$

In a microgrid system, assuming that other parts exhibit sufficient reliability, and no converters are equipped as redundancy, the overall system-level reliability can be formulated in the same approach:

$$R_{\text{MG}} = \prod_{j} R_{\text{conv}}^{(j)} \tag{3.8}$$

where, the B_{10} lifetime of the system can also be concluded by identifying the time t when R_{MG} = 90%.

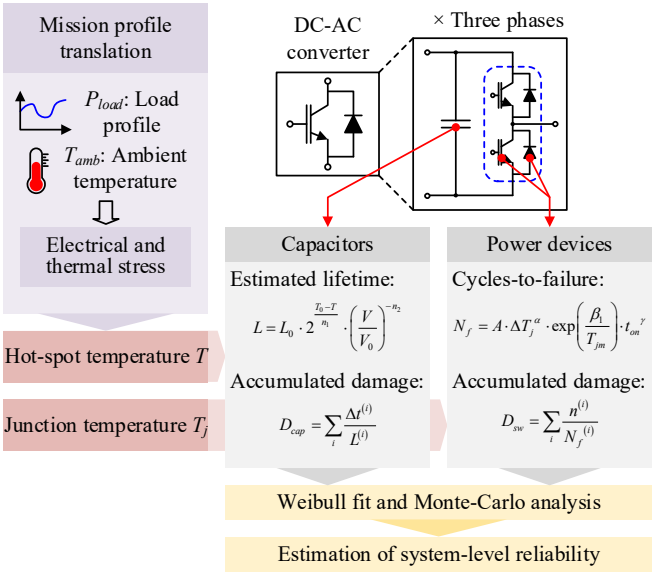

Fig. 3.1: Reliability Evaluation of a three-phase DC-AC converter system. Source: [J2], [J3] and [J4].

The entire procedure is summarized in Fig. 3.1. Through PoF-based reliability analysis, the significance of mission profiles can be effectively emphasized, indicating more accurate evaluation of long-term system performance. In particular, when accounting for the uncertainty of component parameters, the

Monte-Carlo method can typically be employed to statistically estimate the system-level reliability.

3.3. Reliability-Oriented Power Sharing in Microgrids

The lifetime model of power electronics components and systems in Section 3.2 has been incorporated into reliability-oriented power sharing like [81], [82], where the loadings of converters are redistributed for balancing the stresses. For a microgrid system, the probabilistic reliability is dominated by the converter with the least available lifetime, and it thereby becomes essential to ensure that the degradation rates of converters in the system are aligned, allowing for an optimized overall lifetime. Hence, an operation principle is formed as: *converters having consumed more lifetime should share less loading* [92], [93], [J2], [J3].

Therefore, a reliability-oriented power sharing strategy is given in [81] and [82] based on the lifetime model in Section 3.2. For an AC microgrid controlled by droop controllers as specified in (1.1), it is practical to redistribute the loadings by adjusting the droop gains of the converters as:

$$m_p = m_{p0} \cdot \left[\alpha + (1-\alpha) \cdot \left(\frac{D_i}{D_0} \right)^{\lambda} \right] \tag{3.9}$$

where, $0 \le a \le 1$ is a weighting factor to incorporate reliability consideration into the droop characteristic, and $\lambda > 0$ stands for the rate of reliability metrics shaping the droop gain. D_0 denotes the reference value of the accumulated damage of converters in the microgrid system, which is specifically D_i for the i-th converter.

> **Remark 3.2.2:**
> In [92] and [93], the accumulated damage D formulated in (3.7) is considered as the reliability metric incorporated into droop control. Alternatively, other reliability metrics like the probabilistic reliability/unreliability, indirect indicators like junction temperatures [91], or cost-related indicators used in [90] can similarly serve as the optimization targets. Nevertheless, the underlying principles essentially remain similar.

Yet this strategy specified in (3.9) can be inadequate when confronted with load fluctuations. With $1-a \ge 0$, a higher value of D_i will consistently lead to a larger droop gain m_p. This one-way adjustment can potentially contradict the objective of achieving higher reliability when the power deviation ($P-P_0$) in (1.1) crosses zero, especially e.g., when P_0 is updated by higher-level system operators.

In order to address this concern and improve the generality of reliability-oriented power sharing, a two-conditional droop adjustment is thereby derived in [J2]. The two-converter system in Fig. 3.2 is selected as an example, which is configured based on Fig. 1.10 and Table 1.2.

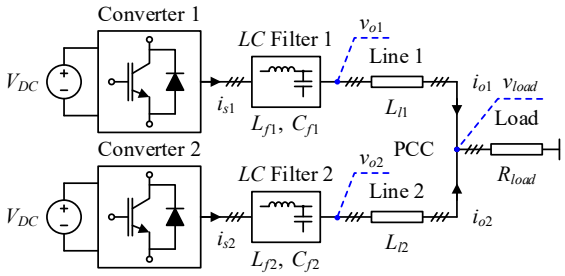

Fig. 3.2: Architecture of the study case for conditional droop adjustment. Source: [J2].

The initial droop gain of both converters is assumed to be m_{p0} and the nominal operation point (P_0, f_0). The following equation should hold in that $f_1 = f_2$ when the system reaches steady state:

$$\Delta f = m_{p1}\left(P_1 - P_0\right) = m_{p2}\left(P_2 - P_0\right) \Rightarrow \frac{m_{p1}}{m_{p2}} = \frac{P_2 - P_0}{P_1 - P_0} \tag{3.10}$$

If the accumulated damage of Converter 1 is higher, or $D_1 \geq D_2$, then the power sharing should be $P_1 \leq P_2$. Three operating conditions could be concluded based on Fig. 3.3:

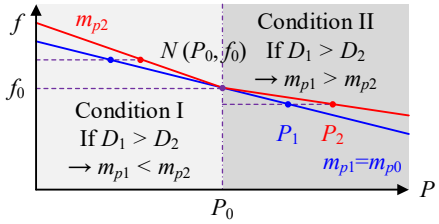

Fig. 3.3: Illustration of the conditions for droop adjustment. Source: [J2].

(a) Condition I: If $P_1 \leq P_2 < P_0$: $P_1 - P_0 \leq P_2 - P_0 < 0$, then

$$\frac{P_2 - P_0}{P_1 - P_0} \leq 1 \Rightarrow m_{p2} \geq m_{p1} > 0 \tag{3.11}$$

When the operation point of a converter locates below its nominal power, *smaller droop gain corresponds to less loading*.

(b) Condition II: If $P_0 < P_1 \leq P_2$: $P_2 - P_0 \geq P_1 - P_0 > 0$, then

$$\frac{P_2 - P_0}{P_1 - P_0} \geq 1 \Rightarrow m_{p1} \geq m_{p2} > 0 \tag{3.12}$$

When the operation point of a converter locates above its nominal power, *larger droop gain corresponds to less loading*.

(c) Condition III: If $P_1 \leq P_0 \leq P_2$, then the only equilibrium operation point is $P_1 = P_0 = P_2$ to maintain the alignment in frequencies.

In normal cases, the droop gain should be adjusted subject to Conditions I or II, and the rules for droop gain adjustment are accordingly formulated as:

$$m_p = m_{p0} \cdot \left[\alpha + (1-\alpha) \cdot \beta_m^{\lambda} \right] \tag{3.13}$$

where, β_m is the adjustment coefficient for the active droop gain m_p indicating the consideration of accumulated damages. The adjustment strategies are exemplified in Table 3.1 [J2]. The droop gains can be updated with the same frequency as the tertiary power commands.

TABLE 3.1: ALTERNATIVE STRATEGIES FOR ACTIVE DROOP GAIN ADJUSTMENT BASED ON THE PROPOSED TWO-CONDITIONAL PRINCIPLE

Strategies of Active Power Droop Adjustment	**Value of β_m under Condition I**	**Value of β_m under Condition II**
Proportional Adjustment	$\beta_{m,\mathrm{I}} = \frac{D_0}{D_i}$	$\beta_{m,\mathrm{II}} = \frac{D_i}{D_0}$
Complementary Adjustment	$\beta_{m,\mathrm{I}} = 1 - D_i$	$\beta_{m,\mathrm{II}} = D_i$
Composite Adjustment	$\beta_{m,\mathrm{I}} = \frac{1 - D_i}{1 - D_0}$	$\beta_{m,\mathrm{II}} = \frac{1 - D_0}{1 - D_i}$

Source: [J2].

Accordingly, the following tests have been carried out to showcase the proposed strategy, covering short-term experimental tests and long-term simulations.

A. Experimental Tests on Short-Term Performance

The experiments are conducted on the platform shown in Fig. 1.10 and configured as specified in Table 1.2. The rated load power is set at 1.38 kW (28.75 Ω per phase), thus requiring each converter to initially share 0.69 kW. By assuming the normalized accumulated damages of the two converters as $D_1 = D_0$ and $D_2 = 0.6\ D_0$, respectively, the shown tests are designed into four stages, where an

increase in P_0 leads to a change in the conditions as specified in Fig. 3.3. The proportional droop adjustment strategy in Table 3.1 is employed, with $a = 0$ and $\lambda = 1$. The results are shown in Fig. 3.4.

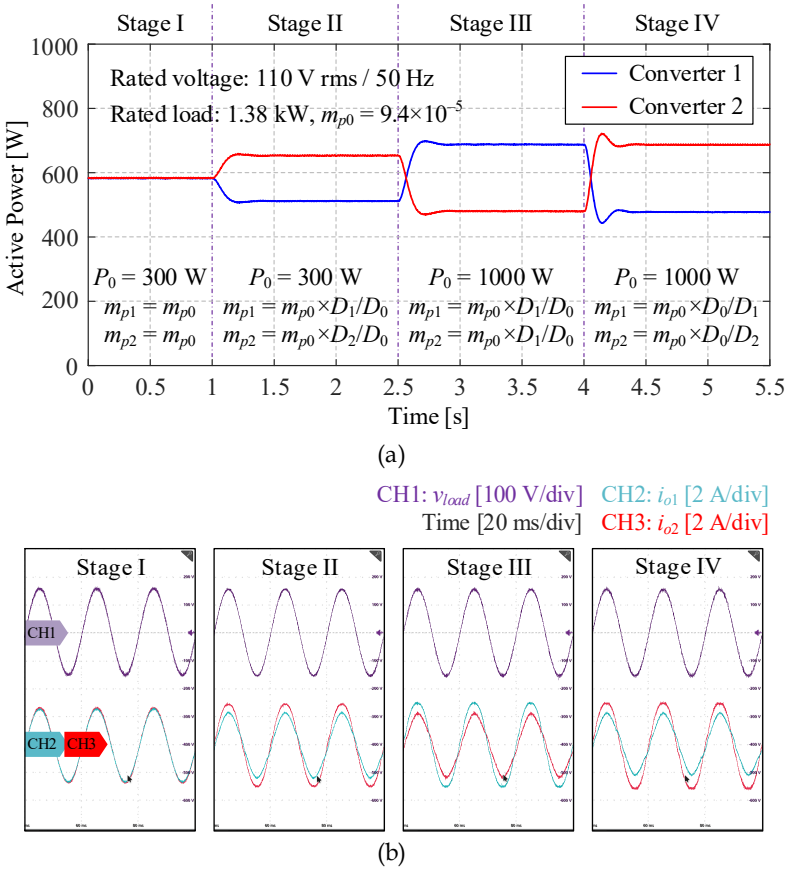

Fig. 3.4: Experimental results demonstrating the two-conditional strategy, including: (a) the active powers of the two converters, and (b) the load voltage v_{load} and output currents i_{o1} & i_{o2}. Source: [J2].

In Stage II where both P_1 and P_2 are higher than P_0, Converter 1 is assigned with less loading given $D_1 > D_2$, but in Stage III, the load-sharing relationship undergoes a reversal when P_0 goes above P_1 and P_2, namely the Condition I. In order to address the reliability consideration in such scenarios, the proposed strategy is thereby employed, which can accordingly accommodate the tertiary update of the nominal operation points as planned.

B. Validation on Long-Term Performance

The long-term tests involve simulations and corresponding reliability analysis on the system shown in Fig. 3.5. The key parameters are listed in Table 3.2, and the rated active powers of Converters 1 & 2 are set to be changed by month. The droop gains are updated monthly by the proportional adjustment strategy with a = 0.5 and λ = 1. The accumulated damages of all components are assumed to be zero in the beginning.

TABLE 3.2: KEY PARAMETERS OF THE STUDY CASE FOR LONG-TERM EVALUATION

Parameters	Values
Type of the power devices	Infineon FS100R12KT3 (1200 V/100 A) for Conv. 1 FS25R12KT3 (1200 V/25 A) for Conv. 2, 3, 4, 5
Initial active droop gain m_{p0}	1.9×10^{-5} [Hz/W] for Conv. 1, 2, 3, 5 9.5×10^{-6} [Hz/W] for Conv. 4
Power cycling period t_{on}	0.01 s
Number of cycles per month	(24×60×60×30) ×50

Source: [J2].

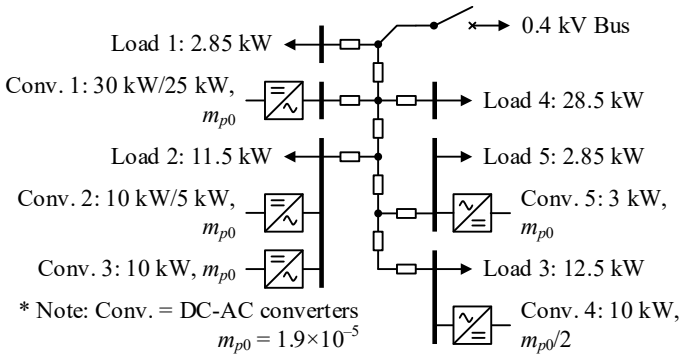

Fig. 3.5: Exemplary system for long-term reliability evaluation based on the CIGRE LV benchmark system. It operates in islanded mode. Source: [J2].

By comparing the proposed two-conditional strategy with conventional single-way adjustment, the system performances over a period of 12 months are depicted in Fig. 3.6 (a), and the analysis is further extended to the EOL of the system in Fig.3.6 (b). In Fig. 3.6 (a), the load sharing in the 2nd, 4th, … months corresponds to Condition II in Fig. 3.3, where both methods can reduce the loading of the studied Converter 1 as intended. On the other hand, in the remaining months when the system falls into Condition I, only the proposed strategy can yield higher system-level reliability. This conclusion is further

substantiated in Fig. 3.6 (b), where the B_{10} lifetime of the system is prolonged by approximately 10%, highlighting the effectiveness of the proposed two-conditional strategy.

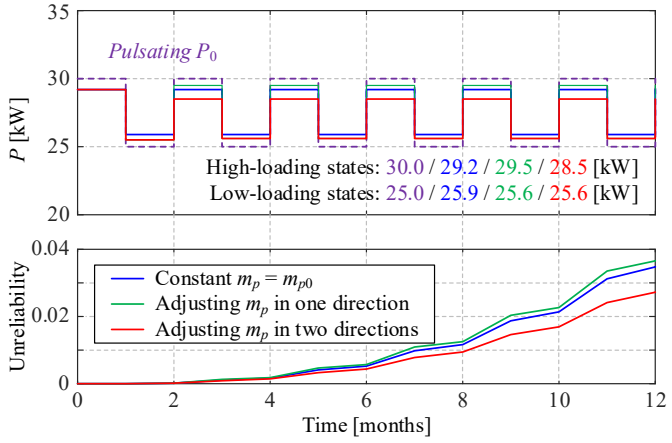

(a)

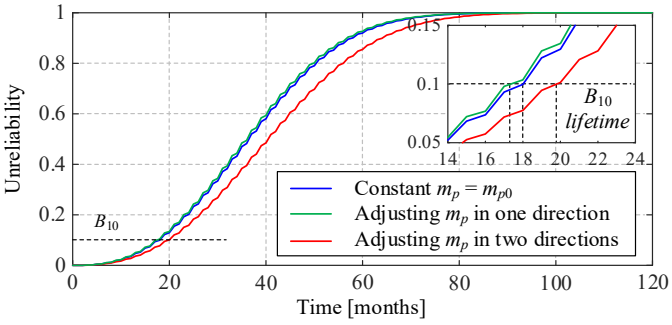

(b)

Fig. 3.6: Comparison of the performances of different droop adjustment policies, including: (a) the loading of Converter 1 in Fig. 3.5 when its rated active power is changed between 30 kW and 25 kW by month, and (b) the unreliability curve of the system. Source: [J2].

Nevertheless, it is important to acknowledge that there exists a boundary for droop adjustment, which is determined by the stability of the system. It can be inferred that the stability imposes a constraint on the maximum reliability or lifetime that can be achieved in the system, which will be further elaborated in *Chapter 4*.

3.4. Real-Time Thermal Simulation for Reliability Validation

The methodologies for reliability validation have also been explored as possible manners to test the strategies proposed in previous sections. In real-time reliability tests of power electronics systems, the observation of thermal performances is critical, but acquiring the junction temperatures using thermal sensors might not always be feasible in practice. On the other hand, there is an appeal in reducing the requirement on computational capability, or sampling frequency, for real-time simulations, as the converters in microgrids are frequently simplified into AC sources by averaging over switching periods, as shown in Fig. 3.7 (a) and (b), and simulating the switching transients will take much computational capability. Consequently, this section aims to present a method to simplify the real-time thermal simulations while maintaining an acceptable level of accuracy especially when applied in complicated systems.

The DC-AC converter in Fig. 3.7 is selected as the study case, which is a three-phase two-level converter consisting of IGBTs (indexed as T_k) and antiparallel diodes (indexed as D_k). The upper and lower legs are denoted by the subscripts H and L, respectively. As per [116], the junction temperature, which are decisive in the lifetime model in Section 3.2, is inherently determined by the current flowing through the device. In light of this, with the comparison between Fig. 3.7 (a) and (b), a rational way to minimizing the sampling frequency is to reconstruct the device current solely by the AC voltage v_o and current i_o.

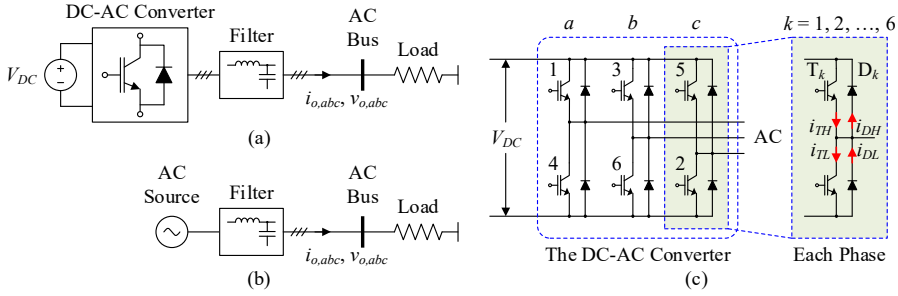

Fig. 3.7: A DC-AC converter in a microgrid, (a) the way it is interfaced by an LC filter, (b) its equivalence as an AC source to be used in real-time simulations, and (c) its detailed internal topology and indices of the power devices. Source: [C4].

The thermal evaluation approach is thereby formalized in Fig. 3.8 [C4]. The entire approach can be decomposed into three major steps:

(1) The reconstruction of device currents,
(2) The calculation of device power dissipations (or losses),
(3) The calculation of the junction temperatures.

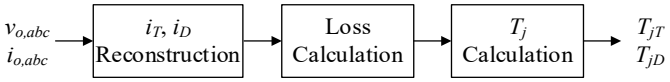

Fig. 3.8: Procedures of the proposed real-time thermal evaluation. Source: [C4].

A. Reconstruction of Device Currents

The reconstruction of the device currents is formed by the Kirchhoff's current law (KCL). As shown in Fig. 3.9, the AC current may flow into or out of a certain phase, while the ON-state devices are different. If the case shown in Fig. 3.9 (b) is defined as $i_o > 0$, then the device currents should satisfy:

$$\begin{cases} i_{TH} + i_{DL} = i_{o,pos} = \begin{cases} |i_o| \text{ if } i_o > 0 \\ 0 \text{ otherwise} \end{cases} \\ i_{TL} + i_{DH} = i_{o,neg} = \begin{cases} |i_o| \text{ if } i_o < 0 \\ 0 \text{ otherwise} \end{cases} \end{cases} \tag{3.14}$$

where, $i_{o,pos}$ and $i_{o,neg}$ are the positive and negative half of i_o, respectively. Since the device current considered for loss calculation is always unidirectional, the absolute value of the AC current i_o is taken to eliminate the influence of its sign.

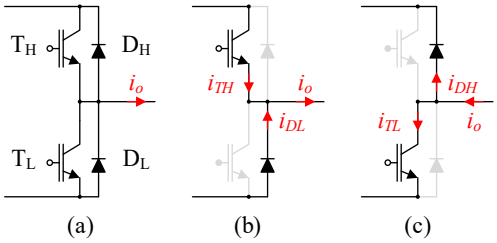

Fig. 3.9: Illustration of the currents through the IGBTs and the diodes, (a) the upper and lower legs of a single phase, (b) when i_o flows out of the phase, and (c) when i_o flows into the leg. Source: [C4].

The current of each device is further derived based on Fig. 3.10, where the relationship between the AC current and the device currents is illustrated.

The ON-state of the IGBT in the upper arm T_H corresponds to the high level of the PWM drive signal, and the diode D_L serves as the freewheeling diode in the complementary situation. Similarly, T_L and D_H operate based on the inverse of the PWM drive signal. By neglecting the OFF-state leakage current, the following equations hold if the currents are averaged over switching periods:

$$\begin{cases} i_{TH} = Di_{o,pos} \\ i_{TL} = \overline{D}i_{o,neg} \end{cases} \tag{3.15}$$

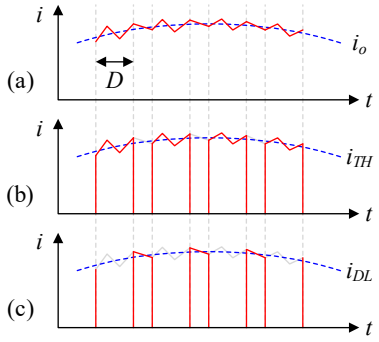

Fig. 3.10: Illustration of the relationship between the AC current and the device currents when $i_o > 0$, (a) the AC output current i_o, (b) the upper IGBT current i_{TH}, and (c) the lower diode current i_{DL}. Source: [C4].

$$\begin{cases} i_{DL} = i_{o,pos} - i_{TH} \\ i_{DH} = i_{o,neg} - i_{TL} \end{cases} \tag{3.16}$$

where, D is the duty cycle, and $\overline{D} = 1–D$ is its complement.

Therefore, the reconstruction of device currents can be obtained as shown in Fig. 3.11. The sampling frequency can be effectively reduced given that only the fundamental-frequency AC voltage v_o and current i_o are sampled.

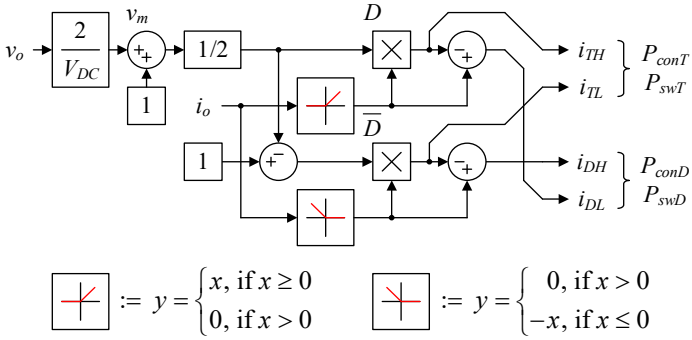

Fig. 3.11: Reconstruction of the device currents using the fundamental-frequency AC voltage v_o and current i_o. Source: [C4].

> **Remark 3.2.3:**
> It should be acknowledged that the current harmonics could also contribute to the power losses of the devices, but the influence could be negligible when the AC current is sinusoidal with low total harmonic distortion (THD) in normal operation.

B. Calculation of Device Power Dissipation

According to [116], the power losses of a power device can be subdivided into conduction loss P_{con} and the switching loss P_{sw}. The two parts can be calculated as following respectively:

(a) The conduction loss is the power dissipation during ON-state, which can be estimated by Joule's law. With the voltage-current (*V-I*) characteristics of the device from the datasheet, the ON-state device voltage drop (v_T or v_D) can be obtained at certain device current (i_T or i_D). The conduction loss P_{con} can thereby be mathematically formulated as the multiplication of the device current and the averaged ON-state voltage by neglecting the current ripples.

$$P_{con} \approx i_T \cdot v_T \tag{3.17}$$

(b) The switching loss is the power dissipation during switching transients. It is normally given by pulsing energy values E_{on} or E_{off} over a single switching action in data sheets. By averaging E_{on} and E_{off} over time, the switching loss can be derived as a power value P_{sw}.

$$P_{sw} = P_{on} + P_{off} = \frac{1}{T_{sw}}\left(E_{on} + E_{off}\right) \tag{3.18}$$

Hence, the estimation of power losses is summarized as shown in Fig. 3.12.

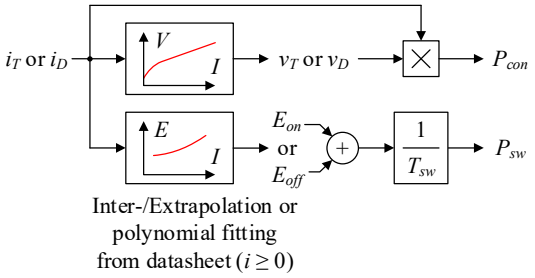

Fig. 3.12: Estimation of power losses using reconstructed device currents. Source: [C4].

> **Remark 3.2.4:**
> The voltage-current (*V-I*) or loss-current (*E-I*) relationships in Fig. 3.11 are normally nonlinear. The relationships can alternatively be fit by constructing look-up tables and using piecewise-linear inter-/extrapolation techniques or by high-order polynomials.

C. Calculation of Junction Temperatures

The junction temperatures can subsequently be estimated by the power losses obtained by Fig. 3.12. The thermal network of power semiconductor modules can be constructed as shown in Fig. 3.13, including the thermal impedances through the junctions, the module case, the heat sink and the ambient. The thermal paths are typically in the form of Cauer or Foster network [72], and the thermal impedance networks exhibits slow dynamics, thus requiring lower sampling rate.

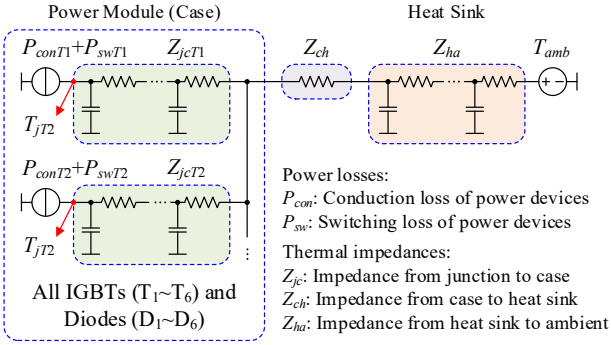

Fig. 3.13: Estimation of junction temperatures using the power losses in a three-phase converter. The thermal path is modeled in the form of Cauer networks. Source: [C4].

> **Remark 3.2.5:**
> The thermal network in Fig. 3.13 can be further simplified by the Thevenin (temperature source in series with a thermal impedance) or Norton (power source in parallel with a thermal impedance) equivalence.

> **Remark 3.2.6:**
> The thermal network in Fig. 3.13 can be constructed in more details [56], e.g., including the thermal coupling among devices, but this will not lead to higher sampling frequency if the thermal model only involves time-invariant thermal resistances and capacitances.

The proposed approach has been validated by real-time simulations on the OPAL-RT platform as mentioned in Section 1.6. The study case in Fig. 3.7 is simulated at a step size of 10 µs (100 kHz sampling rate). Key parameters are listed in Table 3.2, and the results are shown in Fig. 3.14.

From Fig. 3.14, the proposed method can generate junction temperature profiles using a much lower sampling rate, compared to the simulation of switching transients. The accuracy is acceptable for microgrid applications (with around 10% deviations in IGBT junction temperatures). This can basically facilitate reliability-oriented tests of controllers or new design strategies.

TABLE 3.2: KEY PARAMETERS OF THE STUDY CASE TO VALIDATE THE PROPOSED APPROACH BY REAL-TIME SIMULATIONS

Parameters	Values
Rated phase voltage and frequency	230 V_{RMS}, 50 Hz
Rated switching frequency	10 kHz
Resistive load power (three phases)	10 kW or 20 kW as specified
Parameters of the *LC* filter	L_f = 2.0 mH, C_f = 10 µF
Type of the power devices	Infineon FS75R12KT3 (1200 V/75 A, IGBT module)

Source: [C4].

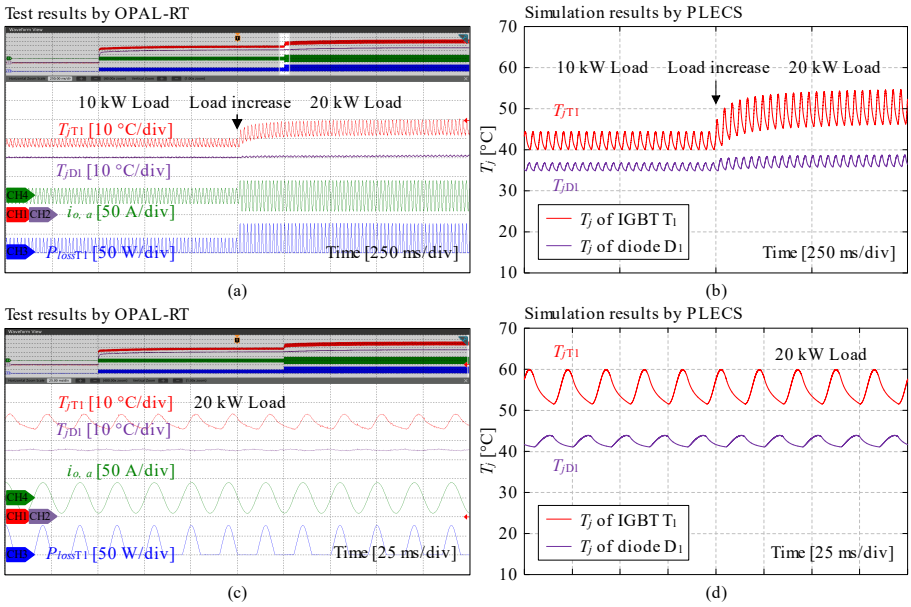

Fig. 3.14: Comparison of the test results obtained by real-time simulations using an OPAL-RT platform and the thermal simulation by PLECS as a benchmark, including: (a) & (b) comparison in dynamic performances, (c) & (d) comparison in steady-state performances, where (a) & (c) are obtained by the proposed method. Source: [C4].

Meanwhile, the presence of errors in T_{jD} should also be acknowledged, which can be attributed to (3.17). The T_{sw}-averaging approximation used for power calculation may bring about inaccuracy when the conduction time is considerably shorter than the switching period T_{sw}, which particularly applies to the freewheeling diodes. Thus, possible solutions could involve refining the power calculations based on the duty cycles, as a tradeoff between accuracy and complexity.

3.5. Summary

In this chapter, the reliability of microgrids is inspected using the PoF-based lifetime model. The reliability of microgrids primarily hinges on the degradation of power semiconductors and capacitors, while the overall performance follows statistical and probability theories. With this, the project emphasizes the reliability-oriented power sharing, as a practical approach to enhance the reliability of microgrids at system level. The proposed conditional droop adjustment has demonstrated improved adaptability to more varied scenarios, but some stability concern can emerge as a potential bottleneck. Additionally, a method for real-time thermal evaluation of power converters has been presented and validated, enabling both simplified and quantitative reliability validation of microgrids.

Related Publications:

- **Section 3.3:**

[J2] **Y. Song**, S. Sahoo, Y. Yang, and F. Blaabjerg, "Conditional Droop Adjustment for Reliability-Oriented Power Sharing in Microgrid Systems," *IEEE Trans. Circuits Syst. II Express Briefs*, vol. 70, no. 7, pp. 2465-2469, Jul. 2023. doi: 10.1109/TCSII.2023.3242139.

- **Section 3.4:**

[C4] **Y. Song**, S. Sahoo, Y. Yang, F. Blaabjerg, and Y. W. Li, "Real-Time Thermal Evaluation of Power Converters in Microgrids by Device Current Reconstruction," accepted by *IEEE CPE-POWERENG 2023*, Tallinn, Estonia, Jun. 2023.

Chapter 4

Stability Constraints on Reliability-Oriented Control

4.1. Background

With the basics of stability and microgrids being scrutinized in *Chapters 2* and *3*, this chapter starts to bridge the two performance indices, composing the major contributions of this project. It has been underlined in Section 1.1.4 that the stability and reliability are often considered separately, which can be principally attributed to two aspects: the disparity in their timescales and the physics behind the respective modeling methods. Consequently, stability analysis and reliability analysis are typically conducted by assuming sufficient reliability and stability. However, it is crucial to understand the connections behind the two performance indices in practical applications, thus motivating the researches presented in *Chapter 4* and *5*, which are aimed at encompassing this point through physical interactions and mathematical combinations of the two indices, respectively.

This chapter thereby focuses on delving into physical interactions between the two indices. Specifically, the reliability-oriented power sharing mentioned in Section 3.3 is studied, which serves as an evident link between the stability and reliability in that the control parameters are modified. Under this scenario, it necessitates the validation of system dynamics. Previous work [91] has examined the system stability after assigning control parameters based on thermal indices, implying the logic for stability considerations, but the relationships between stability and reliability remain unclear. Hence, this chapter sheds light on the mutual impacts of stability and reliability considerations under this scenario, thus providing an intuitive understanding of the connections between the two performance indices [J3].

Moreover, in addition to revealing the stability boundary in reliability-oriented control, this chapter has also presented a solution to this underlying issue, enabling concurrent guarantee of stability and reliability. With this, the framework of stability-constrained reliability-oriented control is eventually formed in [J3], being a highly practical guideline for microgrid design and operation planning.

4.2. Stability Analysis on the Reliability-Oriented Power Sharing

As outlined in Section 3.3, the reliability-oriented power sharing aims to redistribute the loadings of converters subject to individual reliability performances. Specifically, in this chapter, the proportional adjustment as specified in (3.13) and Table 3.1 is first reviewed, which is given as following:

$$m_p = m_{p0} \cdot \left[\alpha + (1-\alpha) \cdot \beta_m^{\ \lambda}\right], \quad \beta_m = \begin{cases} D_0/D_i & \text{if } P < P_0 \\ D_i/D_0 & \text{if } P \geq P_0 \end{cases} \tag{4.1}$$

In [J2], this strategy has been proved to be effective in enhancing the system-level reliability performance, but the adjustment alone does not guarantee system stability which is eventually determined by the dynamics of the system. Since there are chances that the droop gains are increased, stability concerns may be raised similar to the case in [27].

To this end, simulations have been performed on the system shown in Fig. 4.1, which is configured based on the system specified in Section 1.6. Different from Table 1.2, the load resistance is exclusively set as 12 kW (3 Ω per phase), and the base values of the droop gains m_{p0} and n_{q0} are set as 9.4×10^{-5} Hz/W and 1.3×10^{-3} V/Var, respectively.

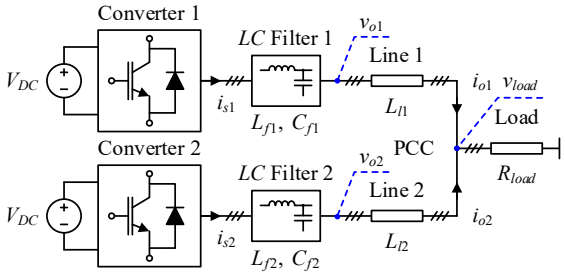

Fig. 4.1: Architecture of the study case for illustrating the stability concerns in reliability-oriented power sharing. Source: [J3].

The simulation results are presented in Fig. 4.2 [J3]. In Fig. 4.2, as the droop gain m_{p1} of Converter 1 is increased, the loading of Converter 1 will decrease due to the droop relationship (1.1), but when m_{p1} is increased up to $40m_{p0}$, the oscillations in frequency will escalate into a divergence, indicating an instability in the system. The results agree with the experimental waveforms depicted in Fig. 4.3, where the instability eventually triggers a shutdown of the system. The results have provided an initial insight that the droop gains cannot be always adjusted as desired to address the reliability concerns. Instead, stability analysis is crucial in identifying the boundary of system reliability performance. Hence, the

subsequent part of this section is dedicated to elaborating on this concern through stability modeling and analysis. Additionally, stabilization techniques can be favorable solutions to broaden the reliability boundary, thereby being a second focus of this chapter.

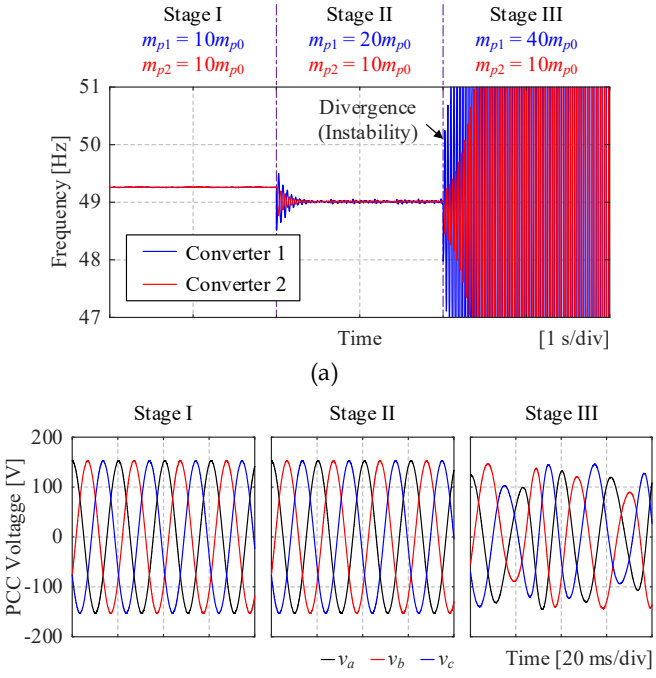

Fig. 4.2: Simulation results illustrating the instability when the droop gain m_{p1} of Converter 1 is increased, including: (a) the frequencies of the two converters, and (b) PCC voltage. Source: [J3].

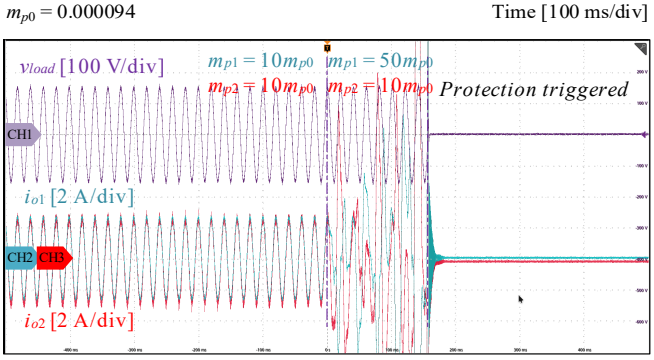

Fig. 4.3: Experimental results illustrating the instability when m_{p1} is increased. The load is 28.75 Ω per phase. Source: [J3].

The exemplary system is then modeled in [J3] similarly as described in Section 2.3.3. To simplify the analysis, the primary voltage control loops are disregarded as specified in Section 1.3.2. Consequently, the state vectors $\Delta x_{conv}^{(k)}$ (k = 1 or 2 for the two converters) of the system is:

$$\Delta \boldsymbol{x}_{\text{conv}}^{(k)} = \Delta\left[\delta^{(k)} \;\; P^{(k)} \;\; Q^{(k)} \;\; i_s^{(k)} \;\; v_o^{(k)} \;\; i_o^{(k)}\right]^T \tag{4.2}$$

And the state space can be constructed as:

$$\frac{\mathrm{d}}{\mathrm{d}t}\begin{bmatrix}\Delta \boldsymbol{x}_{\text{conv}}^{(1)} \\ \Delta \boldsymbol{x}_{\text{conv}}^{(2)}\end{bmatrix} = \boldsymbol{A}_{MG}\begin{bmatrix}\Delta \boldsymbol{x}_{\text{conv}}^{(1)} \\ \Delta \boldsymbol{x}_{\text{conv}}^{(2)}\end{bmatrix} \tag{4.3}$$

where, compared with (2.5), the model is simplified by only considering the state variables of the converters. The voltage at PCC (load voltage) is passively governed by the load resistance and the sum of output currents i_{o1} and i_{o2}.

With this model, the eigenvalue loci of the system are plotted in Fig. 4.4. In Fig. 4.4 (b), a pair of eigenvalues shift towards the right-half plane (RHP) when the droop gain m_{p1} increases, which confirms the observation of instability. Besides, the eigenvalue loci have also provided an insight into the unstable modes, which are located at an angular frequency of around 300 rad/s. This frequency is close to the fundamental frequency ω_1 = 314 rad/s, implying the presence of low-frequency oscillations when the system goes unstable.

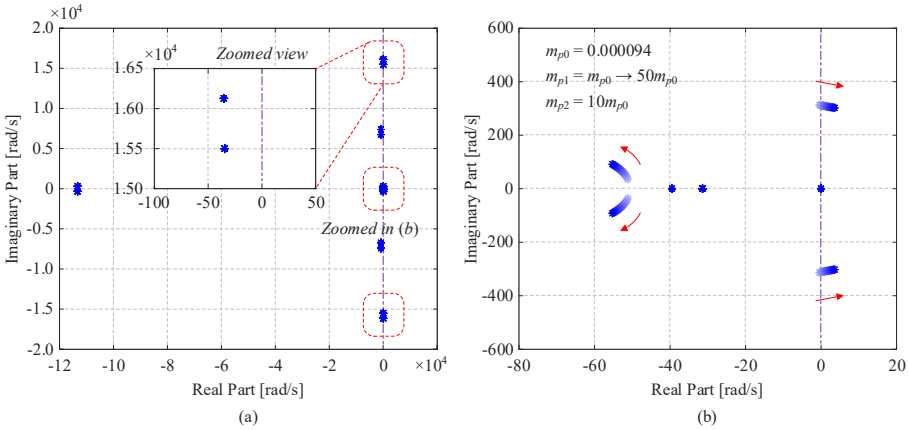

Fig. 4.4: Eigenvalue loci of the study case when m_{p1} ranges from m_{p0} to $50m_{p0}$, including: (a) all the eigenvalues, and (b) zoomed view near the original point. Source: [J3].

Accordingly, the stability modeling has been further validated through experimental tests, as presented in Fig. 4.5. When m_{p1} is increased from $16m_{p0}$ to $20m_{p0}$ representing a relatively small transient, the operation points cross the stability boundary, leading to the emergence of instability in the form of frequency

oscillations. Such instability causes the distortion of output currents i_{o1} and i_{o2}. The experimental results are also demonstrating the significance of stability constraints when adjusting the control parameters for enhancing the system reliability.

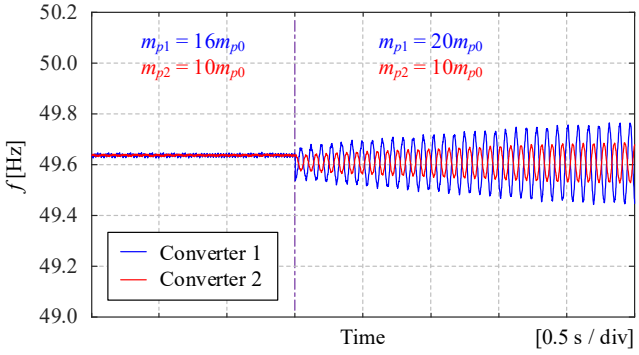

(a)

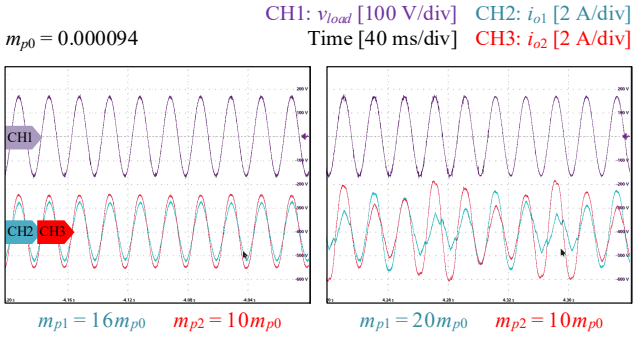

(b)

Fig. 4.5: Experimental results illustrating the instability of the system shown in Fig. 4.1 when m_{p1} is varied from $16m_{p0}$ to $20m_{p0}$, including: (a) the divergence in frequencies, and (b) the load voltage v_{load} and distorted output currents i_{o1} & i_{o2}. The load is 28.75 Ω per phase. Source: [J3].

4.3. Stability Constraints on System Reliability and Solutions

The stability boundary discussed in Section 4.2 is then integrated into reliability analysis as illustrated in Fig. 4.6. Infineon FS25R12KT3 (1200 V/25 A) and FP30R12KE3 (1200 V/30 A) are selected as the power devices of Converters 1 and 2 in Fig. 4.1, respectively. Considering that Converter 1 is more stressed with lower rated current, its droop gain should be increased to improve the overall lifetime of the system. However, the system crosses the stability boundary when

m_{p1} reaches $30m_{p0}$ or larger, indicating that the stability criteria are serving as constraints which can prevent the system from achieving longer lifetime.

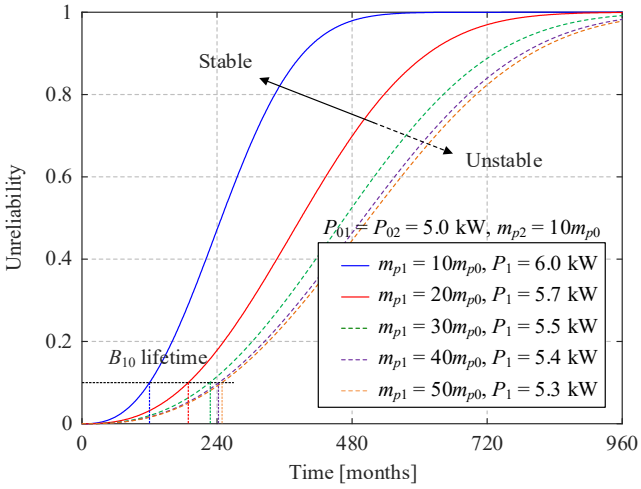

Fig. 4.6: System unreliability over time when m_{p1} ranges from $10m_{p0}$ to $50m_{p0}$. It should be noted that system stability is constraining the achievable B_{10} lifetime. Source: [J3].

Another example is given as following to validate the stability constraints in a larger system. The system has the same topology of Fig. 3.5 based on the CIGRE LV benchmark system, but it is configured differently as specified Fig. 4.7 (a) and Table 4.1. When the droop gains m_{p2} and m_{p3} are varied, the B_{10} lifetime of the system is estimated as illustrated in Fig. 4.7 (b). It is noteworthy that the stability criteria of the system impose constraints on the available parameter combinations, limiting them within a confined region. The achievable lifetime is eventually influenced. This example has also shown the significance of addressing stability concern when enhancing system reliability through reliability-oriented controls.

TABLE 4.1: KEY PARAMETERS OF THE STUDY CASE IN FIG. 4.7 ON LONG-TERM RELIABILITY PERFORMANCE

Parameters	Values
Nominal AC voltage V_n	230 V_{RMS}, 50 Hz
Type of the power devices	Infineon FS100R12KT3 (1200 V/100 A) for Conv. 1 FS75R12KT3 (1200 V/75 A) for Conv. 2 and 3 FS25R12KT3 (1200 V/25 A) for Conv. 4 and 5
Initial active droop gain m_{p0}	9.4×10^{-5} [Hz/W]
Power cycling period t_{on}	0.01 s
Number of cycles per month	(24×60×60×30) ×50

Source: [J3].

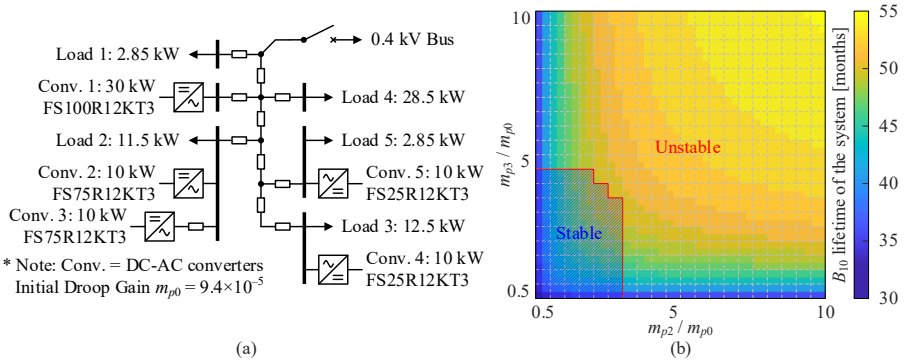

Fig. 4.7: Validation of stability constraints in a larger system, including: (a) the configuration of the system, and (b) estimated lifetime of the study case when m_{p2} and m_{p3} are varied, with the stable region of the system marked by shaded area with red borderlines. Source: [J3].

Therefore, in order to further enhance the reliability performance at system level, it is critical to adopt stabilization techniques to exceed the original stability boundary. Having in mind that the power sharing is governed by reliability metrics, two solutions have been implemented in [J3]: modifying the low-pass filter (LPF) in droop controllers to suppress power transients, or using lead-lag power system stabilizers (PSS) to compensate for the arising oscillations. The two solutions are elaborated based on the system specified in Fig. 4.1 consisting of two DC-AC converters in parallel.

A. Stability Enhancement by Modifying the Low-Pass Power Filter

As clarified in Section 4.2, the instability may emerge in the form of frequency oscillations due to the increase of the active droop gain m_p. The first solution is to utilize the low-pass filters (LPF) in droop controllers to suppress the oscillations. A typical droop controller is depicted in Fig. 4.8, where there are LPFs for both active and reactive power to smoothen the measured powers. The LPFs can be first-order filters as expressed in (4.2), which is exemplified in this section.

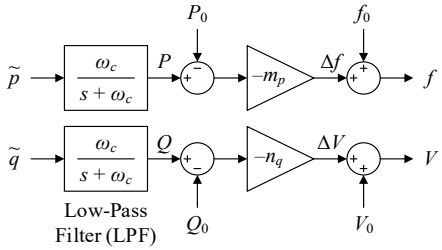

Fig. 4.8: Droop controller with a low-pass power filter, where $\tilde{p}$ and $\tilde{q}$ are the measured power obtained from the sampled voltage v_o and current i_o. Source: [J3].

$$G_{\mathrm{LPF},P}(s)=\frac{P}{\tilde{p}}=\frac{\omega_c}{s+\omega_c},\quad G_{\mathrm{LPF},Q}(s)=\frac{Q}{\tilde{q}}=\frac{\omega_c}{s+\omega_c} \tag{4.2}$$

In the same study case as specified in Section 4.2, the eigenvalue loci are re-plotted in Fig. 4.9 when the bandwidth of the said LPF is varied. The cutoff frequency ω_c is decreased to 1/2, 1/4 and 1/10 of the initial frequency ω_0, which is 31.4 rad/s, 10% of the fundamental frequency. It is seen that the critical modes move further away from the LHP when ω_c is smaller. Though the eigenvalues are still approaching the imaginary axis when m_p increases, the stability margin is increased, allowing for higher capability of reliability enhancement.

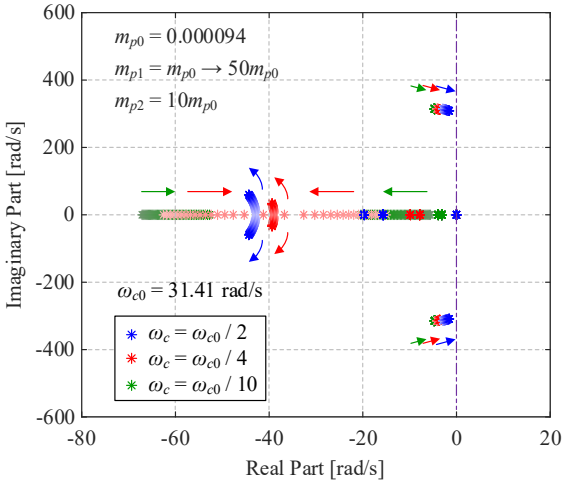

Fig. 4.9: Eigenvalue loci of the study case when m_{p1} ranges from m_{p0} to $50m_{p0}$ with different values of ω_c. Source: [J3].

This approach is validated by simulations with the cutoff frequency ω_c decreased to $\omega_0/2$, and the results are shown in Fig. 4.10. Compared with Fig. 4.2 (a), the oscillations have been suppressed, encompassing a larger stable region and prolonged achievable system lifetime. However, it should be acknowledged that lower bandwidth ω_c also introduces certain tradeoffs, specifically more delays and larger inertia (slower dynamics). The dynamic performances of the system are impaired by longer settling time t_s and larger overshoot during transients. This issue may be more severe when the closed control loops for voltage regulation are employed.

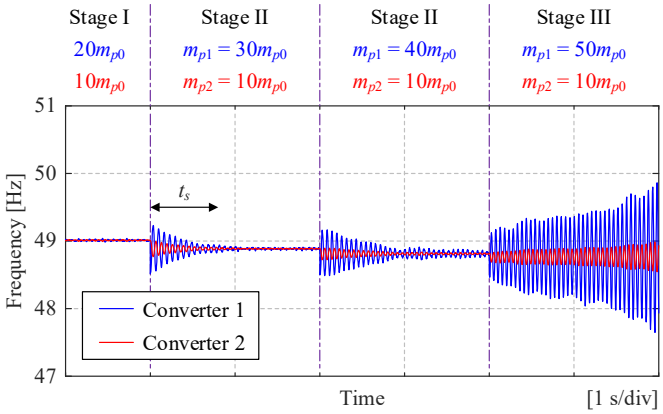

Fig. 4.10: System stability as indicated by frequencies of the two converters when m_{p1} is increased. The cutoff frequency ω_c of power filters is reduced to $\omega_{c0}/2$. Source: [J3].

B. Stability Enhancement by Designing Power System Stabilizer (PSS)

The power system stabilizer (PSS) using a lead-lag regulator as mentioned in [117] is an alternative solution to mitigate the oscillations. The PSS essentially generates a feedforward signal with the same amplitude and complementary phase, such that the frequency oscillations can be compensated to zero. The PSS can be implemented as shown in Fig. 4.11.

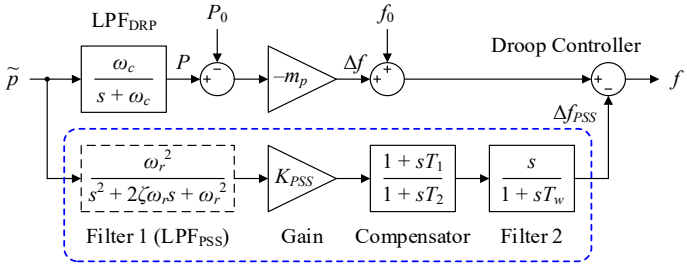

Fig. 4.11: Active power control employing a power system stabilizer (PSS). Source: [J3].

The PSS is designed through the procedure introduced in [117], including:

(a) *A lead-lag compensator* (the Compensator in Fig. 4.11): The phase shift in the original droop controller is primarily determined by the phase of the LPF in the droop controller ($\mathrm{LPF_{DRP}}$ in Fig. 4.11). The phase shift of the compensator at the oscillation frequency should thereby be complimentary to that of $\mathrm{LPF_{DRP}}$.

(b) *A washout filter* (Filter 2 in Fig. 4.11): The washout filter is used to eliminate the DC offset in the measured active power $\tilde{p}$. To ensure the performance of the lead-lag compensator, the washout filter should be designed with negligible phase shift at the oscillation frequency.

(c) *A gain K_{PSS} for amplitude alignment*: The gain K_{PSS} aims to align the amplitudes of the oscillation component and the generated compensation signal. Thus, it is designed by comparing the amplitude of the droop path and the compensation path at the oscillation frequency.

(d) *An anti-harmonic filter* (Filter 1 (LPF_{PSS}) in Fig. 4.11): Another filter is employed to minimize the influence of high-order harmonics or noises and to smoothen the compensation signal. It is important that this filter should not introduce significant phase deviation at the oscillation frequency either. Therefore, its cut-off frequency should be positioned between the oscillation frequency and the harmonic frequency, while the damping ratio is a tradeoff between the dynamic performance and minimizing the said phase deviation.

In the same study case as specified in Section 4.2, the oscillation is measured to be approximately 83.14 rad/s by Fig. 4.5 (a), indicating a phase delay of –69.3° in the LPF_{DRP}. The PSS of Converter 2 is accordingly designed as specified in Table 4.2, and the PSS of Converter 1 is proportionally configured based on the droop gains, namely $K_{PSS,1} = K_{PSS,2} \times m_{p1}/m_{p2}$.

Experimental results are shown in Fig. 4.12. Compared with Fig. 4.5, the frequency oscillations have been effectively suppressed by the PSS, extending the stable region to $m_{p1} = 40m_{p0}$. Hence, it can be concluded that the PSS is an adequate solution to this scenario.

Nevertheless, the frequency decrease resulting from the droop relationships is also noteworthy. The frequency limits associated with source or transmission line capacities could be considered in terms of the steady-state stability as mentioned in Section 1.1.2. Additional boundaries could be formed that similarly limit the reliability performances of the system.

TABLE 4.2: DESIGNED PARAMETERS OF THE PSS IN THE EXPERIMENTAL STUDY CASE

Variables of the PSS in Fig. 4.10	**Values**	**Units**
Time constant T_1	0.0421	s
Time constant T_2	0.001	s
Time constant T_w	3	s
Gain of the PSS for Converter 2 $K_{PSS,2}$	0.000275	–
Resonance frequency of the LPF_{PSS} ω_r	942	rad/s
Damping ratio of the LPF_{PSS} ζ	0.02	–

Source: [J3].

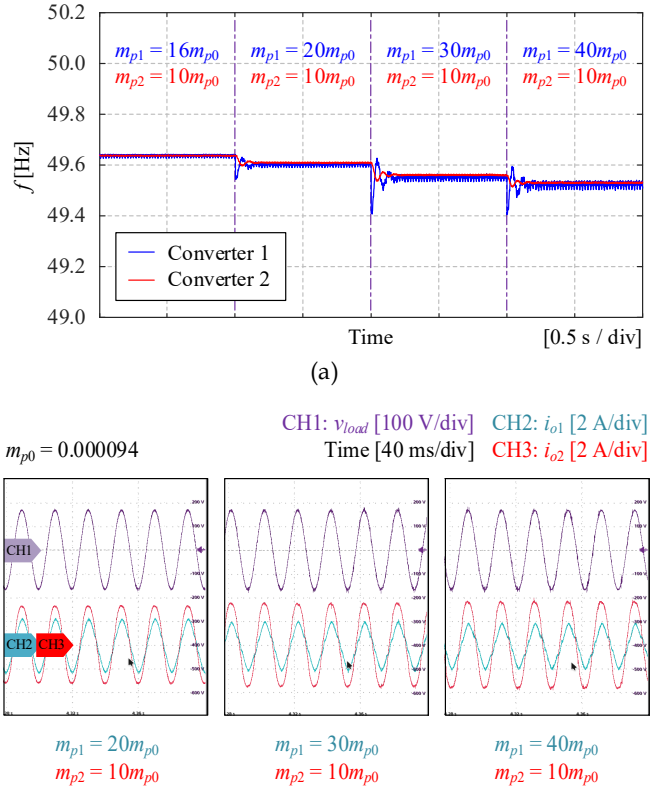

Fig. 4.12: Effectiveness of the PSS when m_{p1} is varied from $16m_{p0}$ to $40m_{p0}$, including: (a) the stabilized frequencies, and (b) the load voltage v_{load} and output currents i_{o1} & i_{o2}. Source: [J3].

4.4. Framework of Stability-Constrained Reliability-Oriented Control

Based on the detailed discussions in Sections 4.2 and 4.3, stability analysis and enhancement can be thereby incorporated into the reliability-oriented control and design, prompting the framework of stability-constrained reliability-oriented control as presented in Fig. 4.13.

In the framework, system power flow or the loadings of the converters are calculated for reliability evaluation, and the droop gains are adjusted to accordingly improve the system reliability. Meanwhile, the stability criteria are also supposed to be considered, which define the boundaries of droop adjustment. In general, the stability criteria could encompass small-signal stability as

demonstrated in Sections 4.2 and 4.3, and the voltage or frequency constraints that are related to the droop relationships.

If the system fails to satisfy the stability criteria, then a review of the design objective of system reliability is required, or the stability enhancement techniques (e.g., PSS) are necessary. In cases where the two performances cannot be simultaneously satisfied, such as when the system reaches its EOL, a maintenance is necessary to ensure safe operation of the system.

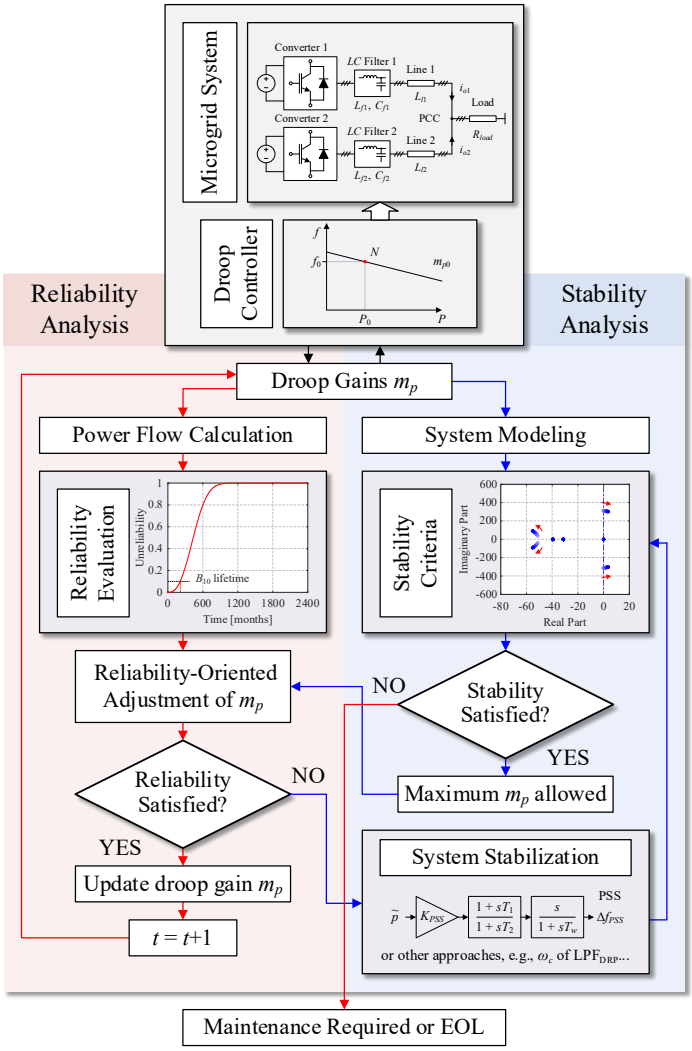

Fig. 4.13: Framework of stability-constrained reliability-oriented droop control for microgrids. Source: [J3].

Remark 4.4.1:
As system reliability is a long-term performance, the proposed framework does not require high sampling rate or high communication capability. The droop gains can be updated according to the secondary or tertiary control periods, e.g., on a monthly basis.

4.5. Summary

This chapter discusses the relationships of stability and reliability from a practical perspective, accentuating their inherent interdependencies. By exemplifying reliability-oriented power sharing in microgrids, the impacts of stability criteria on system reliability have been verified, which delineates a boundary of the achievable system lifetime. The stability validation is thereby necessitated in reliability-oriented planning or reliability enhancement of microgrids, motivating the development of a framework of stability-constrained reliability-oriented control for microgrids. In order to address this issue more comprehensively, possible solutions are also demonstrated, expanding the stability boundary and facilitating more possibilities for reliability enhancement. Nevertheless, this framework should be further validated in larger-scale systems to account for multiple unstable modes or heterogeneous dynamics.

Related Publications:

- **Sections 4.2, 4.3 and 4.4:**

[J3] **Y. Song**, S. Sahoo, Y. Yang, and F. Blaabjerg, "Stability Constraints on Reliability-Oriented Control of AC Microgrids – Theoretical Margin and Solutions," *IEEE Trans. Power Electron*. vol. 38, no. 8, pp. 9459-9468, Aug. 2023. doi: 10.1109/TPEL.2023.3270640.

Chapter 5

Performance Evaluation Considering Stability and Reliability

5.1. Background

As revealed in *Chapter 4*, the stability and reliability of microgrids can essentially interact with each other. It becomes evident that s*ystem stability does not guarantee optimal reliability, and a highly reliable system may still encounter the risk of instability*. The stability-constrained reliability-oriented control has thereby been outlined to address this point. However, apart from the emphasis on the mutual interactions under certain scenarios, it is also essential to adopt a more comprehensive unification of stability and reliability that can reflect the collective performance of the system, prompting the primary objective of this chapter.

This chapter first clarifies the two concerns mentioned in Section 4.1 as following: Long-timescale reliability performances are decomposed into events with smaller time frames to match the stability evaluation in the time domain, and uncertainties and contingencies are introduced to facilitate probabilistic approaches for both stability and reliability. Compared with *Chapter 4*, this chapter principally forms the logic from a more mathematical perspective. The *operational risk* of microgrid systems can be reorganized to collectively include both stability and reliability, and the *lifetime* is accordingly generalized [J4].

The formulated probabilistic stability and reliability are also allowing for an interpretation of their connections using theorems from the probability theory. For instance, the Bayesian inference is employed in [C5] to interpret the relationship between stability and reliability based on events or observed states, where the degradation of capacitors is exemplified, which may direct shape the system-level stability. This scheme is also promising in establishing links between probabilistic evaluations with real-world data. As such, the foundation is laid for inspiring potential applications leveraging advanced data-driven methodologies in the evaluation of stability and reliability in microgrids.

5.2. Operational Risk Considering Stability and Reliability

Both instability and unreliability can potentially lead to malfunctions or failures of microgrids systems, thus being significant to be considered simultaneously. As *Chapter 4* has addressed interactions between stability and reliability, it is also practical to intuitively describe the two performances with metrics in more general cases. Notably, the concept of *probabilistic stability* that encloses the system uncertainties has been formulated in literature like [16], while it is also able to facilitate the alignment of stability and reliability analysis in a probabilistic way. With this, by decomposing long-term reliability into instantaneous probabilities, it is justifiable to treat stability and reliability as events. They can be subsequently synthesized using probability theories based on their logical relationships.

5.2.1. Probabilistic Stability in Microgrids

The probabilistic stability is essentially a generalization of deterministic stability by considering the underlying uncertainties in the system. In [J4], this extension is first demonstrated by including uncertainties into the same study case used in Section 4.2, which is configured in Fig. 5.1 with a resistive load of 12 kW and initial droop gains m_{p0} and n_{q0} of 9.4×10^{-5} Hz/W and 1.3×10^{-3} V/Var, respectively. The system is modeled with the same approach as expressed in (4.2) and (4.3), yielding the eigenvalues listed in Table 5.1.

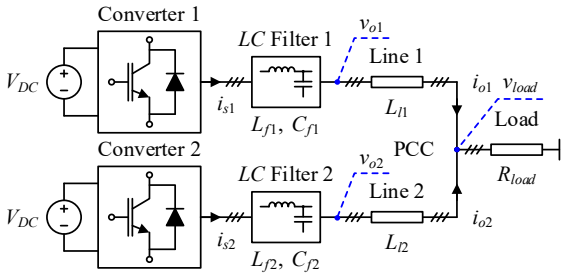

Fig. 5.1: Architecture of the study case for probabilistic stability and reliability evaluation. Source: [J4].

From Table 5.1, the conjugate eigenvalues λ_{11} and λ_{12} are concluded to be the critical modes, as they are located close to the imaginary axis and are sensitive to the variation of m_p. It has also been confirmed by modeling with more varied parameter combinations that λ_{11} and λ_{12} are the only eigenvalues that satisfy the two criteria and could move into RHP under the exemplary scenarios. Thus, the stability analysis can be simplified by focusing specifically on the critical modes λ_{11} and λ_{12}.

TABLE 5.1: EIGENVALUES OF THE STUDIED SYSTEM

Index of the eigenvalues	Eigenvalues in default case $m_{p1} = m_{p2} = m_{p0}$	Eigenvalues when $m_{p1} = 2m_{p2} = 2m_{p0}$
$\lambda_{1,2}$	–35.38 ± j16125	–35.38 ± j16125
$\lambda_{3,4}$	–34.60 ± j15497	–34.60 ± j15497
$\lambda_{5,6}$	–4735 ± j14527	–4735 ± j14527
$\lambda_{7,8}$	–4734 ± j13898	–4734 ± j13898
$\lambda_{9,10}$	–2740 ± j308.62	–2740 ± j308.62
$\lambda_{11,12}$	–1.17 ± j315.44	–1.10 ± j315.23
λ_{13}	–0.32	–0.30
λ_{14}	–61.29	–51.20 ± j5.68
λ_{15}	–41.11	
λ_{16}	–30.95	–31.10
λ_{17}	–31.41	–31.41
λ_{18}	–39.50	–39.50

Source: [J4].

The uncertainties in microgrid systems mentioned in Section 1.1.1 [16] are then introduced to embody the probability of system stability. The uncertainties of the configuration parameters are considered herein, which typically follow Gaussian distribution with the Probability Density Function (PDF) expressed as:

$$f(X) = \frac{1}{\sigma_{\text{par}}\sqrt{2\pi}} \cdot \exp\left[-\frac{1}{2}\cdot\left(\frac{X-\mu_{\text{par}}}{\sigma_{\text{par}}}\right)^2\right] \tag{5.1}$$

where, for a certain parameter X, μ_{par} is its mean value (typically the nominal value), and σ_{par} is its standard deviation. Such distribution is denoted as N (μ_{par}, σ_{par}^2) in this chapter. It is also assumed that all parameter uncertainties follow the 3-σ rule, i.e., the rated uncertainty of X corresponds to $3\sigma_{\text{par}}$.

The evaluation of the probabilistic stability can subsequently be implemented following the procedure as outlined in Fig. 5.2. System stability corresponds to the condition that the real parts of all critical modes satisfy $\text{Re}\{\lambda\} \le 0$, and the Monte-Carlo method can be employed to fit the probability of stability from a statistical perspective.

The uncertainties of the configuration parameters studied in this chapter are given in per-unit values and are assumed equal. For example, in this section (Section 5.2), L_f, C_f, L_l, and parasitic resistances r_{Lf} and r_{Ll} are initially assigned with

an uncertainty of 10%, namely $3\sigma_{par} = 10\%\mu_{par}$, then the probability distribution of the real part of the critical modes can be obtained as shown in Fig. 5.3. Most data points fall into the 3-σ region [μ_{eig}–$3\sigma_{eig}$, μ_{eig}+$3\sigma_{eig}$], and the distribution of the data points can be fit by a Gaussian PDF. The probability of system stability $P(Stable)$ corresponds to the area surrounded by the Gaussian PDF curve and the x-axis in the LHP.

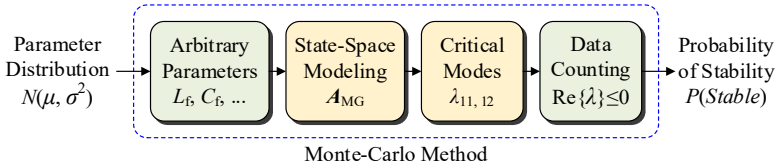

Fig. 5.2: Evaluation of probabilistic stability using Monte-Carlo analysis. Source: [J4].

Remark 5.2.1:
In this chapter, parameters with uncertainties are assumed to be independent variables. In cases where the correlations of parameters are not negligible, the Monte-Carlo method should be conducted by inputting compatible parameter groups or stratified samples subject to particular parameter groups.

Remark 5.2.2:
In more general cases, a system is stable when all the eigenvalues are located in LHP. The probability of the system stability should be formulated as:

$$P(Stable) = P\left(\bigcap_{j=1}^{k}\left\{\mathrm{Re}\left\{\lambda_j\right\} \le 0\right\}\right) \tag{5.2}$$

where k is the total number of the eigenvalues.
In this case, considering the critical modes that may move into the RHP, (5.2) can be simplified into:

$$P(Stable) = P\left(\mathrm{Re}\left\{\lambda_{11,12}\right\} \le 0\right) = \int_{-\infty}^{0} f(\sigma)\,\mathrm{d}\sigma \tag{5.3}$$

which is the basis of Fig. 5.3.
If more critical modes should be considered, then (5.3) should be extended to include all the critical modes.

Upon this, the probabilistic stability is explored in [J4] by examining two major influence factors: the droop gains, which affect the mean values of the eigenvalues μ_{eig}, and system uncertainties, which affect the standard variance of the eigenvalues σ_{eig}. The Monte-Carlo simulation results are depicted in Fig. 5.4 with Gaussian fitting, and the following conclusions can be drawn based on the results:

(a) The probability of system stability is more sensitive to parameter variation when the mean values of the real parts of critical modes are close to zero, which also agrees with the deterministic stability modeling.

(b) Different from deterministic stability modeling, the probability of system instability can be nonzero even when the mean values of the real parts of all critical modes are negative.

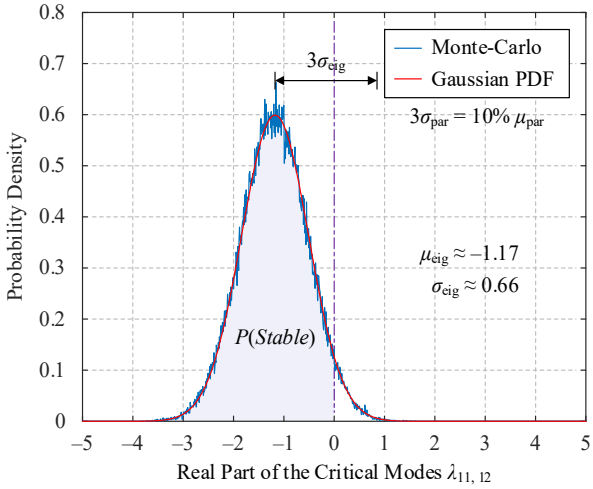

Fig. 5.3: Distribution of the real parts of the critical modes $\lambda_{11,\ 12}$ by Monte-Carlo simulations and Gaussian fit of the probability distribution. Source: [J4].

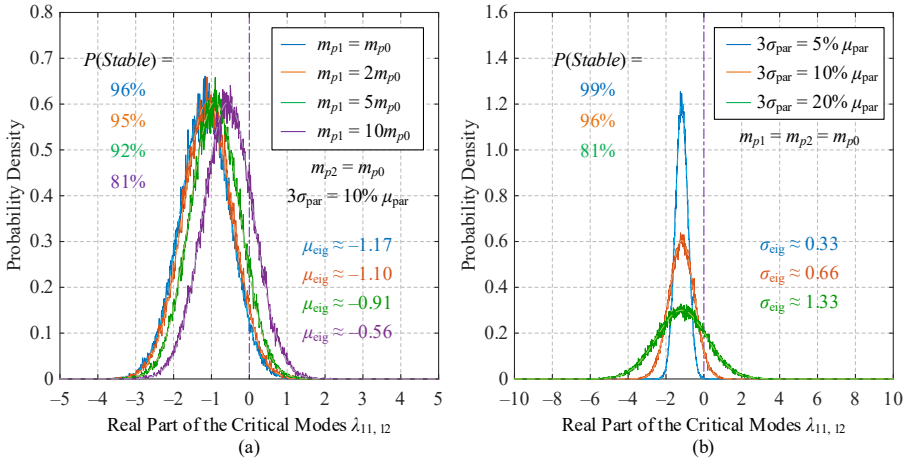

Fig. 5.4: Distribution of the real parts of the critical modes $\lambda_{11,\ 12}$ as influenced by: (a) the variation of the droop gain m_{p1}, and (b) the variation of parameter uncertainties. Source: [J4].

Fig. 5.5 presents a summary on the probability of system stability in terms of the variation of the droop gain m_{p1} and the parameter uncertainty $3\sigma_{\text{par}}$. These curves are dependent on both the CDF of the distribution of the critical modes and the sensitivity of the droop gains affecting the critical modes ($\partial \text{Re}\{\lambda\}/\partial m_p$). With the symmetric Gaussian distribution studied in this case, the conventional deterministic stability corresponds to a 50% probability of system stability.

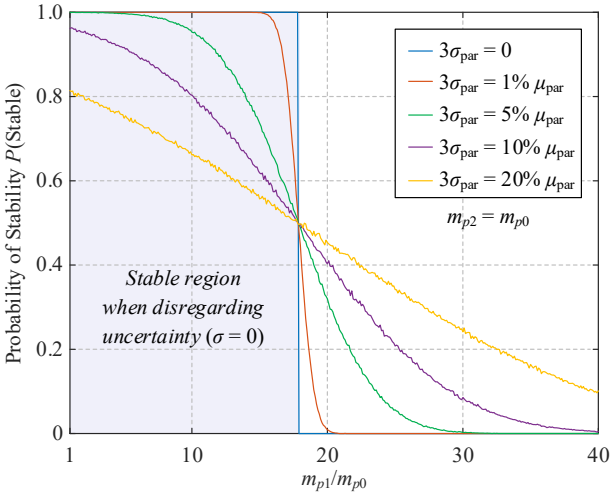

Fig. 5.5: Illustration of the influences of the droop gain m_{p1} and the parameter uncertainty $3\sigma_{\text{par}}$ on the probabilistic stability. Source: [J4].

5.2.2. Probabilistic Relationships of Stability and Reliability

With the probabilistic stability formulated in Section 5.2.1, the probabilistic relationships of stability and reliability can be illustrated as in Fig. 5.6 [J4], including the following two types:

(a) Figs. 5.6 (a) & (b) outline the conditional probability. This can elucidate the cases where one of the two performance metrics is constrained by the other, or where the posterior probability is preferred under the observation of a certain system state.

(b) Fig. 5.6 (c) represents an explication of the collective probability. It encompasses both stability and reliability, which gives the overall probability of safe operation.

Recognizing that the operational risk of microgrid systems should address both stability and reliability concerns, [J4] further delves into this point by extending the study case discussed in Section 5.2.1, which is presented in the following section.

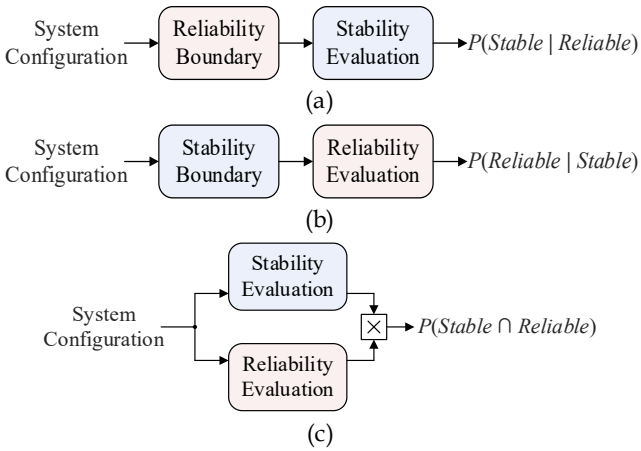

Fig. 5.6: Probabilistic relationships of microgrid stability and reliability, including: (a) stability subject to reliability conditions, (b) reliability subject to stability conditions, and (c) collective performance of stability and reliability. Source: [J4].

5.2.3. Operational Risk Considering Both Stability and Reliability

The concept of risk has been originally specified in [96]-[98] as a reflection of operational security, which is mentioned in Section 1.1.4, while both instability and unreliability can essentially result in failures or service interruptions. Building upon this, the following definition of the *probabilistic risk* of microgrid systems has been yielded as an extension to emphasize the joint consideration of stability and reliability more specifically:

> **Definition 5.1: The probabilistic risk of a microgrid system**
> The *probabilistic risk* of a microgrid system is the probability that the system cannot conform to its essential function with both sufficient stability and reliability. The system can be said to be secure when there is a low probability of risk.

Therefore, the risk should be formulated as following, which is the converse of the intersection between stability and reliability:

$$Risk = 1 - P\left(Stable \cap Reliable\right) \tag{5.4}$$

The stability and reliability of the study case are mathematically independent given a specific system configuration Γ. (5.4) can be rewritten into:

$$Risk\big|_{\Gamma} = 1 - P\left(Stable\right)\big|_{\Gamma} \cdot P\left(Reliable\right)\big|_{\Gamma} \tag{5.5}$$

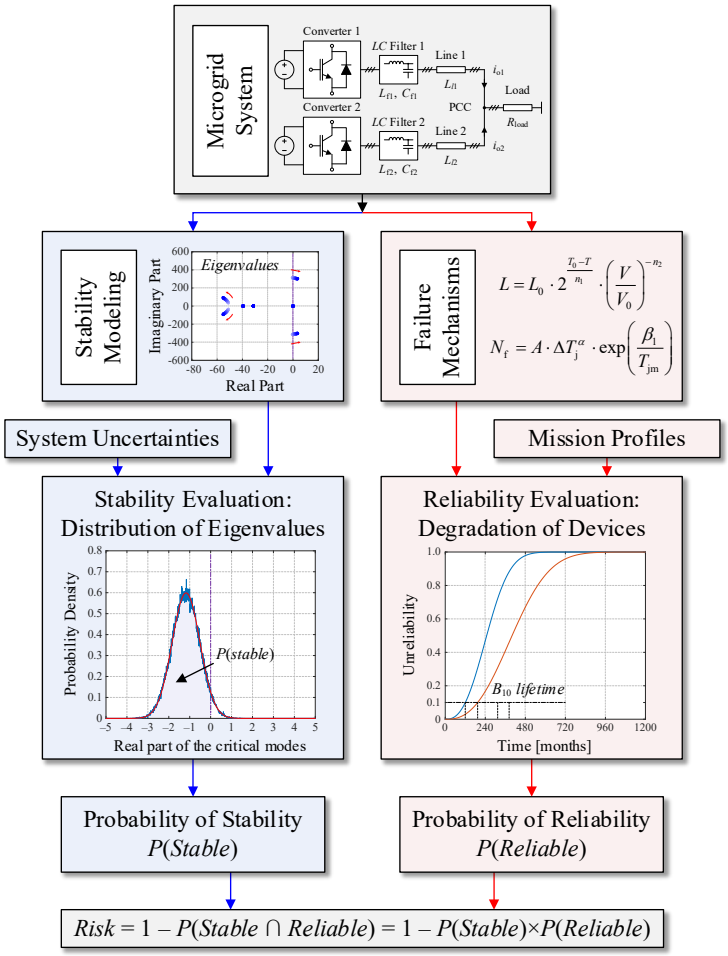

Fig. 5.7: Framework of operational risk evaluation of a microgrid system, where both stability and reliability analysis are considered. Source: [J4].

> **Remark 5.2.3:**
> If stability and reliability are not mathematically independent where (5.5) does not hold (e.g., the degradation of components leads to critical parameter variation that causes instability), the risk can be evaluated based on (5.4) alongside time-dependent Monte-Carlo simulations or Markov approaches. The concept of decomposing long-timescale performances into short-timescale events remains applicable.

Accordingly, the framework of operational risk evaluation can be formalized as shown in Fig. 5.7 [J4]. The system uncertainties and mission profiles are shaping

the system stability and reliability, respectively, while their contribution to the overall risk can both be reflected by the framework, which is practical for understanding the two performance indices collectively.

5.2.4. Extension of the Risk Evaluation Framework

Fig. 5.7 is subsequently applied to the study case, of which the results are compared with those of the plain reliability evaluation in Fig. 5.8. With the risk-evaluation framework, the B_{10} *lifetime* in reliability analysis can be generalized into the timespan before which the system maintains an overall operational risk below 10%, as marked in Fig. 5.8 (b).

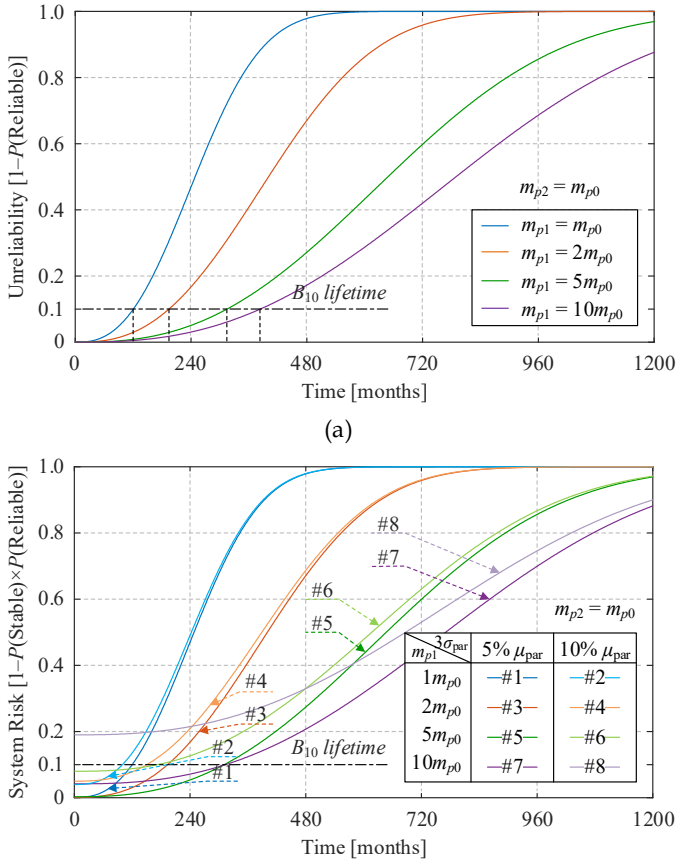

Fig. 5.8: Long-term operational risk of the study case, (a) when only reliability is considered, and (b) when parameter uncertainties and probabilistic stability are incorporated into the analysis. Source: [J4].

The findings highlight the consequences introduced by probabilistic stability, including higher operational risk from the beginning. Besides, a larger droop gain m_{p1} cannot ensure longer low-risk lifetime. Considering this aspect during the system design and planning can be advantageous in practice, by which system failures due to parameter errors can be anticipated.

The low-risk lifetime is further examined in Fig. 5.9 considering the droop gain m_{p1} and parameter uncertainties. The curves are located within the stable region, which aligns with Fig. 5.5, but as the probability of the system instability increases, the low-risk lifetime will eventually decrease to zero. For each of Cases #1-#4, the local maximum of the low-risk lifetime corresponds to the optimal droop gain under the scenario, whereas Case #5 reveals the existence of conditions where the high probability of instability induces elevated operational risk. This further necessitates the combination of stability and reliability evaluations in system planning, and it should be even more accentuated when a stricter threshold of operational risk (e.g., B_1 instead of B_{10}) is enforced.

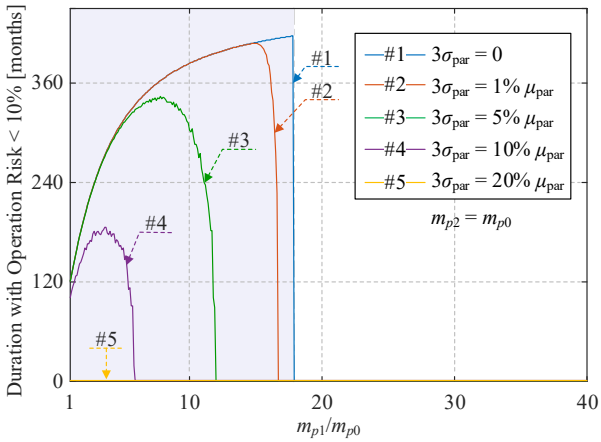

Fig. 5.9: The low-risk (below 10%) lifetime considering the droop gain m_{p1} and parameter uncertainties. Source: [J4].

5.3. Reliability under Stability Conditions Based on Bayesian Inference

The probabilistic relationships of stability and reliability falls into two major concerns in Section 5.2.2, of which the collective probability has been addressed in Section 5.2. Nevertheless, the posterior stability or reliability could be recognized concerning posterior probability based on state observations. To this end, [C5] thereby expands on this point by exemplifying the degradation of capacitors and inspecting its impacts on the system stability.

5.3.1. Bayesian Inference and Posterior Reliability

The Bayes' theorem is one of the basic theorems in probability theory, which describes the conditional probability of an event given prior knowledge of the condition, as [118]:

$$P(A \mid B) = \frac{P(A \cap B)}{P(B)} = \frac{P(B \mid A)P(A)}{P(B)} \tag{5.6}$$

where, A and B are two events with respective probabilities $P(A)$ and $P(B)$, and $P(A \mid B)$ is the probability of A under the condition that B is true.

In data science, the Bayesian inference is frequently applied, which is derived based on the Bayes' theorem:

$$P(H \mid E) = \frac{P(E \mid H)P(H)}{P(E)} \tag{5.7}$$

where, H is a hypothesis and E is the data obtained by tests. The posterior probability $P(H \mid E)$ of H given E is accordingly calculated out of its prior probability $P(H)$, and the likelihood $P(E \mid H)$ of the data E under the hypothesis H.

The conditional probability of stability and reliability can likewise be mapped. As the long-timescale reliability is decomposed into shorter-timescale frames, the stability performance in each time frame can be observed through tests, and in practice, the probability of reliability should be described as the probability under observed system states or conditions, namely the posterior reliability. If the stability and reliability of a microgrid system are denoted as the events S and R, respectively, then the reliability under stability conditions can be formulated based on the Bayesian inference given as [C5]:

$$P(R \mid S) = \frac{P(S \mid R)P(R)}{P(S)} \tag{5.8}$$

In particular, if stability and reliability are mathematically independent, then (5.8) can be re-organized as:

$$\begin{cases} P(S \cap R) = P(S)P(R) \\ P(R \mid S) = P(R) \\ P(S \mid R) = P(S) \end{cases} \tag{5.9}$$

which does not conflict with the framework for collective probability in Section 5.2.3.

5.3.2. Case Study on the Conditional Evaluation of System Reliability

To showcase the applications of posterior reliability, a typical grid-forming converter (voltage-source converter) system in microgrids is studied, as illustrated in Fig. 5.10. The system configurations resemble the converters described in Table 1.2, except that the filter capacitor C_f is 15 μF by default, and the load power P_{load} is 5 kW for three phases. In the case study, the degradation of capacitors is emphasized, and the parameters of the double-loop voltage controllers in Fig. 5.9 are designed as: K_{pv} = 0.04, K_{iv} = 78, K_{pi} = 10.5, K_{ic} = 16000.

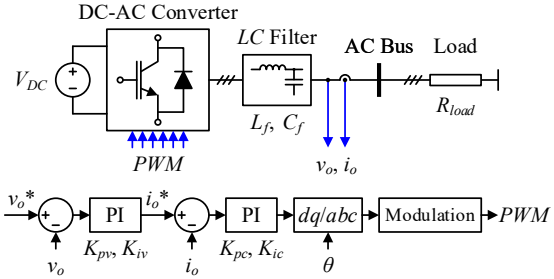

Fig. 5.10: Exemplary grid-forming converter system in microgrids with a resistive load and double-loop voltage controllers. Source: [C5].

A. Stability Analysis

To characterize the stability of the system, it can be modeled into a closed-loop transfer function as:

$$G_{sys}(s) = \frac{V_o(s)}{V_o^*(s)} \tag{5.10}$$

where, V_o* and V_o denote the Laplacian forms (in the frequency domain) of v_o* and v_o, respectively.

The stability of the system can be assessed by analyzing the characteristic roots (poles) of G_{sys}, which are equivalent to the eigenvalues if modeled into a state matrix. The root loci are plotted in Fig. 5.11 considering the variation of the filter capacitance C_f. Notably, the system becomes unstable when C_f falls below 11 μF.

The stability boundary is preliminarily verified by simulation results shown in Fig. 5.12. When C_f is decreased from 15 μF to 10 μF, the load voltage becomes highly distorted with the presence of harmonics. As the degradation of capacitors is often associated with a decrease in capacitances [78], [119], instability could thereby arise in the long run.

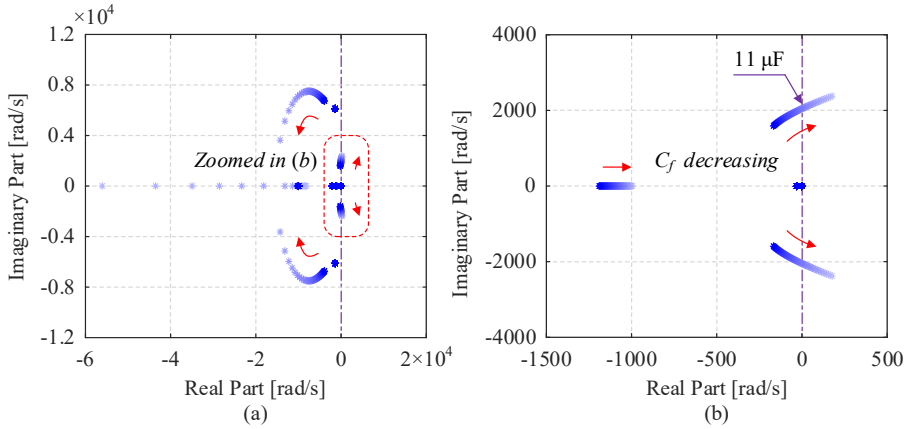

Fig. 5.11: Root loci of the exemplary system, including: (a) all the poles, and (b) zoomed view near the original point. Source: [C5].

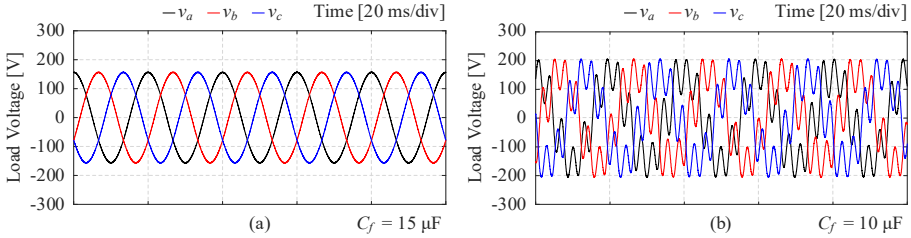

Fig. 5.12: Load voltage of the system in Fig. 5.9 when (a) C_f = 15 μF, and (b) C_f = 10 μF. The voltage waveforms are distorted when C_f is decreased, showing the system instability. Source: [C5].

B. Reliability Analysis

For reliability analysis, the filter capacitors are considered to be Metallized Polypropylene Film Capacitors (MPPF-Caps). The constant n_2 of MPPF-Caps in the lifetime model described by (3.3) typically ranges 7~10, thus assigned as 7 in this case. The capacitor R75H series from KEMET is exemplified, of which the rated parameters are given in Table 5.2.

TABLE 5.2: RATED PARAMETERS OF STUDIED CAPACITORS (KEMET R75H)

Parameters	Values
Rated lifetime[1] of the capacitor	1000 h
Rated AC voltage of the capacitor	160 V
Uncertainty of the capacitance[2]	±10%

Note 1: The rated lifetime is treated as B_{20} lifetime, which is similar in [78].
Source: [C5].

Meanwhile, the model in [119] is applied to describe the degradation of capacitors, which is formulated as:

$$C_t = C_0 \cdot (1 - \alpha \cdot t),\ \alpha > 0 \tag{5.10}$$

where, C_0 is the initial capacitance (15 µF in this case), and C_t is the capacitance at time t. The capacitance decreases as usage time goes on.

If the capacitors are considered to be worn out when the capacitances drop by 20% (as adopted in [78]), then the B_{20} lifetime is the time t when $C_t < 80\%C_0$. By simplifying the study case with balanced capacitances in three phases and Gaussian uncertainties as formulated (5.1), system unreliability turns out to be the value of CDF at $0.8C_0$, i.e., $F(0.8C_0)$, with the mean value μ equal to the time-variant capacitance C_t. Accordingly, the reliability curves are presented in Fig. 5.13, where the B_{10} lifetime of the system is observed to be around 9178 h under the AC voltage of 110 V.

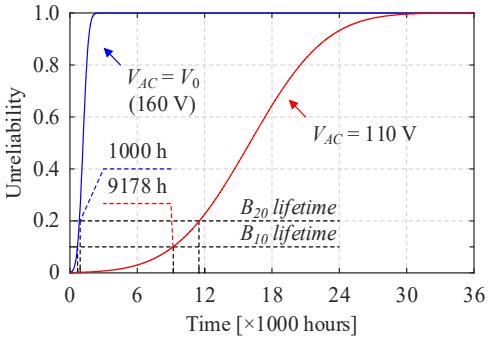

Fig. 5.13: System unreliability due to the degradation of capacitors. Source: [C5].

C. Conditional Reliability Analysis Based on Bayesian Inference

Therefore, to merge the preceding discussions in this section, the stable and reliable regions of the study case are illustrated in Fig. 5.14 (a), which satisfy:

$$\begin{cases} P(S) = P(C \geq C_S)\big|_t \\ P(R) = P(C \geq C_R)\big|_t \end{cases} \tag{5.11}$$

where, C_S and C_R are the minimum capacitance of C_f to ensure system stability and reliability. In this case, C_R is $80\%C_0$, i.e., 12 µF.

If some stability margin is reserved by assigning C_S as 11.5 μF, then the probability of stability under the condition that the system is reliable should be:

$$P(S \mid R) = \frac{P(C \geq C_S)}{P(C \geq C_R)}\bigg|_t = 1 \tag{5.12}$$

The degradation of capacitors is accordingly visualized in Fig. 5.14 (b), where C_1 denotes the mean capacitance value when F ($0.8C_0$) equals 10%, which corresponds to the B_{10} lifetime.

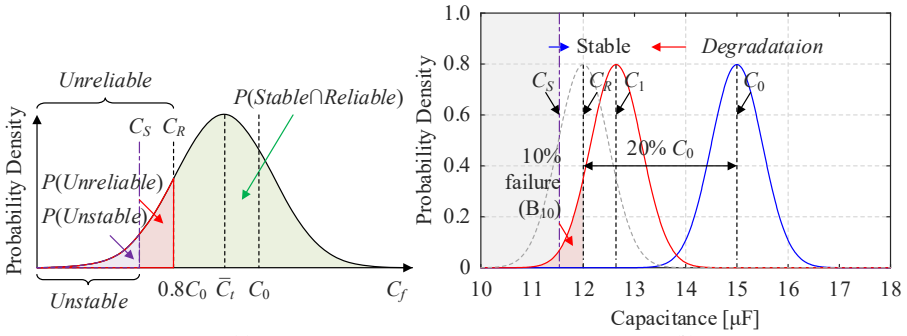

Fig. 5.14: Illustration of (a) stable and reliable regions of the system and the corresponding probabilities, and (b) the degradation of filter capacitors over time. Source: [C5].

With this, given that the system stability has been observed, the Bayesian relationship in (5.8) allows for the derivation of posterior reliability in Fig. 5.15. In this case, the observation of system stability influences the posterior reliability, which is more significant when, e.g., the system is designed with high uncertainty or operates closely to the stability boundary. Consequently, the revision on the long-term performance evaluation is recommended when real-time data or observations are available, prompting further improvement of the planning of system maintenance to reduce the overall costs.

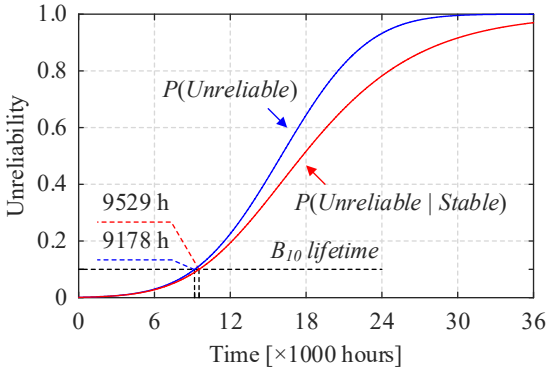

Fig. 5.15: Comparison of conditional and unconditional reliability analysis on the study case. Source: [C5].

5.4. Experimental Results and Further Reflections

The experimental results for the systems in [J4] and [C5] are presented in Fig. 5.16 and Fig. 5.17, respectively. In both groups of figures, instability occurs in the form of harmonics when there is a variation in the system parameters, when the system operates close to its stability boundary. Such instability stemming from parameter mismatch should also be categorized as dynamic stability as explained in *Chapter 2*. The figures can demonstrate the impacts of parameter uncertainty on the stability of microgrid systems, while Fig. 5.17 has additionally shed light on the interconnection between component degradations and stability concerns. In general, these results solidify the essence of integrating stability alongside reliability analysis, forming the basis for the proposed framework for operational risk evaluation.

Furthermore, the results may also inspire data-informed stability and reliability analysis, which could be advantageous in addressing the possible deviation between mathematical models and real-world systems. For instance, short-term tests could serve to delineate the stability boundary [120], while long-term parameter estimation or condition monitoring helps to calibrate the reliability evaluations [121]. By thus bridging stability and reliability, more authentic performances of microgrid systems can be concluded, yielding more informed decision-making and optimization of the operation planning in microgrids.

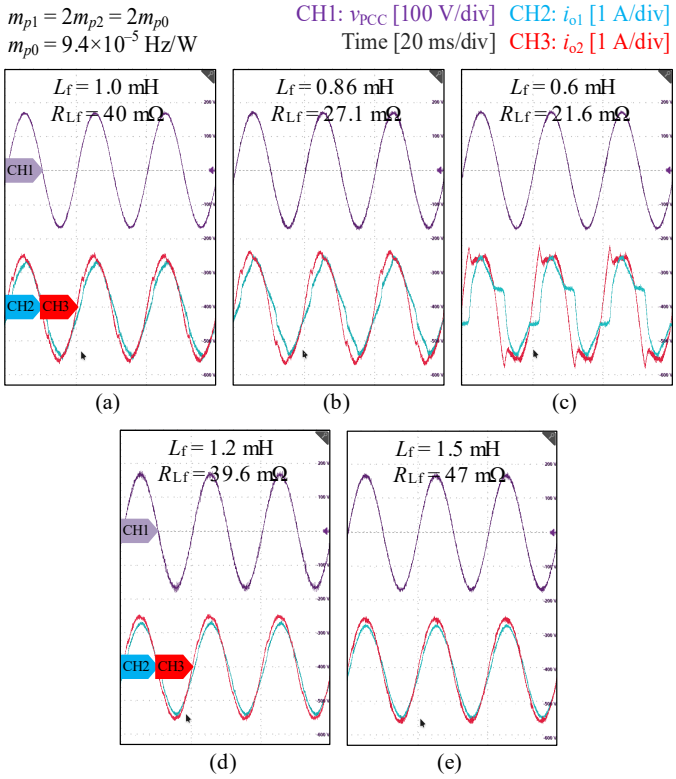

Fig. 5.16: Experimental results of the stability performance of the system used in Section 5.2 when the filter inductor L_f is varied. The load is downscaled to 0.63 kW (57 Ω per phase). Source: [J4].

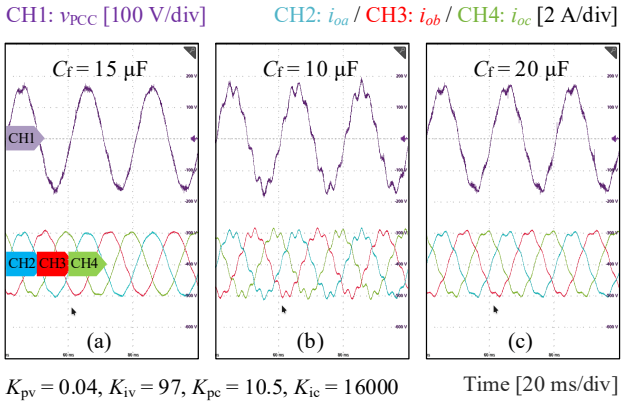

Fig. 5.17: Experimental results of the stability performance of the system used in Section 5.3 when the filter capacitor C_f is varied. The load is downscaled to 0.5 kW (80 Ω per phase). Source: [C5].

5.5. Summary

This chapter bridges the theoretical gap between stability and reliability in microgrids using probability theories. By incorporating system uncertainties, the concept of probabilistic stability has introduced new possibilities for a mathematical combination of stability and reliability. This chapter explores two major types of the connections in terms of probability analysis: the collective probability quantifies the overall operational risk of microgrids systems, while the conditional probability reflects the interdependencies of stability and reliability or the posterior performances subject to state observations. Additionally, it has also been exemplified how observed data or state variables influence the identification of system performances through the Bayesian inference. The data-informed analysis may possibly inspire more accurate system planning and anticipation of the stability and reliability risks of the microgrid systems.

Related Publications:

- **Sections 5.2 and 5.4:**

[J4] **Y. Song**, S. Sahoo, Y. Yang, and F. Blaabjerg, "Probabilistic Risk Evaluation of Microgrids Considering Stability and Reliability," *IEEE Trans. Power Electron.*, vol. 38, no. 8, pp. 10302-10312, Aug. 2023. doi: 10.1109/TPEL.2023.3278037.

- **Sections 5.3 and 5.4:**

[C5] **Y. Song**, S. Sahoo, Y. Yang, and F. Blaabjerg, "Probabilistic Mapping of Stability and Reliability in Microgrids – A Bayesian Interpretation," accepted by *EPE'23 ECCE Europe*, Aalborg, Denmark, Sept. 2023.

Chapter 6

Conclusions and Future Work

This chapter encapsulates the outcomes of this Ph.D. project – *Stability and Reliability Validation of Microgrid Systems* – as well as summarizes the main technical contributions of this project. Perspectives on potential future extensions are also provided, aiming to stimulate subsequent new research topics in relation to this emerging field.

6.1. Summary

This Ph.D. project has bridged stability and reliability analysis of microgrids for the first time and provide comprehensive validation methodologies for the two key performance indices. Through individual investigations on the stability and reliability of microgrids, the major research question specified in *Chapter 1* is preliminarily started from reliability-oriented control, recognizing its eligibility for involving stability and reliability simultaneously. Subsequently, the research question has been addressed by exploring the interactions and combinative metrics for these two performance indices. To this end, a summary is given as following for each chapter of this thesis:

Chapter 1 inaugurates the thesis by revisiting the state-of-the-art and revealing research gaps in the stability and reliability of microgrids. Both stability and reliability are desired for the safe operation of microgrid systems, wherein challenges are posed by their mismatches in timescales and modeling methodologies, thus highlighting clear motivations behind this Ph.D. project. The major research question is formed to bridge the two performance metrics, and it is partitioned into sub-questions inducing the following chapters: *Chapters 2* and *3* inspect the stability and reliability validation individually, whilst *Chapters 4* and *5* delve into comprehensive exploration from practical and theoretical perspectives, providing solutions to the major research question.

Chapter 2 accentuates the stability evaluation of microgrids at system level. The instability of microgrids is examined based on the CIGRE LV benchmark system, and the scope of this project is narrowed down to small-signal dynamic stability. In this context, a comparative study on the two typical modeling methods, state-space and impedance-based modeling, are conducted, where new quantitative

metrics are proposed for intuitively benchmarking them. Moreover, in order to facilitate the stability studies through real-time tests, model-aggregated emulation of converters has also been implemented as practical validation methodologies.

Chapter 3 expands on the system-level reliability of microgrids, underlining the reliability metrics that are derived from the PoF of power semiconductors and capacitors and leveraged into subsequent studies. With this, reliability-oriented control is formulated for enhancing the overall reliability of microgrid systems, where the loadings of converters are strategically redistributed based on their individual available lifetimes. A conditional droop adjustment strategy is proposed accordingly, showcasing improved adaptability to a wider range of loading scenarios. In terms of real-time tests, a thermal evaluation method via device current reconstruction has also been presented and validated.

Chapter 4 continues the exploration of reliability-oriented control and sheds light on the underlying stability concerns, which represents a practical connection between the two performance indices. Since reliability considerations potentially require larger control gains, the stability criteria become decisive in constraining the achievable system reliability. To this end, stability validation is necessitated, yielding the framework of stability-constrained reliability-oriented control. To address this challenge, solutions are demonstrated, providing more opportunities to expand the stability boundary and to enhance the reliability of microgrid systems.

Chapter 5 is dedicated to interpreting the combinations of stability and reliability. The perception of system uncertainties induces probabilistic stability analysis, elucidating the mathematical connections of stability and reliability in two aspects: the operational risk is redefined to merge stability and reliability into a holistic view of system performances, whilst the conditional probability describes their interdependencies and the posterior estimations subject to state observations. In addition, the exemplary results are also reflected, which inspires data-informed methodologies and may foster more pragmatic operational planning of microgrid systems.

6.2. Main Contributions of the Thesis

The main contributions of the thesis are concluded as following, highlighting the outcomes in pursuit of the research objectives specified in *Chapter 1*:

- **Contributions on the modeling and evaluation of microgrid stability:**

  The stability in microgrids and its validation has been scrutinized, providing an intuitive mapping of the modeling methods using proposed quantitative metrics. The validation of microgrid stability is substantiated by a case study,

establishing a solid foundation for the stability analysis throughout the project as well as for future PEPS.

- **Contributions on the study of microgrid reliability and improved reliability-oriented control:**

  The PoF-based reliability evaluation for microgrid systems has been revisited with specific emphasis on power semiconductors and capacitors. Upon this, a conditional reliability-oriented power sharing strategy has been developed, exhibiting improved performance and adaptability to more varied loading conditions, which can also be applicable for larger-scale PEPS.

- **Contributions on the stability constraints on microgrid reliability:**

  This project has performed an in-depth stability analysis on the reliability-oriented power sharing and revealed the underlying boundary of microgrid reliability, namely a practical connection between stability and reliability. The stability-constrained reliability-oriented control is accordingly formalized, and viable solutions have been demonstrated to tackle the potential stability concerns.

- **Contributions on the indices connecting microgrid stability and reliability:**

  This project has bridged the stability and reliability of microgrids for the first time by facilitating probabilistic analysis accounting for system uncertainties and decomposing long-term reliability performances into short-timescale frames. The operational risk is redefined for microgrid systems to manifest the collective performances, and the conditional probability is explicated using Bayesian inferences, which mathematically links the stability and reliability of microgrids.

- **Contributions on test methodologies for stability and reliability validation:**

  New methodologies for stability and reliability validation have also been suggested. Model-aggregated emulations of multi-converter buses is demonstrated for stability tests, and simplified real-time thermal evaluation of power converters is streamlined for reliability tests.

6.3. Future Research Perspectives

Nevertheless, this Ph.D. project is subject to certain assumptions, which inevitably introduce limitations that could be more extensively addressed, and the findings and outcomes could also be inspiring for future research. Thereupon, some

research perspectives as potential extensions of the scope of this project are given as following:

- **To cast light on more intricate interactions between stability and reliability:**

  This project is conducted within the context of dynamic stability, and the reliability-oriented control of AC microgrids is exemplified. However, in practice, the interactions between stability and reliability can be manifested in more diverse ways, necessitating extensive investigations on the PoF of power components. For instance, the evaluation of reliability may deviate due to the presence of harmonics in the microgrid systems or inadequate voltage/frequency stability, and the stability-reliability interdependencies are supposed to be analyzed with respect to DC microgrids or DC links as well.

- **To validate stability and reliability of microgrids considering multiple modes or more heterogeneous dynamics:**

  In this project, the stability analysis has been performed by focusing on the critical modes in small-signal models, whereas a microgrid system may potentially involve multiple unstable modes or large-signal transients. Besides, the heterogeneous dynamics of DERs and non-resistive loads in microgrids may also introduce additional interactions between stability and reliability. It is thereby favorable to incorporate these stability concerns into the reliability validation and evaluate the proposed methodologies in more general multi-dynamic microgrid systems.

- **To accommodate the proposed methodologies to larger-scale PEPS:**

  The methodologies developed in this project have been tested on small-scale systems utilizing basic droop controllers. Nevertheless, it is also essential to validate the proposed methodologies for larger-scale PEPS. To this end, the methodologies could be further accommodated to system-level operational conditions, including source and line capacities, redundancies, scheduling of maintenances, and load priorities, etc.

- **Data-based probabilistic evaluation of microgrid stability and reliability:**

  In the future, the evaluation of microgrid stability and reliability could be further improved through data-based approaches. Condition monitoring techniques can be employed to calibrate the stability and reliability evaluation either during operation or offline, where the observed data and the Bayesian inference can be leveraged to estimate operational risks more accurately. Artificial intelligence (AI) algorithms could be trained and

integrated into the proposed methodologies as more efficient tools, especially for large-scale systems with considerable amounts of data. Promising scenarios include probabilistic stability and reliability modeling, AI-driven system optimization, and contingency prediction for long-term system planning, etc.

- **Connections of microgrid stability and reliability with system resilience:**

  In modern microgrids or PEPS, the resilience is also a critical performance metric, accentuating the capability of fault ride-through or rapid system restoration when confronted with disruptive events. Hence, exploring the impacts of stability and reliability considerations on system resilience can be a future extension of this project. The combinative study of stability, reliability and resilience can aim at achieving more dependable power supplies in PEPS and minimizing system downtime during unforeseen contingencies.

Bibliography

References

[1] REN21. Renewables 2022 Global Status Report, 2022. Accessed: Feb. 2023. [Online]. Available: https://www.ren21.net/gsr-2022/

[2] Danish Energy Agency. Global Report, Apr. 2022. Accessed: Feb. 2023. [Online]. Available: https://ens.dk/en/our-services/projections-and-models/global-report

[3] Electric Power Research Institute (EPRI). Net-Zero 2050: U.S. Economy-Wide Deep Decarbonization Scenario Analysis, Dec. 2022. Accessed: Feb. 2023. [Online]. Available: https://lcri-netzero.epri.com/

[4] International Electrotechnical Commission (IEC). Electropedia: Microgrid. Dec. 2017. Accessed: Feb. 2023. [Online]. Available: https://www.electropedia.org/iev/iev.nsf/display?openform&ievref=617-04-22

[5] S. Papathanassiou, N. D. Hatziargyriou, and K. Strunz, "A Benchmark Low Voltage Microgrid Network," in *Proc. CIGRE Symposium: Power Systems with Dispersed Generation*, Athens, Greece, Apr. 2005, pp. 1-8.

[6] S. Peyghami, P. Davari, M. Fotuhi-Firuzabad, and F. Blaabjerg, "Standard Test Systems for Modern Power System Analysis: An Overview," *IEEE Ind. Electron. Mag.*, vol. 13, no. 4, pp. 86-105, Dec. 2019, doi: 10.1109/MIE.2019.2942376.

[7] J. Fang, H. Li, Y. Tang, and F. Blaabjerg, "On the Inertia of Future More-Electronics Power Systems," *IEEE J. Emerging Sel. Top. Power Electron.*, vol. 7, no. 4, pp. 2130-2146, Dec. 2019, doi: 10.1109/JESTPE.2018.2877766.

[8] M. G. Taul, "Synchronization Stability of Grid-Connected Converters under Grid Faults," Ph.D. thesis, Aalborg University, Denmark, 2020.

[9] CRO Forum. Power Blackout Risks – Risk Management Options: Emerging Risk Initiative – Position Paper, Nov. 2011. Accessed: Feb. 2023. [Online]. Available: https://www.thecroforum.org/cro-forum-positioning-on-power-blackout-risks

[10] H. H. Alhelou, M. E. Hamedani-Golshan, T. C. Njenda, and P. Siano, "A Survey on Power System Blackout and Cascading Events: Research Motivations and Challenges," *Energies*, vol. 12, no. 4, Feb. 2019, doi: 10.3390/EN12040682.

[11] U.S.-Canada Power System Outage Task Force. Final Report on the August 14, 2003 Blackout in the United States and Canada: Causes and Recommendations, 2004. Accessed: Feb. 2023. [Online]. Available: https://www.energy.gov/

[12] S.-K. Joo, J.-C. Kim, and C.-C. Liu, "Empirical Analysis of the Impact of 2003 Blackout on Security Values of U.S. Utilities and Electrical Equipment Manufacturing Firms," *IEEE Trans. Power Syst.*, vol. 22, no. 3, pp. 1012-1018, Aug.

2007, doi: 10.1109/TPWRS.2007.901278.

[13] Electricity Consumers Resource Council (ELCON). The Economic Impacts of the August 2003 Blackout, Feb. 2004. Accessed: Sept. 2020. [Online]. Available: https://elcon.org/

[14] EPRI. Enhancing Energy System Reliability and Resiliency in a Net-Zero Economy, Jan. 2022. Accessed: Mar. 2023. [Online]. Available: https://www.epri.com/research/products/000000003002023437

[15] Energy Systems Integration Group (ESIG). Design Study Requirements for a U.S. Macrogrid: A Path to Achieving the Nation's Energy System Transformation Goals, Feb. 2022. Accessed: Mar. 2023. [Online]. Available: https://www.esig.energy/design-study-requirements-for-a-u-s-macrogrid/

[16] K. N. Hasan, R. Preece, and J. V. Milanovic, "Existing Approaches and Trends in Uncertainty Modelling and Probabilistic Stability Analysis of Power Systems with Renewable Generation," *Renewable Sustainable Energy Rev.*, vol. 101, pp. 168-180, Mar. 2019, doi: 10.1016/J.RSER.2018.10.027.

[17] S. Q. Bu, W. Du, H. F. Wang, Z. Chen, L. Y. Xiao, and H. F. Li, "Probabilistic Analysis of Small-Signal Stability of Large-Scale Power Systems as Affected by Penetration of Wind Generation," *IEEE Trans. Power Syst.*, vol. 27, no. 2, pp. 762-770, May 2012, doi: 10.1109/TPWRS.2011.2170183.

[18] E. Carpaneto and G. Chicco, "Evaluation of the Probability Density Functions of Distribution System Reliability Indices with a Characteristic Functions-Based Approach," *IEEE Trans. Power Syst.*, vol. 19, no. 2, pp. 724-734, May 2004, doi: 10.1109/TPWRS.2003.821627.

[19] K. Ogata, *Modern Control Engineering*, 5th ed. Pearson, 2010, ISBN: 978-0-13-615673-4.

[20] P. Kundur, *Power System Stability and Control*, 1st ed. McGraw-Hill, 1994, ISBN: 978-0-07-035958-X.

[21] P. Kundur, J. Paserba, V. Ajjarapu, G. Andersson, A. Bose, C. A. Cañizares, N. Hatziargyriou, D. Hill, A. Stankovic, C. Taylor, T. V. Cutsem, and V. Vittal, "Definition and Classification of Power System Stability – IEEE/CIGRE Joint Task Force on Stability Terms and Definitions," *IEEE Trans. Power Syst.*, vol. 19, no. 3, pp. 1387-1401, May 2004, doi: 10.1109/TPWRS.2004.825981.

[22] N. Hatziargyriou, J. V. Milanovic, C. Rahmann, V. Ajjarapu, C. Cañizares, I. Erlich, D. Hill, I. Hiskens, I. Kamwa, B. Pal, P. Pourbeik, J. Sanchez-Gasca, A. Stankovic, T. Van Cutsem, V. Vittal, and C. Vournas, "Definition and Classification of Power System Stability – Revisited & Extended," *IEEE Trans. Power Syst.*, vol. 36, no. 4, pp. 3271-3281, Jul. 2021, doi: 10.1109/TPWRS.2020.3041774.

[23] M. Farrokhabadi, C. A. Cañizares, J. W. Simpson-Porco, E. Nasr, L. Fan, P. A. Mendoza-Araya, R. Tonkoski, U. Tamrakar, N. Hatziargyriou, D. Lagos, R. W. Wies, M. Paolone, M. Liserre, L. Meegahapola, M. Kabalan, A. H. Hajimiragha, D. Peralta, M. A. Elizondo, K. P. Schneider, F. K. Tuffner, and J. Reilly, "Microgrid

Stability Definitions, Analysis, and Examples," *IEEE Trans. Power Syst.*, vol. 35, no. 1, pp. 13-29, Jan. 2020, doi: 10.1109/TPWRS. 2019.2925703.

[24] Z. Shuai, Y. Sun, Z. J. Shen, W. Tian, C. Tu, Y. Li, and X. Yin, "Microgrid Stability: Classification and a Review," *Renewable Sustainable Energy Rev.*, vol. 58, pp. 167-179, May 2016, doi: 10.1016/J.RSER.2015.12.201.

[25] X. Wang and F. Blaabjerg, "Harmonic Stability in Power Electronic-Based Power Systems: Concept, Modeling, and Analysis," *IEEE Trans. Smart Grid*, vol. 10, no. 3, pp. 2858-2870, May 2019, doi: 10.1109/TSG.2018.2812712.

[26] Q. Peng, Q. Jiang, Y. Yang, T. Liu, H. Wang, and F. Blaabjerg, "On the Stability of Power Electronics-Dominated Systems: Challenges and Potential Solutions," *IEEE Trans. Ind. Appl.*, vol. 55, no. 6, pp. 7657-7670, Nov./Dec. 2019, doi: 10.1109/TIA.2019.2936788.

[27] N. Pogaku, M. Prodanovic, and T. C. Green, "Modeling, Analysis and Testing of Autonomous Operation of an Inverter-Based Microgrid," *IEEE Trans. Power Electron.*, vol. 22, no. 2, pp. 613-625, Mar. 2007, doi: 10.1109/TPEL.2006.890003.

[28] Y. Wang, X. Wang, F. Blaabjerg, and Z. Chen, "Harmonic Instability Assessment Using State-Space Modeling and Participation Analysis in Inverter-Fed Power Systems," *IEEE Trans. Ind. Electron.*, vol. 64, no. 1, pp. 806-816, Jan. 2017, doi: 10.1109/TIE.2016.2588458.

[29] Y. Wang, X. Wang, Z. Chen, and F. Blaabjerg, "Small-Signal Stability Analysis of Inverter-Fed Power Systems Using Component Connection Method," *IEEE Trans. Smart Grid*, vol. 9, no. 5, pp. 5301-5310, Sept. 2018, doi: 10.1109/TSG.2017.2686841.

[30] J. Sun, "Impedance-Based Stability Criterion for Grid-Connected Inverters," *IEEE Trans. Power Electron.*, vol. 26, no. 11, pp. 3075-3078, Nov. 2011, doi: 10.1109/TPEL.2011.2136439.

[31] L. Harnefors, "Modeling of Three-Phase Dynamic Systems Using Complex Transfer Functions and Transfer Matrices," *IEEE Trans. Ind. Electron.*, vol. 54, no. 4, pp. 2239-2248, Aug. 2007, doi: 10.1109/TIE.2007.894769.

[32] L. Harnefors, M. Bongiorno, and S. Lundberg, "Input-Admittance Calculation and Shaping for Controlled Voltage-Source Converters," *IEEE Trans. Ind. Electron.*, vol. 54, no. 6, pp. 3323-3334, Dec. 2007, doi: 10.1109/TIE.2007.904022.

[33] X. Wang, F. Blaabjerg, and W. Wu, "Modeling and Analysis of Harmonic Stability in an AC Power-Electronics-Based Power System," *IEEE Trans. Power Electron.*, vol. 29, no. 12, pp. 6421-6432, Dec. 2014, doi: 10.1109/TPEL.2014.2306432.

[34] X. Wang, F. Blaabjerg, and P. C. Loh, "An Impedance-Based Stability Analysis Method for Paralleled Voltage Source Converters," in *Proc. IPEC 2014 – ECCE Asia*, Hiroshima, Japan, May 2014, pp. 1529-1535, doi: 10.1109/IPEC.2014. 6869788.

[35] X. Wang, L. Harnefors, and F. Blaabjerg, "Unified Impedance Model of Grid-Connected Voltage-Source Converters," *IEEE Trans. Power Electron.*, vol. 33, no. 2, pp. 1775-1787, Feb. 2018, doi: 10.1109/TPEL.2017.2684906.

[36] Y. Li, Y. Gu, Y. Zhu, A. Junyent-Ferre, X. Xiang, and T. C. Green, "Impedance

Circuit Model of Grid-Forming Inverter: Visualizing Control Algorithms as Circuit Elements," *IEEE Trans. Power Electron.*, vol. 36, no. 3, pp. 3377-3395, Mar. 2021, doi: 10.1109/TPEL.2020.3015158.

[37] C. Zhang, X. Cai, A. Rygg, and M. Molinas, "Sequence Domain SISO Equivalent Models of a Grid-Tied Voltage Source Converter System for Small-Signal Stability Analysis," *IEEE Trans. Energy Convers.*, vol. 33, no. 2, pp. 741-749, Jun. 2018, doi: 10.1109/TEC.2017.2766217.

[38] X. Wang, M. G. Taul, H. Wu, Y. Liao, F. Blaabjerg, and L. Harnefors, "Grid-Synchronization Stability of Converter-Based Resources – An Overview," *IEEE Open J. Ind. Appl.*, vol. 1, pp. 115-134, Aug. 2020, doi: 10.1109/OJIA.2020.3020392.

[39] H. Wu and X. Wang, "Design-Oriented Transient Stability Analysis of Grid-Connected Converters with Power Synchronization Control," *IEEE Trans. Ind. Electron.*, vol. 66, no. 8, pp. 6473-6482, Aug. 2019, doi: 10.1109/TIE.2018.2875669.

[40] H. Wu and X. Wang, "Design-Oriented Transient Stability Analysis of PLL-Synchronized Voltage-Source Converters," *IEEE Trans. Power Electron.*, vol. 35, no. 4, pp. 3573-3589, Apr. 2020, doi: 10.1109/TPEL.2019.2937942.

[41] Y. Zhang and L. Xie, "Online Dynamic Security Assessment of Microgrid Interconnections in Smart Distribution Systems," *IEEE Trans. Power Syst.*, vol. 30, no. 6, pp. 3246-3254, Nov. 2015, doi: 10.1109/TPWRS.2014.2374876.

[42] Y. Zhang and L. Xie, "A Transient Stability Assessment Framework in Power Electronic-Interfaced Distribution Systems," *IEEE Trans. Power Syst.*, vol. 31, no. 6, pp. 5106-5114, Nov. 2016, doi: 10.1109/TPWRS.2016.2531745.

[43] Q. Xu, X. Wang, M. G. Taul, and F. Blaabjerg, "Conceptual Systematic Stability Analysis of Power Electronics based Power Systems," in *Proc. 2019 IEEE ECCE*, Baltimore, MD, USA, Sept.-Oct. 2019, pp. 2232-2238, doi: 10.1109/ECCE.2019.8912806.

[44] L. Fan and Z. Miao, "Admittance-Based Stability Analysis: Bode Plots, Nyquist Diagrams or Eigenvalue Analysis?" *IEEE Trans. Power Syst.*, vol. 35, no. 4, pp. 3312-3315, Jul. 2020, doi: 10.1109/TPWRS.2020.2996014.

[45] L. Huang, C. Wu, D. Zhou, and F. Blaabjerg, "Comparison of Three Small-Signal Stability Analysis Methods for Grid-Following Inverter," in *Proc. 2021 ACEMP & OPTIM*, Brasov, Romania, Sept. 2021, pp. 34-41, doi: 10.1109/OPTIM-ACEMP50812.2021.9590036.

[46] A. M. Hakami, K. N. Hasan, M. Alzubaidi, and M. Datta, "A Review of Uncertainty Modelling Techniques for Probabilistic Stability Analysis of Renewable-Rich Power Systems," *Energies*, vol. 16, no. 1, Dec. 2022, doi: 10.3390/EN16010112.

[47] R. Preece, N. C. Woolley, and J. V. Milanovic, "The Probabilistic Collocation Method for Power-System Damping and Voltage Collapse Studies in the Presence of Uncertainties," *IEEE Trans. Power Syst.*, vol. 28, no. 3, pp. 2253-2262, Aug. 2013, doi: 10.1109/TPWRS.2012.2227837.

[48] W. Chen, X. Xie, D. Wang, H. Liu, and H. Liu, "Probabilistic Stability Analysis of

Subsynchronous Resonance for Series-Compensated DFIG-Based Wind Farms," *IEEE Trans. Sustainable Energy*, vol. 9, no. 1, pp. 400-409, Jan. 2018, doi: 10.1109/TSTE.2017.2737599.

[49] K. Ye, J. Zhao, N. Duan, and Y. Zhang, "Physics-Informed Sparse Gaussian Process for Probabilistic Stability Analysis of Large-Scale Power System with Dynamic PVs and Loads," *IEEE Trans. Power Syst.*, 2022, early access, doi: 10.1109/TPWRS.2022.3188182.

[50] A. Birolini, *Reliability Engineering: Theory and Practice*, 8th ed. Springer, 2017, ISBN: 978-3-662-54208-8.

[51] R. Billinton and R. N. Allan, *Reliability Evaluation of Power Systems*, 2nd ed. Springer, 1996, ISBN: 978-1-4899-1862-8.

[52] S. Peyghami, P. Palensky, and F. Blaabjerg, "An Overview on the Reliability of Modern Power Electronic Based Power Systems," *IEEE Open J. Power Electron.*, vol. 1, pp. 34-50, Feb. 2020, doi: 10.1109/OJPEL.2020.2973926.

[53] J. Choi, T. D. Mount, and R. J. Thomas, "Transmission Expansion Planning Using Contingency Criteria," *IEEE Trans. Power Syst.*, vol. 22, no. 4, pp. 2249-2261, Nov. 2007, doi: 10.1109/TPWRS.2007.908478.

[54] US MIL-HDBK-217F. *Reliability Prediction of Electronic Equipment.* Dec. 1991.

[55] M. J. Cushing, D. E. Mortin, T. J. Stadterman, and A. Malhotra, "Comparison of Electronics-Reliability Assessment Approaches," *IEEE Trans. Reliab.*, vol. 42, no. 4, pp. 542-546, Dec. 1993, doi: 10.1109/24.273574.

[56] H. Wang and F. Blaabjerg, "Power Electronics Reliability: State of the Art and Outlook," *IEEE J. Emerging Sel. Top. Power Electron.*, vol. 9, no. 6, pp. 6476-6493, Dec. 2021, doi: 10.1109/JESTPE.2020.3037161.

[57] U.-M. Choi, S. Jørgensen, and F. Blaabjerg, "Advanced Accelerated Power Cycling Test for Reliability Investigation of Power Device Modules," *IEEE Trans. Power Electron.*, vol. 31, no. 12, pp. 8371-8386, Dec. 2016, doi: 10.1109/TPEL.2016.2521899.

[58] U.-M. Choi, F. Blaabjerg, and S. Jørgensen, "Power Cycling Test Methods for Reliability Assessment of Power Device Modules in Respect to Temperature Stress," *IEEE Trans. Power Electron.*, vol. 33, no. 3, pp. 2531-2551, Mar. 2018, doi: 10.1109/TPEL.2017.2690500.

[59] Z. Wang, B. Tian, W. Qiao, and L. Qu, "Real-Time Aging Monitoring for IGBT Modules Using Case Temperature," *IEEE Trans. Ind. Electron.*, vol. 63, no. 2, pp. 1168-1178, Feb. 2016, doi: 10.1109/TIE.2015.2497665.

[60] Y. Zhu, K. Ma, and X. Cai, "Thermal Characterization Method of Power Semiconductors Based on H-Bridge Testing Circuit," *IEEE Trans. Power Electron.*, vol. 34, no. 9, pp. 8268-8273, Sept. 2019, doi: 10.1109/TPEL.2019.2900253.

[61] Y. Peng, Y. Shen, and H. Wang, "A Converter-Level ON-State Voltage Measurement Method for Power Semiconductor Devices," *IEEE Trans. Power Electron.*, vol. 36, no. 2, pp. 1220-1224, Feb. 2021, doi: 10.1109/TPEL. 2020.3009934.

[62] B. Yao, Q. Wang, H. Wang, K. Hasegawa, and H. Wang, "A Robust Testing

Method for DC and AC Capacitors with Minimum Required Power Supply," *IEEE Trans. Power Electron.*, vol. 37, no. 5, pp. 4942-4946, May 2022, doi: 10.1109/TPEL.2021.3130085.

[63] H. Soliman, H. Wang, and F. Blaabjerg, "A Review of the Condition Monitoring of Capacitors in Power Electronic Converters," *IEEE Trans. Ind. Appl.*, vol. 52, no. 6, pp. 4976-4989, Nov./Dec. 2016, doi: 10.1109/TIA.2016.2591906.

[64] S. Yang, A. Bryant, P. Mawby, D. Xiang, L. Ran, and P. Tavner, "An Industry-Based Survey of Reliability in Power Electronic Converters," *IEEE Trans. Ind. Appl.*, vol. 47, no. 3, pp. 1441-1451, May/Jun. 2011, doi: 10.1109/TIA.2011.2124436.

[65] H. Wang, M. Liserre, F. Blaabjerg, P. d. P. Rimmen, J. B. Jacobsen, T. Kvisgaard, and J. Landkildehus, "Transitioning to Physics-of-Failure as a Reliability Driver in Power Electronics," *IEEE J. Emerging Sel. Top. Power Electron.*, vol. 2, no. 1, pp. 97-114, Mar. 2014, doi: 10.1109/JESTPE.2013.2290282.

[66] M. Ciappa, F. Carbognani, and W. Fichtner, "Lifetime Prediction and Design of Reliability Tests for High-Power Devices in Automotive Applications," *IEEE Trans. Device Mater. Reliab.*, vol. 3, no. 4, pp. 191-196, Dec. 2003, doi: 10.1109/TDMR.2003.818148.

[67] H. Wang, K. Ma, and F. Blaabjerg, "Design for Reliability of Power Electronic Systems," in *Proc. 2012 IEEE IECON*, Montreal, QC, Canada, Oct. 2012, pp. 33-44, doi: 10.1109/IECON.2012.6388833.

[68] W. Lai, M. Chen, L. Ran, O. Alatise, S. Xu, and P. Mawby, "Low ΔT_j Stress Cycle Effect in IGBT Power Module Die-Attach Lifetime Modeling," *IEEE Trans. Power Electron.*, vol. 31, no. 9, pp. 6575-6585, Dec. 2016, doi: 10.1109/TPEL.2015.2501540.

[69] H. Wang and F. Blaabjerg, "Reliability of Capacitors for DC-Link Applications in Power Electronic Converters - An Overview," *IEEE Trans. Ind. Appl.*, vol. 50, no. 5, pp. 3569-3578, Sep.-Oct. 2014, doi: 10.1109/TIA.2014.2308357.

[70] A. Albertsen, "Electrolytic Capacitor Lifetime Estimation," *Jianghai Europe GmbH*, pp. 1-13, Apr. 2010.

[71] Y. Shen, A. Chub, H. Wang, D. Vinnikov, E. Liivik, and F. Blaabjerg, "Wear-Out Failure Analysis of an Impedance-Source PV Microinverter Based on System-Level Electrothermal Modeling," *IEEE Trans. Ind. Electron.*, vol. 66, no. 5, pp. 3914-3927, May 2019, doi: 10.1109/TIE.2018.2831643.

[72] Infineon. AN2015-10: Transient Thermal Measurements and Thermal Equivalent Circuit Models, Apr. 2020. [Online]. Available: https://www.infineon.com/dgdl/Infineon-Thermal_equivalent_circuit_models-ApplicationNotes-v01_02-EN.pdf?fileId=db3a30431a5c32f2011aa65358394dd2

[73] K. Ma, N. He, M. Liserre, and F. Blaabjerg, "Frequency-Domain Thermal Modeling and Characterization of Power Semiconductor Devices," *IEEE Trans. Power Electron.*, vol. 31, no. 10, pp. 7183-7193, Oct. 2016, doi: 10.1109/TPEL.2015.2509506.

[74] H. Wang, R. Zhu, H. Wang, M. Liserre, and F. Blaabjerg, "A Thermal Modeling

Method Considering Ambient Temperature Dynamics," *IEEE Trans. Power Electron.*, vol. 35, no. 1, pp. 6-9, Jan. 2020, doi: 10.1109/TPEL.2019.2924723.

[75] H. Wang and H. Wang, "Analytical Modeling and Design of Capacitor Bank Considering Thermal Coupling Effect," *IEEE Trans. Power Electron.*, vol. 36, no. 3, pp. 2629-2640, Mar. 2021, doi: 10.1109/TPEL.2020.3014913.

[76] M. Xu, K. Ma, B. Liu, and X. Cai, "Modeling and Correlation of Two Thermal Paths in Frequency-Domain Thermal Impedance Model of Power Module," *IEEE J. Emerging Sel. Top. Power Electron.*, vol. 9, no. 4, pp. 3971-3981, Aug. 2021, doi: 10.1109/JESTPE.2020.3034574.

[77] M. Xu, K. Ma, X. Cai, G. Cao, and Y. Zhang, "Lumped Thermal Coupling Model of Multichip Power Module Enabling Case Temperature as Reference Node," *IEEE Trans. Power Electron.*, vol. 37, no. 10, pp. 11502-11506, Oct. 2022, doi: 10.1109/TPEL.2022.3173653.

[78] D. Zhou, H. Wang, and F. Blaabjerg, "Mission Profile Based System-Level Reliability Analysis of DC/DC Converters for a Backup Power Application," *IEEE Trans. Power Electron.*, vol. 33, no. 9, pp. 8030-8039, Sept. 2018, doi: 10.1109/TPEL.2017.2769161.

[79] A. Sangwongwanich, Y. Yang, D. Sera, and F. Blaabjerg, "Lifetime Evaluation of Grid-Connected PV Inverters Considering Panel Degradation Rates and Installation Sites," *IEEE Trans. Power Electron.*, vol. 33, no. 2, pp. 1225-1236, Feb. 2018, doi: 10.1109/TPEL.2017.2678169.

[80] Q. Xu, Y. Xu, P. Tu, T. Zhao, and P. Wang, "Systematic Reliability Modeling and Evaluation for On-Board Power Systems of More Electric Aircrafts," *IEEE Trans. Power Syst.*, vol. 34, no. 4, pp. 3264-3273, Jul. 2019, doi: 10.1109/TPWRS.2019.2896454.

[81] S. Peyghami, H. Wang, P. Davari, and F. Blaabjerg, "Mission-Profile-Based System-Level Reliability Analysis in DC Microgrids," *IEEE Trans. Ind. Appl.*, vol. 55, no. 5, pp. 5055-5067, Sept./Oct. 2019, doi: 10.1109/TIA.2019.2920470.

[82] S. Peyghami, F. Blaabjerg, and P. Palensky, "Incorporating Power Electronic Converters Reliability into Modern Power System Reliability Analysis," *IEEE J. Emerging Sel. Top. Power Electron.*, vol. 9, no. 2, pp. 1668-1681, Apr. 2021, doi: 10.1109/JESTPE.2020.2967216.

[83] Y. Song and B. Wang, "Survey on Reliability of Power Electronic Systems," *IEEE Trans. Power Electron.*, vol. 28, no. 1, pp. 591-604, Jan. 2013, doi: 10.1109/TPEL.2012.2192503.

[84] M. Liserre, G. Buticchi, J. I. Leon, A. M. Alcaide, V. Raveendran, Y. Ko, M. Andresen, V. G. Monopoli, and L. G. Franquelo, "Power Routing: A New Paradigm for Maintenance Scheduling," *IEEE Ind. Electron. Mag.*, vol. 14, no. 3, pp. 33-45, Sept. 2020, doi: 10.1109/MIE.2020.2975049.

[85] M. Andresen, K. Ma, G. Buticchi, J. Falck, F. Blaabjerg, and M. Liserre, "Junction Temperature Control for More Reliable Power Electronics," *IEEE Trans. Power Electron.*, vol. 33, no. 1, pp. 765-776, Jan. 2018, doi: 10.1109/TPEL.2017.2665697.

[86] M. Andresen, V. Raveendran, G. Buticchi, and M. Liserre, "Lifetime-Based Power Routing in Parallel Converters for Smart Transformer Application," *IEEE Trans. Ind. Electron.*, vol. 65, no. 2, pp. 1675-1684, Feb. 2018, doi: 10.1109/TIE.2017.2733426.

[87] J. Falck, G. Buticchi, and M. Liserre, "Thermal Stress Based Model Predictive Control of Electric Drives," *IEEE Trans. Ind. Appl.*, vol. 54, no. 2, pp. 1513-1522, Mar.-Apr. 2018, doi: 10.1109/TIA.2017.2772198.

[88] A. Sangwongwanich, Y. Yang, D. Sera, and F. Blaabjerg, "Mission Profile-Oriented Control for Reliability and Lifetime of Photovoltaic Inverters," *IEEE Trans. Ind. Appl.*, vol. 56, no. 1, pp. 601-610, Jan./Feb. 2020, doi: 10.1109/TIA.2019.2947227.

[89] M. Andresen, G. Buticchi, and M. Liserre, "Thermal Stress Analysis and MPPT Optimization of Photovoltaic Systems," *IEEE Trans. Ind. Electron.*, vol. 63, no. 8, pp. 4889-4898, Aug. 2016, doi: 10.1109/TIE.2016.2549503.

[90] I. U. Nutkani, P. C. Loh, P. Wang, and F. Blaabjerg, "Cost-Prioritized Droop Schemes for Autonomous AC Microgrids," *IEEE Trans. Power Electron.*, vol. 30, no. 2, pp. 1109-1119, Feb. 2015, doi: 10.1109/TPEL.2014.2313605.

[91] Y. Wang, D. Liu, P. Liu, F. Deng, D. Zhou, and Z. Chen, "Lifetime-Oriented Droop Control Strategy for AC Islanded Microgrids," *IEEE Trans. Ind. Appl.*, vol. 55, no. 3, pp. 3252-3263, 2019, doi: 10.1109/TIA.2019.2898847.

[92] S. Peyghami, P. Davari, and F. Blaabjerg, "System-Level Reliability-Oriented Power Sharing Strategy for DC Power Systems," *IEEE Trans. Ind. Appl.*, vol. 55, no. 5, pp. 4865-4875, Sept./Oct. 2019, doi: 10.1109/TIA.2019.2918049.

[93] J. Jiang, S. Peyghami, C. Coates, and F. Blaabjerg, "A Decentralized Reliability-Enhanced Power Sharing Strategy for PV-Based Microgrids," *IEEE Trans. Power Electron.*, vol. 36, no. 6, pp. 7281-7293, Jun. 2021, doi: 10.1109/TPEL.2020.3040991.

[94] S. Peyghami, P. Palensky, and F. Blaabjerg, "An Overview on the Reliability of Modern Power Electronic Based Power Systems," *IEEE Open J. Power Electron.*, vol. 1, pp. 34-50, Feb. 2020, doi: 10.1109/OJPEL.2020.2973926.

[95] D. Boroyevich, I. Cvetković, D. Dong, R. Burgos, F. F. Wang, and F. C. Lee, "Future Electronic Power Distribution Systems – A Contemplative View," in *Proc. OPTIM 2010*, Brasov, Romania, May 2010, pp. 1369-1380, doi: 10.1109/OPTIM.2010.5510477.

[96] J. D. McCalley, A. A. Fouad, V. Vittal, A. A. Irizarry-Rivera, B. L. Agrawal, and R. G. Farmer, "A Risk-Based Security Index for Determining Operating Limits in Stability-Limited Electric Power Systems," *IEEE Trans. Power Syst.*, vol. 12, no. 3, pp. 1210-1219, Aug. 1997.

[97] CIGRE Task Force 38.03.12. "Power System Security Assessment: A Position Paper," *Electra*, vol. 175, pp. 49-77, 1997.

[98] K. Morison, L. Wang, and P. Kundur, "Power System Security Assessment," *IEEE Power Energy Mag.*, vol. 2, no. 5, pp. 30-39, Sept.-Oct. 2004.

[99] J. Rocabert, A. Luna, F. Blaabjerg, and P. Rodríguez, "Control of Power

Converters in AC Microgrids," *IEEE Trans. Power Electron.*, vol. 27, no. 11, pp. 4734-4749, Nov. 2012, doi: 10.1109/TPEL.2012.2199334.

[100] Infineon. AN2019-05: PC and TC Diagrams, Rev. 2.1, Feb. 2021. Accessed: Apr. 2022. [Online] Available: https://www.infineon.com/dgdl/Infineon-AN2019-05_PC_and_TC_Diagrams-ApplicationNotes-v02_01-EN.pdf?fileId=5546d46269e1c019016a594443e4396b

[101] K. Ma, J. Wang, X. Cai, and F. Blaabjerg, "AC Grid Emulations for Advanced Testing of Grid-Connected Converters – An Overview," *IEEE Trans. Power Electron.*, vol. 36, no. 2, pp. 1626-1645, Feb. 2021, doi: 10.1109/TPEL. 2020.3011176.

[102] J. Liu and M. Molinas, "Impact of Digital Time Delay on the Stable Grid-Hosting Capacity of Large-Scale Centralised PV Plant," *IET Renewable Power Gener.*, vol. 15, no. 7, pp. 1422-1435, May 2021, doi: 10.1049/RPG2.12097.

[103] C. Dong, S. Yang, H. Jia, and P. Wang, "Padé-Based Stability Analysis for a Modular Multilevel Converter Considering the Time Delay in the Digital Control System," *IEEE Trans. Ind. Electron.*, vol. 66, no. 7, pp. 5242-5253, Jul. 2019, doi: 10.1109/TIE.2018.2868008.

[104] S. Golestan, J. M. Guerrero, and J. C. Vasquez, "Three-Phase PLLs: A Review of Recent Advances," *IEEE Trans. Power Electron.*, vol. 32, no. 3, pp. 1894-1907, Mar. 2017, doi: 10.1109/TPEL.2016.2565642.

[105] P. Vorobev, P.-H. Huang, M. Al Hosani, J. L. Kirtley, and K. Turitsyn, "High-Fidelity Model Order Reduction for Microgrids Stability Assessment," *IEEE Trans. Power Syst.*, vol. 33, no. 1, pp. 874-887, Jan. 2018, doi: 10.1109/TPWRS. 2017.2707400.

[106] A. Gorbunov, J. C.-H. Peng, and P. Vorobev, "Identification of Critical Clusters in Inverter-Based Microgrids," *Electr. Power Syst. Res.*, vol. 189, 106731, Dec. 2020, doi: 10.1016/J.EPSR.2020.106731.

[107] K. Ma and Y. Song, "Power-Electronic-Based Electric Machine Emulator Using Direct Impedance Regulation," *IEEE Trans. Power Electron.*, vol. 35, no. 10, pp. 10673-10680, Oct. 2020, doi: 10.1109/TPEL.2020.2976143.

[108] Z. Zhou, M. S. Khanniche, P. Igic, S. T. Kong, M. Towers, and P. A. Mawby, "A Fast Power Loss Calculation Method for Long Real Time Thermal Simulation of IGBT Modules for a Three-Phase Inverter System," in *Proc. EPE'05*, Sept. 2006, pp. 33-46, doi: 10.1109/EPE.2005.219598.

[109] W. Wang, H. R. Wickramasinghe, K. Ma, and G. Konstantinou, "Real-Time Co-Simulation for Electrical and Thermal Analysis of Power Electronics," in *Proc. 2019 ICPES*, Perth, WA, Australia, Dec. 2019, doi: 10.1109/ICPES47639. 2019.9105352.

[110] Q. Li, H. Bai, E. Breaz, R. Roche, and F. Gao, "Lookup Table-based Electro-Thermal Real-Time Simulation of Output Series Interleaved Boost Converter for Fuel Cell Applications," in *Proc. IECON 2021*, Toronto, ON, Canada, Oct. 2021, pp. 1-6, doi: 10.1109/IECON48115.2021.9589447.

[111] T. Horiguchi, T. Oi, M. Harakawa, A. Imanaka, and T. Nagano, "Real-time

Electro-Thermal Simulation of a Motor Drive System," in *Proc. EPE'09*, Sept. 2009, pp. 1-7.

[112] A. T. Bryant, P. A. Mawby, P. R. Palmer, E. Santi, and J. L. Hudgins, "Exploration of Power Device Reliability Using Compact Device Models and Fast Electrothermal Simulation," *IEEE Trans. Ind. Appl.*, vol. 44, no. 3, pp. 894-903, May/Jun. 2008, doi: 10.1109/TIA.2008.921388.

[113] R. Bayerer, T. Herrmann, T. Licht, J. Lutz, and M. Feller, "Model for Power Cycling Lifetime of IGBT Modules - Various Factors Influencing Lifetime," in *Proc. 5th International Conference on Integrated Power Electronics Systems*, Nuremberg, Germany, Mar. 2008, pp. 1-6.

[114] J. Lutz, C. Schwabe, G. Zeng, and L. Hein, "Validity of Power Cycling Lifetime Models for Modules and Extension to Low Temperature Swings," in *Proc. EPE'20 ECCE Europe*, Lyon, France, Sept. 2020, pp. P.1-P.9, doi: 10.23919/EPE20ECCE Europe43536.2020.9215609.

[115] M. A. Miner, "Cumulative Damage in Fatigue," *J. Appl. Mech.*, vol. 12, no. 3, pp. A159-A164, 1945, doi: 10.1115/1.4009458.

[116] Semikron. Application Manual Power Semiconductors, 2nd ed, 2015. [Online]. Available: https://www.semikron-danfoss.com/service-support/application-manual.html

[117] A. Firdaus and S. Mishra, "Mitigation of Power and Frequency Instability to Improve Load Sharing Among Distributed Inverters in Microgrid Systems," *IEEE Syst. J.*, vol. 14, no. 1, pp. 1024-1033, Mar. 2020, doi: 10.1109/JSYST. 2019.2920018.

[118] A. N. Kolmogorov, *Foundations of the Theory of Probability*, 2nd English ed. Chelsea Publishing Company, 1956.

[119] B. Sun, X. Fan, C. Qian, and G. Zhang, "PoF-Simulation-Assisted Reliability Prediction for Electrolytic Capacitor in LED Drivers," *IEEE Trans. Ind. Electron.*, vol. 63, no. 11, pp. 6726-6735, Nov 2016, doi: 10.1109/TIE.2016. 2581156.

[120] S. Sahoo and F. Blaabjerg, "Data-Driven Controllability of Power Electronics Under Boundary Conditions – A Physics-Informed Neural Network Based Approach," in *Proc. 2023 IEEE APEC*, Orlando, FL, USA, Mar. 2023, pp. 2801-2806, doi: 10.1109/APEC43580.2023.10131654.

[121] Y. Peng, S. Zhao, and H. Wang, "A Digital Twin Based Estimation Method for Health Indicators of DC-DC Converters," *IEEE Trans. Power Electron.*, vol. 36, no. 2, pp. 2105-2118, Feb. 2021, doi: 10.1109/TPEL.2020.3009600.

ISSN (online): 2446-1636
ISBN (online): 978-87-7573-670-6

AALBORG UNIVERSITY PRESS